UNIVERSIDAD COMPLUTENSE DE MADRID

FACULTAD DE CIENCIAS GEOLÓGICAS
DEPARTAMENTO DE PETROLOGÍA Y GEOQUÍMICA

TESIS DOCTORAL

Ironstone occurrences in the northern part of the Bahariya Depression, Western Desert, Egypt: Geology, mineralogy, geochemistry and origin

Depósitos de hierro al norte de la Depresión de Bahariya, Desierto Occidental, Egipto: Geología, mineralogía, geoquímica y génesis

MEMORIA PARA OPTAR AL GRADO DE DOCTOR

PRESENTADA POR

Adel Mady Afify Mohammed

DIRECTORES

María Esther Sanz-Montero
José Pedro Calvo Sorando

Madrid, 2017

Ironstone occurrences in the northern part of the Bahariya Depression, Western Desert, Egypt: Geology, mineralogy, geochemistry and origin

PhD Thesis

Adel Mady Afify Mohammed

UNIVERSIDAD COMPLUTENSE DE MADRID
FACULTAD DE CIENCIAS GEOLÓGICAS
Departamento de Petrología y Geoquímica

Madrid, 2016

UNIVERSIDAD COMPLUTENSE DE MADRID

FACULTAD DE CIENCIAS GEOLÓGICAS

DEPARTAMENTO DE PETROLOGÍA Y GEOQUÍMICA

PhD Thesis

Ironstone occurrences in the northern part of the Bahariya Depression, Western Desert, Egypt: Geology, mineralogy, geochemistry and origin

Depósitos de hierro al norte de la Depresión de Bahariya, Desierto Occidental, Egipto: Geología, mineralogía, geoquímica y génesis

Dissertation submitted for the degree of Doctor of Philosophy in

Geological Sciences

Adel Mady Afify Mohammed

Supervisors:

Dr. María Esther Sanz-Montero

Dr. José Pedro Calvo Sorando

Madrid, 2016

Acknowledgements

The PhD thesis presented here is a result of an intense and long work, which has come to fruition thanks to several people who have supported me over the years. In the following paragraphs I want to thank in a special way to those without whom this thesis would not have been.

Firstly, thanks to God destiny that grants me the opportunity to reach the end of this work and inspire me how to finish it.

Secondly, I want to express my deep thanks and gratitude to my supervisors; Prof. Dr. Jose Pedro Calvo and Prof. Dr. Maria Esther Sanz-Montero, who taught me how to think freely and critically. From the first moment you accepted me, you gave me access to the labs of the faculty and help me to know many people from the Complutense University as well as from other institutes in Spain. My gratitude to you is for your kind supervision, guidance in the field, fruitful discussions and continued help, especially in the practical preparation of the work, critical reading and revision of this thesis. Thanks for everything you´ve done and thanks for doing more than you "should".

My deep gratitude to the Ministry of Higher Education, the Egyptian Government and the Geology Department of the Faculty of Science of Benha University, Egypt, for their financial and administrative support during the whole period of study of my PhD thesis in the Complutense University of Spain. Many thanks for giving me such opportunity to travel abroad and get more knowledge, culture and science.

I want to express my deep sincere to Prof. Dr. Wanas, Geology Department, Faculty of Science, Menoufia University, Egypt, for his help to know my supervisors here in Spain. Many thanks for him in helping us during the fieldwork and his collaboration in one of the articles published in the thesis. All my gratitude to my

friends, Dr. Mohammed Kamal Zobaa and Dr. Emad Samir Sallam, Geology Department, Faculty of Science, Benha University, Egypt, for their support during all the fieldtrips that were done during 2012-2014 seasons. Thanks to Dr. Zobaa for his kindly help and using his car during the first fieldtrip. Thank you Dr. Emad for your help and collaboration in one of the articles published in the thesis.

I want to express my sincere thanks to Prof. Dr. Josep Serra-Kiel, Stratigraphy, Paleontology and Marine Geosciences Department, University of Barcelona, Spain, for his kindly help in identification of the larger foraminifera and his collaboration in one of the articles published and used in the thesis.

All my gratitude to Dr. Laura Gonzalez Acebron, Maria Belen Muñoz-Garcia and Valle Lopez (Stratigraphy Department, Faculty of Geological Sciences, University of Complutense of Madrid), for their great help during the thesis. Laura helped me so much for the petrography and fluid inclusions microthermometry, thanks for everything she has done for me. Belen and Valle supported me with the geological mapping and tectonic studies, ´´ Many thanks to you.´´.

I´m grateful to Dr. Cecilia Pérez-Soba Aguilar (Petrology and Geochemistry Department, Faculty of Geological Sciences, University of Complutense, Madrid), for her help and comments on the geochemical studies of the thesis and her encouragement for me during the whole period of the thesis ´´Muchas Gracias.´´.

Special thanks to Prof. Dr. Ana Alonzo-Zarza, Rafaela Marfil and Carlos Rossi (professors of Petrology and Geochemistry Department, Faculty of Geological Sciences, University of Complutense, Madrid) for their scientific help and comments during the long period of the thesis.

I’m so grateful to Prof. Dr. María del Pilar Andonaegui Moreno (Ex-Head of Petrology and Geochemistry Department), Prof. Dr. Jacobo Abati Gómez (Head of Petrology and Geochemistry Department), Prof. Dr. César Casquet Martin, Prof. Dr. Ricardo Arenas Martin, Dr. Carmen Galindo, Dr. Javier Fernández Suárez, Dr. David Orejana, Dr. Miguel Gómez Heras, for many facilities they had done for me during this long period of study in the Petrology and Geochemistry Department, ´´Many thanks to you.´´.

My deep thanks for all of the professors of Petrology and Geochemistry Department of the Faculty of Geological Sciences, Complutense University of Madrid for their help and encouragement during the work. Special thanks for my big family (my colleagues) in the department, especially Oscar Cabestrero Aranda, for their help during the progress of the work. Many thanks to Angela Claro Moreno, Alejandra Gomez Ulla Rubíra, Alvaro Rodríguez, Richard Albert Roper, Alberto Fernández-Mort for their support during the thesis.

Quiero agradecer al personal del taller de Petrología y Geoquímica, a Marián Barajas, Carmen Valdehita, Pedro Lozano e Iván Serrano Muñoz, por el excelente trato recibido, por enseñarme todo lo relacionado con la preparación de muestras y de láminas delgadas y por preparar diligentemente aquellas muestras urgentes que en su momento necesité. También agradecer al CAI de Técnicas Geológicas, a Dra. Sol López Andrés, Xabier Arroyo Rey, Isabel Gómez Pinilla y Teresa Benito Criado. Durante la larga temporada que pasé en el laboratorio aprendí multitud de cosas, preparación de muestras, análisis con los espectrómetros y un largo etcétera, en el que por supuesto incluyo las técnicas. ´´Muchas gracias.´´

Agradezco a todos los miembros del grupo de investigación del departamento por el día a día, el trato amigable, y su disposición, al Departamento de Petrología y Geoquímica por acogerme y facilitarme los medios materiales necesarios, con una

mención especial a Isabel, Beatriz y Miguel Ángel; a la Facultad de Ciencias Geológicas por formarme y a Lidia por hacer que funcione.

Agradezco a los revisores anónimos de la tesis doctoral y a los revisores internacionales de los artículos que se presentan en esta tesis doctoral, que mejoraron considerablemente la calidad de éstos con sus comentarios y apreciaciones.

Special thanks to Prof. Dr. Cecilio Quesada, Prof. Dr. Manuel Pozo and Prof. Dr. David Loope for their comments during several meetings, fieldtrips and conferences as well as their revisions for some manuscripts and short abstracts during the period of the thesis. Really, their comments and annotations greatly improved and added to our knowledge about the project.

My deep gratitude to my family, that without them I couldn´t reach to that point. Many thanks to my parents, my brothers and my lovely sisters who encouraged me all the time. My gratitude to my wife who suffered a lot during the whole period of my study, encouraging me and looking after our kids, Retaj, and the twin Hamza and Moaaz. This work dedicated to all my family, my wife, lovely daughter ´´Retaj´´ and my sons: ´´Hamza´´ and ´´Moaaz´´; their smile is my life.

Adel Mady Afify

Index

Abstract **I**
Resumen **III**

Chapter I: Introduction **1**

1.1. General introduction **1**
1.2. Geological background on iron ore deposits **2**
1.2.1. Types of iron ore deposits **2**
1.2.1.1. Banded iron formations (BIFs) **2**
1.2.1.2. Phanerozoic ironstones **4**
1.2.1.3. Bog iron **5**
1.2.2. Types of iron- and manganese- bearing minerals **6**
1.2.3. Factors controlling stability of ferromanganese minerals **7**
1.2.4. Mechanisms of formation of iron ore deposits – hypotheses and modelling **9**
1.2.5. Sources of iron and mechanisms of transportation **11**
1.3. Iron ore deposits in Egypt **12**
1.3.1. Banded iron formations (BIFs) **12**
1.3.2. Phanerozoic ironstones **14**

Chapter II: Objectives and methodology **19**

2.1. Objectives **19**
2.2. Materials and methods **21**
2.2.1. Fieldwork and geological mapping **21**
2.2.2. Sampling and sample preparation **21**
2.2.3. Petrography and high resolution textural analyses **22**
2.2.4. Mineralogy **22**
2.2.4.1. Bulk mineralogy **22**
2.2.4.2. Clay mineralogy **23**
2.2.5. Geochemistry **23**
2.2.5.1. Major and trace elements geochemistry **23**
2.2.5.2. Rare earth elements and yttrium geochemistry **24**
2.2.5.3. Carbon and oxygen isotope geochemistry **25**
2.2.5.4. Sulfur and oxygen isotope geochemistry **62**
2.2.5.5. Fluid inclusions microthermometry **26**

Chapter III: Geologic setting of the Bahariya Depression **27**

3.1. Stratigraphy **27**
3.1.1. Paleozoic **28**
3.1.2. Mesozoic **30**
3.1.2.1. Jurassic and Lower Cretaceous **30**
3.1.2.2. Upper Cretaceous outcropping succession **32**
3.1.2.2.1. The Bahariya Formation **32**
3.1.2.2.2. The El Heiz Formation **32**

3.1.2.2.3. The El Hefhuf Formation **33**
3.1.2.2.4. The Khoman Formation **33**
3.1.3. Cenozoic outcropping succession **33**
3.1.3.1. The Naqb Formation **34**
3.1.3.2. The Qazzun Formation **34**
3.1.3.3. The El Hamra Formation **36**
3.1.3.4. The Radwan Formation **36**
3.1.3.5. The continental carbonate unit **36**
3.1.4. Volcanic-subvolcanic rocks **37**
3.2. Tectonic setting **39**

Chapter IV: Ironstone crusts hosted in Cenomanian clastic rocks **41**

4.1.Diagenetic origin of ironstone crusts in the Lower Cenomanian Bahariya Formation, Bahariya Depression, Western Desert, Egypt (Article) **43**
4.1.1. The article **44**
4.1.2. Conclusions from the article **63**
4.2. Additional data **65**
4.2.1. Clay mineralogy **65**
4.2.2. Carbon and oxygen isotope analyses of host carbonate rocks **69**
4.2.3. Major and trace elements geochemistry **70**
4.2.4. Rare earth elements and yttrium (REY) geochemistry **75**
4.3. Discussion and conclusions on the genesis of the Upper Cretaceous ironstones of the Bahariya area **78**

Chapter V: Ironstone mineralization hosted in Eocene carbonates **83**

5.1. Nummulite biostratigraphy of the Eocene succession in the Bahariya Depression, Egypt: Implications for timing of iron mineralization (Article) **85**
5.1.1. The article **86**
5.1.2. Conclusions from the article **99**
5.2. Ironstone deposits hosted in Eocene carbonates from Bahariya (Egypt) –New perspective on cherty ironstone occurrences (Article) **101**
5.2.1. The article **102**
5.2.2. Conclusions from the article **121**
5.3. Additional data **123**
5.3.1. Mineralogy and petrology **123**
5.3.2. Major and trace elements geochemistry **127**
5.3.3. Rare earth elements and yttrium (REY) geochemistry **132**
5.3.4. Sulfur and oxygen isotope geochemistry **135**
5.3.5. Fluid inclusions geochemistry **137**
5.4. Discussion and interpretation of the Eocene ore-bearing minerals **140**
5.4.1. Ferromanganese minerals and quartz **140**
5.4.2. Phosphates **142**
5.4.3. Sulfate minerals **142**
5.4.4. Clay minerals – clays as geothermal indicators **144**

Chapter VI: Diagenetic and hydrothermal models of ironstone formation: constraints and comparison **145**

6.1. Constraints of host rock sedimentary features in occurrences of ore minerals **145**
6.2. Geochemical constraints as genetic proxies for both ironstone types **146**
6.3. Modelling and interpretation of the two ironstone types **152**

Chapter VII: Summary and conclusions **155**

Chapter VIII: References **157**

Abstract

The PhD thesis deals with two different ironstone rock types encountered in two sedimentary successions (Upper Cretaceous and Lower Cenozoic) in the northern Bahariya, Egypt. Occurrence of the two iron-bearing rock types in a same area offers an opportunity to better understanding the origin of ironstone deposits. The ironstones occur as thin crusts within Cenomanian clastic rocks (Bahariya Formation) and as big ore bodies at three mine areas, associated to Eocene carbonate units. Analysis of the two ironstone types was carried out by means of field, petrographic, mineralogical and geochemical investigations. The ironstones contain similar iron-bearing minerals, mainly goethite and hematite, which display a variety of fabrics, i.e. concretionary, massive, stromatolitic-like, pisolithic, colloidal, reiniform aggregates, boxwork, leisegang, geode-like and brecciated. They show preferential replacement and cementation of carbonates by iron-rich minerals. Thus, the two ironstone types replaced both depositional and diagenetic carbonates (dolomites) with preservation of the structures, fabrics and thickness of their precursors. However, they exhibit some differences in textures, morphology and bed geometries but marked distinction in which refers to origin, mechanisms and timing of formation.

The main mineral paragenesis in the Upper Cretaceous ironstones includes goethite, hematite, Fe-dolomite/ankerite and subordinate amounts of siderite, pyrolusite, todorokite, psilomelane and barite. In contrast, the Eocene ironstones show a more complex mineral paragenesis including goethite, hematite, quartz and subordinate amount of jarosite, alunite, barite, pyrolusite, jacobsite, romanechite, psilomelane, todorokite, apatite, palygorskite and kaolinite.

The ironstone crusts of the Cenomanian Bahariya Formation show selective replacement of the carbonate rocks deposited in coastal environments and paleosols (calcretes) that occur interbedded with the clastic rocks. Iron-rich dolomite crystals replaced the carbonates during diagenesis. The presence of bitumen in sandstone beds and the carbon isotope values of dolomite support that iron was reduced by decomposition of organic matter and then transported in association with hydrocarbons by Fe- and Mg- rich fluids. The tectonic movements taking place in the region during the Turonian – Santonian favored mixing of meteoric waters with reduced fluids

responsible for the oxidizing conditions required for the deposition of the oxyhydroxides. The permeable rocks, partially composed of dissolved dolomite, joint planes and other discontinuities were preferentially mineralized. We postulate that iron needed to form this diagenetic ironstone type was sourced by iron-bearing minerals (Fe-carbonates and pyrite) from the Bahariya Formation with possibly significant contribution of underlying Jurassic carbonate deposits.

Likewise, the Eocene ironstones occur closely related to major faults showing local extensive replacement of the Eocene carbonate host rocks. The deposits are related to structural traps where hydrothermal reducing iron-rich fluids migrated through the major faults and mixed with meteoric water. Association and distribution of quartz, jacobsite, pyrolusite and barite with the ore deposits support their hydrothermal origin from Si, Fe, Mn, Ba- rich fluids. Chronostratigraphic updating of the fossil assemblages collected from the Eocene formations indicate that they span late Ypresian – early Bartonian. Therefore, formation of the ore deposits can be dated later than early Bartonian, most probably during the Priabonian. The mineralization was coeval to outstanding magmatic activity in Bahariya, south of the mine areas. Source of iron related to deep-seated hydrothermal iron-rich solutions associated with the magmatism.

The two ironstone types show slight similarities in major and trace elements geochemistry, which provides evidence for their formation by carbonate replacement. However, rare earth elements and yttrium (REY) values point to different genetic ironstone types. The Upper Cretaceous ironstones display negative Y and Ce anomalies and intermediate Nd concentrations (between 10 and 100 ppm) indicative of diagenetic origin, whilst the negative Ce anomaly, positive Y and Eu anomalies, low Nd concentration (mostly less than 10 ppm) and very low REE concentrations of the Eocene ironstones strongly support a hydrothermal origin. The presence of positive Y anomalies in the Eocene ironstones suggests that iron precipitation occurred rapidly and immediately after reducing, slightly acidic waters reached oxidizing and alkaline water. The contrasted formation mechanisms and the distinctive features, on which these mechanisms are proposed, provide proxies for interpreting more ancient ironstone deposits. Occurrence of chert in the Eocene ironstones and its preferential distribution along faults can help in better understanding of the genetic mechanisms of formation of banded iron formations (BIFs) that were abundant during the Precambrian.

Resumen

El sector Norte de la Depresión de Bahariya (Desierto Occidental de Egipto) ofrece la oportunidad única de estudiar dos tipos de depósitos de hierro formados en distintos contextos geotectónicos. Uno de los tipos se dispone intercalado entre rocas detríticas del Cenomaniense que se sedimentaron en ambientes fluvio-deltaicos (Fm. Bahariya). El segundo tipo de depósitos de hierro, que se explota en minas a cielo abierto, aparece asociado a las formaciones carbonáticas suprayacentes (Fms. Naqb, Qazzum y Hamra) que se depositaron durante el Eoceno en distintos ambientes marinos de plataforma continental.

En la Fm. Bahariya, los depósitos de hierro se presentan como concreciones (nódulos, rizolitos, etc.) y costras de hasta 1 m de espesor siguiendo principalmente las discontinuidades sedimentarias. Las rocas ferruginosas superiores se concentran en las inmediaciones de dos grandes sistemas de falla, donde se muestran como mineralizaciones masivas y voluminosas que pasan lateralmente a carbonatos. El estudio de los depósitos se ha realizado mediante la combinación de técnicas de campo con análisis sedimentológicos, petrográficos, mineralógicos y geoquímicos. Estos análisis muestran que las rocas ferruginosas están mayoritariamente constituidas por óxidos y oxihidróxidos de hierro (hematites y goethita) que adoptan distintas morfologías: masiva, boxwork, brechoide, concreciones, laminada, leisegang, pisolítica, coloidal, etc. Ambos tipos de depósitos de hierro se encuentran reemplazando y/o cementando selectivamente a carbonatos (calizas y dolomías) tanto deposicionales como diagenéticos, mientras que los componentes siliciclásticos asociados se muestran inalterados. En las rocas ferruginosas se pueden reconocer las estructuras, las fábricas, la secuencialidad y el espesor de los precursores carbonáticos.

Cada depósito de hierro, no obstante, presenta unos rasgos específicos que revelan orígenes distintos. El acumulado en la Fm. Bahariya reemplaza/cementa cristales de dolomita ferrosa (hasta 14% de FeO) afectados por disolución. Los valores de isótopos estables de la dolomita ($\delta^{13}C$ hasta -7.22‰) así como la presencia de bitumen en las areniscas, sugieren que el hierro se encontraría en estado reducido a causa de la transformación de compuestos orgánicos y se movilizó junto a los hidrocarburos durante la diagénesis. Se propone que los movimientos tectónicos que

afectaron a la cuenca en el Turoniense – Santoniense propiciaron la mezcla de aguas meteóricas con aguas reductoras lo que favoreció la oxidación y depósito de los óxidos y oxihidróxidos de hierro, preferentemente a favor de las rocas dolomíticas más permeables y las discontinuidades. Las rocas ferruginosas cretácicas se encuadran, por tanto, en un modelo de formación diagenético, dentro del que la principal fuente de hierro se sitúa en los carbonatos ferrosos y pirita de las formaciones jurásicas subyacentes que, a su vez, se reconocen como rocas madre de petróleo.

Los depósitos de hierro cenozoicos se concentran en trampas estructurales donde reemplazan por completo a los carbonatos eocenos más fracturados. En éstos se reconoce una asociación mineral más compleja integrada por goetita, hematites, cuarzo y, en menor medida, por jarosita, alunita, barita, pirolusita, jacobsita, romanechita, psilomelana, todorokita, apatito, palygorskita y caolinita. Estas y otras evidencias, apoyan que esta mineralización se generó a partir de fluidos hidrotermales enriquecidos en Fe, Si, Mn y Ba. Los fluidos ascendieron a favor de las fallas hasta mezclarse con aguas superficiales oxidantes, favoreciendo la precipitación de los minerales transportados. Los resultados microtermométricos de las inclusiones fluidas del cuarzo revelan que las temperaturas de homogeneización variaron en el rango 90-283 °C; mientras que las inclusiones monofásicas líquidas halladas en cristales de barita reflejan una temperatura de formación baja (<50 °C), en ambiente meteórico. Por lo tanto, la mineralización se produjo dentro de un amplio rango de temperaturas.

Las asociaciones de fósiles ferruginizados han permitido determinar que los carbonatos que los contienen se depositaron entre el periodo Ypresiense superior – Bartoniense inferior. Por lo tanto, todo apunta a que el evento formativo se produjo con posterioridad a esta fecha, y más probablemente durante el Priaboniense, coincidiendo con una etapa de intensa actividad tectónica en Egipto que precedió a la sedimentación de las formaciones sedimentarias no ferruginizadas, de edad Priaboniense.

Los análisis geoquímicos de los dos tipos de depósitos de hierro muestran ciertas semejanzas, en cuanto a los elementos mayores y traza, que evidencian su formación a partir de carbonatos. El análisis de las tierras raras e itrio (REY) indica, no obstante, que los depósitos tienen distinto origen. Así, las anomalías negativas de Y y Ce, junto a los valores de concentración intermedios de Nd, entre 10 y 100 ppm, apoyan un origen

diagenético de las rocas cretácicas. Mientras que, en conjunto, las anomalías negativas de Ce, las anomalías positivas de Y y Eu, así como las bajas concentraciones de Nd (< 10 ppm) y de tierras raras medidas, confirman un origen hidrotermal en el caso de los depósitos eocenos. Las anomalías positivas del Y que presentan estos últimos sugieren, además, que la precipitación del hierro se produjo de una forma rápida e inmediata, al mezclarse aguas reductoras y ligeramente ácidas con aguas meteóricas.

Los dos mecanismos de formación propuestos, diagenético e hidrotermal, para los depósitos de hierro cretácicos y eocenos, respectivamente, dejan una impronta mineralógica, geoquímica, de distribución, etc. característica que puede ser utilizada para discriminar distintos mecanismos de formación en rocas ferruginosas más antiguas. Específicamente, los depósitos de hierro con cuarzo del Eoceno pueden ser utilizados como análogos para comprender mejor el origen de las formaciones de hierro bandeado que fueron tan extensas y abundantes durante el Precámbrico y, sin embargo, son muy escasas en el Fanerozoico.

I

Introduction

1.1. General introduction
1.2. Geological background on iron ore deposits
1.2.1. Types of iron ore deposits
1.2.1.1. Banded iron formations (BIFs)
1.2.1.2. Phanerozoic ironstones
1.2.1.3. Bog iron
1.2.2. Types of iron- and manganese- bearing minerals
1.2.3. Factors controlling stability of ferromanganese minerals
1.2.4. *Mechanisms of formation of iron ore deposits – hypotheses and modelling*
1.2.5. *Sources of iron and mechanisms of transportation*
1.3. Iron ore deposits in Egypt
1.3.1. Banded iron formations (BIFs)
1.3.2. Phanerozoic ironstones

1.1. General introduction

This PhD thesis explores the genesis, mechanisms of formation and modelling of ironstone mineralization, especially those occurring in Phanerozoic rocks. The present study deals with a variety of ironstone occurrences in the northern part of the Bahariya Depression, located in the central part of the Western Desert of Egypt. The ironstone occurrences in this area are either hosted in clastic rocks of the Cenomanian Bahariya Formation or associated with Eocene carbonate units. In both cases, the ironstones were correlated with their host rocks by using mineralogical, geochemical and

sedimentological evidence. The results are presented in two blocks according to the two different types of ironstone occurrences. The first block of the thesis deals with ironstone occurrences in the Upper Cretaceous Bahariya Formation whereas the second one includes the ironstones associated with the Eocene carbonates. Last part of the work focuses on integration of the mechanisms that constrained the formation of the ironstone deposits and a modelling for these ironstones is provided.

1.2. Geological background on iron ore deposits

Ferruginous and manganiferous chemical sediments, such as ironstone crusts, ferromanganese crusts, nodules and concretions, ironstones and banded iron formations (BIFs), are widely used as archives of geochemical proxies (Bau et al., 2014; Hein et al., 2016). These rock types are currently being explored and evaluated as potential targets for steel industry and high technology metals, such as Cu, Ni, Co, REE, Mo, etc (e.g., Hein et al., 2013). Formation of Fe-Mn chemical sediments shows different modes of formation, i.e. hydrogenetic, hydrothermal, diagenetic and/or a combination of these processes through different temporal and spatial occurrences. Accordingly, the following subchapters will give an overview on the main types of iron ores, their ore-forming minerals, mechanisms of formation and the main proposed genetic models.

1.2.1. Types of iron ore deposits

In terms of morphology, texture and mineralogy, there are three main types of iron ore that illustrate different ore forming processes including one or more stages during their formation. The three types are banded iron formation (BIF), Phanerozoic ironstone, and bog iron (Evans, 1993; Robb, 2004; Boggs, 2006, and references therein).

1.2.1.1. Banded iron formations (BIFs)

The BIFs represent the most important source of iron ore all over the world, with more reserves and total production value than those of Phanerozoic ironstone and bog iron ores. The banded iron formation is a stratigraphic unit composed largely of ironstone that may be cherty or non-

cherty but with banded appearance (Kimberley, 1989; Klein and Beukes, 1993). BIFs are observed over a wide range of scales, from coarse macrobands (meters in thickness) to mesobands (centimeter-thick units) to millimeter and sub- millimeter layers (Trendall and Blockley, 1970). The BIF term is hyphenated and applies strictly to bedded chemical sediment comprising alternating layers rich in iron and chert (Klein and Beukes, 1993). BIFs were formed during essentially three periods throughout the Archean and Proterozoic Earth history, namely 3500–3000 Ma, 2500–2000 Ma, and 1000–500 Ma. These periods equate with different tectonic settings and are referred to as Algoma, Lake Superior and Rapitan types, respectively (James and Trendall, 1982; James, 1983; Maynard, 1991; Klein and Beukes, 1993; Bekker et al., 2010, 2014).

a) Algoma type BIFs are associated with volcanic arcs and are typically found in Archean greenstone belts. These deposits tend to be fairly small but they are mined in places such as the Abitibi greenstone belt of Ontario, Canada (Holland, 1984; Maynard, 1991; Robb, 2004; Boggs, 2006; Bekker et al., 2014).

b) The Lake Superior or simply Superior type BIFs is located mostly on stable continental platforms and were mainly deposited in Paleoproterozoic times. They represent the most important category of iron ore deposits and the most currently producing iron ore districts. Examples include the Hamersley Basin of Western Australia, the Transvaal Basin of South Africa, the Quadrilatero Ferrifero of Brazil, the Labrador trough of Canada, the Singhbhum region of India and the type area in the Lake Superior region of the USA (Robb, 2004; Bekker et al., 2014).

c) The Rapitan type represents a rather unusual occurrence of iron ores associated with glaciogenic sediments formed during the major Neoproterozoic ice ages. The type occurrence is the Rapitan Group in the McKenzie Mountains of northwest Canada (Holland, 1984; Maynard, 1991; Robb, 2004).

The main iron minerals in the banded iron formation are hematite (Fe_2O_3), magnetite (Fe_3O_4), greenalite ($Fe_3Si_2O_5$ $(OH)_4$), stilpnomelane (2(Fe, Mg)O (Al, Fe)$_2$·O_3·$5SiO_2$·$3H_2O$),

minnesotaite ($(Fe, Mg)_3 Si_4O_{10} (OH)_2$) and pyrite ($FeS_2$) (Table 1.1). The banded iron formation occurs in the form of banded or bedded structure of alternating iron-bearing minerals and chert or other silicate and carbonate minerals.

1.2.1.2. Phanerozoic ironstones

The second type is referred to ironstone deposits formed during the Phanerozoic; they are usually termed as Phanerozoic iron deposits. These ironstone deposits are of widespread occurrence representing an important source of iron, particularly during the first part of the twentieth century. The term iron-rich is restricted to sedimentary rocks that contain at least 15% of total iron (Kimberley, 1994). Iron is present in almost all sedimentary rocks, with average content 4.8 percent in siliciclastic shale, 2.4 percent in sandstone and 0.4 percent in limestone (Blatt, 1982). Boggs (2006) used the term ironstone for non-banded, non-cherty, commonly oolitic, iron-rich sedimentary rocks whilst the term iron formation was allocated to the cherty, well-banded iron-rich sedimentary rocks. Several nomenclatures have been used for the Phanerozoic ironstone (Bottke, 1981; Barnes, 1989; Evans, 1993; Mücke and Farshad, 2005). Thus, ironstone deposits occurring in the Jurassic sediments of England and the Alsace-Lorraine region of France and Germany were referred to as minette or Lorraine-type iron ores. Other types recorded in North America were known as Silurian Clinton type iron ores of Kentucky and Alabama that are analogues of the younger European deposits (Bottke, 1981; Barnes, 1989; Evans, 1993; Mücke and Farshad, 2005).

The ironstone deposits in the Phanerozoic were formed in different ways, the most common being the oolite type. This is mainly present in the Ordovician, Silurian, Jurassic, Cretaceous and Cenozoic periods but shows a wide stratigraphic range from Precambrian to Holocene (Petránek and Van Houten, 1997). Most oolite ores are economically exploited and major development took place during the Ordovician and Jurassic periods. Ordovician iron oolites are found in North Africa, Spain, Portugal, France, Germany, England, Poland, the Czech Republic (Bohemia) and other places (James, 1966). The Ordovician oolite

ironstones occur widely in marine shelf sequences of SW Europe (the Western European Platform), the Avalonian Terranes and in North Africa where they form the most important group of deposits of the two major periods of Phanerozoic ooidal ironstone generation (Ordovician- Devonian and Jurassic – Paleogene; Young and Taylor, 1989). Cenozoic ironstone is also of wide occurrence in the north central Africa and SW Europe in Paleocene, Eocene, Oligocene, Miocene and Pliocene episodes and mostly with ooid fabrics (Van Hutton, 1992). The Cenozoic ironstone occurs in northern Pakistan, western Siberia, southern Germany, northwestern Venezuela, northeastern Colombia, northwestern Romania, south-central USA and central North Africa (Van Hutton, 1992; Petránek and Van Houten, 1997).

The main iron bearing minerals recognized in the Phanerozoic ironstone are hematite (Fe_2O_3), goethite ($FeO{\cdot}OH$), siderite ($FeCO_3$), ankerite ($(Ca, Mg, Fe)(CO_3)_2$), ferroan dolomite ($Ca\ Mg,\ Fe\ (CO_3)_2$), ferroan calcite ($(Ca, Fe)CO_3$), pyrite (FeS_2), jarosite ($KFe_3^{3+}(SO_4)_2(OH)_6$), chamosite ($(3(Fe^{2+},Mg)_5Al\ (AlSi_3O_{10})(OH)_8$), berthierine ($(Fe^{2+},Fe^{3+},Al,\ Mg)_2{\cdot}3(Si, Al)_2O_5(OH)_4$), nontronite ($Na_{0.3}Fe_2\ ((Si, Al)_4O_{10})\ (OH)_2{\cdot}nH_2O$) and glauconite ($(K\ Mg\ (Fe, Al)\ (SiO_3)_6{\cdot}3H_2O$) (Table 1.1).

1.2.1.3. Bog iron

The third type of iron ores is the bog iron deposits. They mainly form in lakes and swamps of the glaciated tundra regions of the northern hemisphere, such as northern Canada and Scandinavia as well as most recent iron deposits (Boggs, 2006). The deposits are typically small and thin, and comprise concentrations of goethite and limonite associated with organic-rich shale. They formed in recent geological periods; even they form locally at present (Stanton, 1972; Robb, 2004; Boggs, 2006). This type of iron ores precipitates where aqueous solutions containing labile ferrous iron (Fe^{2+}), in a relatively reduced environment, are oxidized, with the subsequent formation and precipitation of ferric iron (Fe^{3+}). The bog iron accumulation occurs at the interface between oxygenated surface waters flowing along an aquifer and the reduced iron-rich solutions percolating downwards through a swamp.

1.2.2. Types of iron- and manganese-bearing minerals

Iron minerals present in the three previously-described iron ore types can be included in four different mineral classes, namely oxides, sulfides, carbonates and silicates (James, 1992) (Table 1.1). In addition, manganese minerals are commonly associated with the iron-rich rocks. Where accompanied with iron oxyhydroxides, the manganese minerals are referred as ferromanganese deposits and are mostly composed of pyrolusite, psilomelane, romanechite, todorokite, manganite, etc, mostly oxides and oxyhydroxides (Table 1.1).

Mineral class		Mineral	Chemical formula
Iron-bearing minerals	Oxides	Goethite	FeO·OH
		Hematite	Fe_2O_3
		Magnetite	Fe_3O_4
	Silicates	Chamosite	3 (Fe, Mg)O (Al, Fe) $_2$·O_3·2SiO_2·nH_2O
		Greenalite	$Fe_3Si_2O_5(OH)_4$
		Glauconite	K Mg (Fe, Al) $(SiO_3)_6$·3H_2O
		Minnesotaite	$(Fe, Mg)_3$ Si_4O_{10} $(OH)_2$
		Stilpnomelane	2 (Fe, Mg)O (Al, Fe) $_2$·O_3·5SiO_2·3H_2O
		Nontronite	$Na_{0.3}Fe_2((SiAl)_4O_{10})(OH)_2$·n$H_2O$
	Sulfides	Pyrite	FeS_2
		Marcasite	FeS_2
	Carbonates	Siderite	$FeCO_3$
		Ankerite	Ca (Mg, Fe)$(CO_3)_2$
		Fe-Dolomite	Ca (Mg, Fe) $(CO_3)_2$
		Fe-Calcite	(Ca, Fe) CO_3
Mn-bearing minerals	Mn- Oxyhydroxides	Pyrolusite	MnO_2
		Manganite	MnO·OH
		Rhodochrosite	$MnCO_3$
		Jacobsite	$Mn(Mg, Fe)_2O_4$
		Romanechite	$((Ba,H_2O)_2(Mn^{+4},Mn^{+3})_5O_{10})$
		Psilomelane	$Ba(Mn^{2+})(Mn^{4+})_8O_{16}(OH)_4$
		Manjiroite	$(Na, K)(Mn^{+4}, Mn^{+2})_8O_{16}$·n$(H_2O)$
		Todorokite	(Na, Ca, K, Ba, Sr)1-x(Mn, Mg, Al)$_6O_{12}$•3-4H_2O
		Birnessite	$(Na_{0.3}Ca_{0.1}K_{0.1})(Mn^{4+},Mn^{3+})_2O_4$ · 1.5 H_2O
		cryptomelane	$K(Mn^{4+},Mn^{2+})_8O_{16}$

Table 1.1. Main iron and manganese-bearing minerals and their chemical formula (chemical composition of minerals after Deer, Howie and Zussman, 1992).

1.2.3. Factors controlling stability of ferromanganese minerals

Iron occurs in nature in two valence states: ferrous or divalent state and ferric or trivalent state. The behavior of iron and the precipitation of iron-rich minerals is controlled by the chemistry of surface and diagenetic environments (Tucker, 1981). The ferrous state is stable under relatively reducing and acidic conditions while the ferric state forms and remains under more oxidizing and alkaline conditions. In river water and groundwater iron in true solution occurs in very low concentration (less than 1 ppm) whilst in seawater the concentration is around 0.003 ppm.

Ferromanganese minerals form through different paragenetic stages and their stability depends on the interplay among several factors e.g., pH, Eh, organic content, bacterial activity, carbon activity (pCO_2), sulfur activity (pS^{-2}), temperature, iron and manganese concentration and rate of precipitation (Chao and Theoblad, 1976; Murray, 1979; Schwertmann and Murad, 1983; Brookins, 1987; Alt, 1988; Hein et al., 1997; Fortin and Langley, 2005; Mamet and Préat, 2006; Loope et al., 2011). These factors affecting different ferromanganese minerals occur summarized in Table 1.2.

The pH–Eh relationship of the solution is considered a decisive factor controlling precipitation of the ferromanganese minerals (Fig. 1.1). Regarding the pH-Eh range of natural environments, ferric iron is present as highly insoluble $Fe(OH)_3$ whereas ferrous iron is present in solution (more soluble). Similar to iron, Mn^{3+} and Mn^{4+} are insoluble in natural environments whilst the divalent Mn occurs in solution. The amount of organic matter affects the Eh of the natural aqueous environments since decay of organic matter consumes oxygen and creates reducing conditions. The organic matter deposited in the sediments soon decomposes through aerobic bacterial reduction and the reducing environment form some tens of centimeters below the sediment- water interface so that oxic, near surface environment passes down into anoxic environment. Accordingly, main environments leading to the formation of iron-bearing minerals are subdivided into oxic and anoxic environments. The oxic environment leads to formation of iron minerals with ferric state such as hematite, goethite and MnO_2 minerals.

The anoxic environments led to the formation of iron and manganese minerals in divalent state such as siderite, ankerite, magnetite, pyrite, marcasite, chamosite, greenalite, and manganese mineral rhodochrosite. Some of these anoxic environments are sulfidic. The activity of sulfur is high and the sulfate reducing bacteria will lead to the release of H_2S that will react with the Fe^{+2} forming pyrite or marcasite. The anoxic environments are also characterized by non-sulfidic methanic or post-oxic anoxic conditions (negative Eh, low sulfur activity) under which siderite, ankerite, rhodochrosite and iron silicate minerals formed. Accordingly, the activity of carbonates (pCO_2) and the activity of sulfur (pS^{-2}) are also important factors controlling Fe-Mn formation (Table 1.2). Temperature has also effects on the formation of ferromanganese minerals as decomposition of organic matter is highly depending on that factor; the higher the temperature, the higher the amount of organic matter decomposed.

Factors Minerals	pH	Eh	Organic matter	Activity of carbonates	Activity of sulfur	Occurrence
Hematite	Neutral to alkaline	Positive	Low or no content	Low	Low	In BIF and ironstone
Goethite	Neutral to alkaline	Positive	Low or no content	Low	Low	In ironstone and bog iron
Magnetite	Neutral to alkaline	Negative	Low organic content	Low	Low	In BIF and minor in ironstone
Pyrite	Acidic	Negative	High	Low	High	In BIF and ironstone
Siderite	Acidic	Negative	Moderate to high	High	Low	In BIF and ironstone
Ankerite	Acidic	Negative	Moderate to high	High	Low	In ironstone
Glauconite	Acidic to alkaline	Negative to positive	Low organic matter	Low	Low	In ironstone, sandstone and limestone
Chamosite	Acidic to alkaline?	Negative	Low	Low	Low	In ironstone
Greenalite	Acidic?	Negative	Low organic matter	Low	Low	In BIF

Table 1.2. Stability, occurrence and factors affecting formation of iron-bearing minerals (source of data: Chao and Theoblad, 1976; Murray, 1979; Schwertmann and Murad, 1983; Alt, 1988).

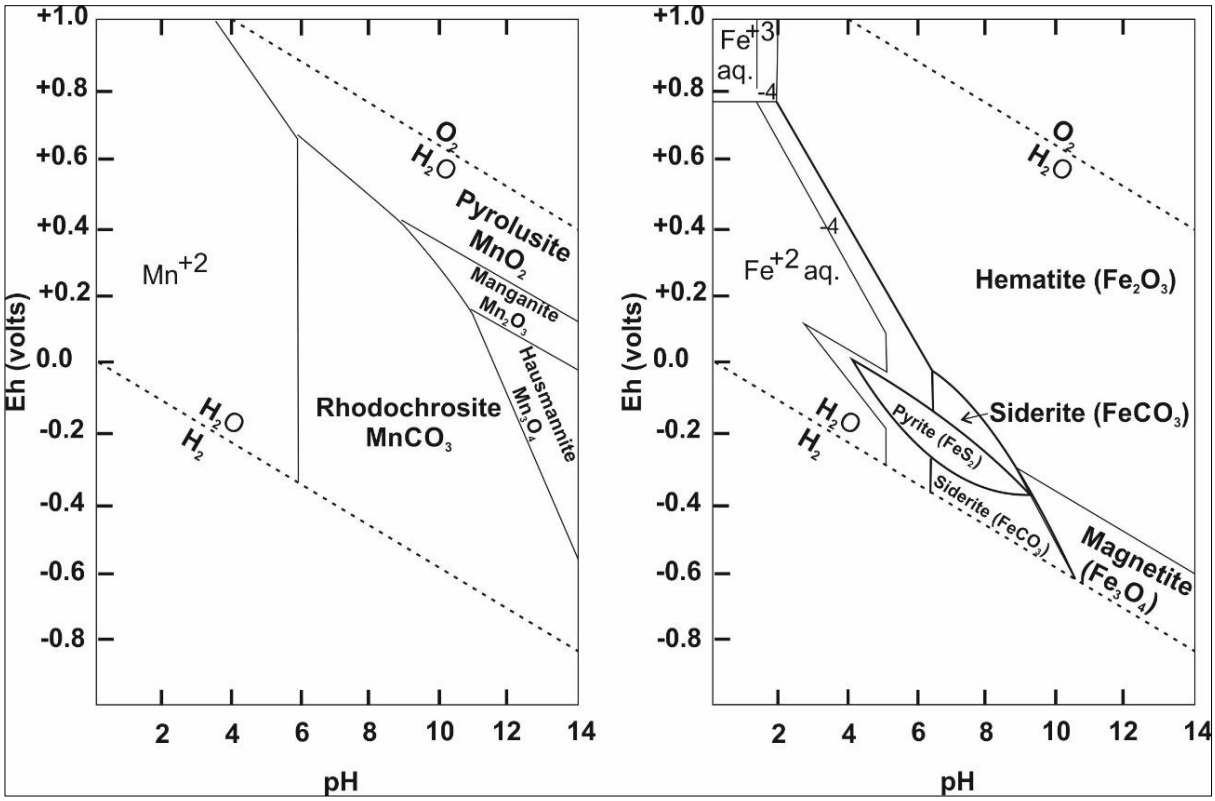

Figure 1.1. Eh-pH diagram showing the stability fields of the common ferromanganese minerals in water at 25 °C and 1 atm total pressure (diagrams after Garrels and Christ, 1965; Brookins, 1987; Krauskopf and Bird, 1995; Takeno, 2005).

1.2.4. Mechanisms of formation of iron ore deposits – hypotheses and modelling

Literature on iron deposits is large and the origin of iron ore deposits has long been subject of discussion and controversies. This resulted in a variety of contrasted hypotheses dealing with the origin of iron ore deposits (James, 1966; Stanton, 1972; Siehl and Thein, 1989; Heikoop et al., 1996; Mücke, 2000; Sturesson et al., 2000; Mücke and Farshad, 2005; Kappler et al., 2005; Bekker et al., 2010; Loope et al., 2011; Rasmussen et al., 2014; Sun et al., 2015; Hein et al., 2016; and references therein).

In this work, more descriptions and interpretations about Phanerozoic ironstones are included where they represent our case study. Young and Taylor (1989) postulated that the sedimentary ironstone deposits are thin sequences that formed in shallow marine or non-marine environments. The formation of iron could involve the mobilization and transport of the ore-forming metals by seawards flowing

groundwater of continental origin (James, 1966) either from shallow unconfined aquifers associated with organic-rich sediments (Borchert, 1965) or from deep aquifers (Stanton, 1972). The formation of ironstone could be related to a pattern of global tectonic cyclicity and specifically to times of continental dispersal and sea-level high stand, as well as periods of warmer climate and increased rates of chemical sedimentation (Van Houten and Authur, 1989). Weathering of a variety of rocks under lateritic conditions and further transportation of iron through fluvial drainage systems into marine basins was pointed out as a model for ironstone formation (Mücke, 2000; Mücke and Farshad, 2005). Mechanical reworking, in-situ weathering and re-deposition from basement rocks in non-marine basins via river systems were proposed as main processes leading to the accumulation of iron under pedogenic conditions (Siehl and Thein, 1989). Their model implies the transfer of the pedogenic pisoids to a marginal marine setting with subsequent mechanical abrasion and reworking/concentration of pisoids.

Otherwise, ferromanganese minerals can form through three main genetic processes, i.e. hydrogenetic, hydrothermal, diagenetic and/or a combination of these processes (Hein et al., 1997). Likewise, hydrothermalism and volcanicity are considered as main factors controlling the formation of ferromanganese ore deposits and their associated minerals (e.g. sulfates, quartz and clay minerals) in different localities, especially in geotectonic settings (Kimberley, 1989, 1994; Sturesson et al., 2000; Hein et al., 2008, 2016). Formation of iron ooids in reef areas under the influence of venting of hydrothermal water associated with volcanic activity has been reported (Heikoop et al., 1996). Hydrothermal solutions produce iron oolites in certain areas today and erosion of volcanic rocks can locally cause enrichment of the elements needed for ooid formation (Sturesson et al., 1999). Volcanism was a major source of iron leading to ironstone formation from volcanic ash with hydrothermal fluids enriching seawater in Fe, Al and Si (Dreesen, 1989; Sturesson, 1992; Sturesson et al., 2000). Besides, Kimberley (1989, 1994) documented precipitation of iron from exhalative fluids associated with active faults.

Most of the aforementioned case studies deal with inorganic precipitation of iron mineral phases. Even though, microbial activity appears to have played a significant role in the formation of ferruginous-coated grains, concretions and ferruginous stromatolitic microbialites (Dahanayake and Krumbein, 1986; Burkhalter, 1995; Préat et al., 2000; Mamet and Préat, 2006; Loope et al., 2011).

In short, a variety of processes has been invoked for the formation of the different types of ironstone deposits, i.e. replacement of carbonates (Kimberley, 1979; Loope et al., 2011), crystallization from precursor iron oxyhydroxide gels (Harder, 1989), mechanical accretion of chamositic clay particles (Bhattacharya and Kakimoto, 1982; Van Houten and Burucker, 1984) and/or precipitation in marine environment linked to sedimentary exhalative hydrothermal processes in tectonically active areas (Rivas-Sánchez et al., 2006; Hein et al., 2008, 2013, 2016).

1.2.5. Sources of iron and mechanisms of transportation

Discussion on the origin of iron-rich and manganese-rich sediments can be summarized into two main concepts: their formation was either due to direct precipitation from solution (groundwater, hydrothermal, magmatic, volcanic sources) or to chemical weathering of Fe- and Mn- rich mafic rocks and heavy minerals (Dreesen, 1989; Young and Taylor, 1989; Kimberly, 1994; Pichler and Veizer, 1999; Pichler et al., 1999; Mücke, 2000; Sturesson et al., 2000; Sturesson, 2003; Needham et al., 2004; Kimberly, 2005; Mücke and Farshad, 2005; Needham et al., 2005; Rivas-Sánchez et al., 2006, and references therein). In the latter case, the source for iron is related to continental intensive weathering under humid tropical climate that releases the iron from mafic and heavy minerals, e.g., igneous and iron-rich rocks, and produces iron-charged ground water and iron-rich lateritic soils precipitated through flocculation of the colloidal suspensions (Siehl and Thein, 1989; Mücke and Farshad, 2005). In the former case, iron related to the volcanic, magmatic and/or hydrothermal activities that can supply considerable amount of iron from iron-rich solutions (Kimberley, 1989, 1994; Sturesson et

al., 2000; Hein et al., 2008). The magmatic and hydrothermal sources usually relate to some specific geotectonic areas.

The three main mechanisms for the transportation of iron described in literature are the following: a) movement through fractures and faults or by groundwater and surface streams of solutions either of ferric hydroxide readily forming insoluble colloidal suspension or more soluble ferrous iron solution; b) iron is transported by adsorption and chelating onto organic matter; c) iron is carried by clay minerals, either as a part of the clay structure or as oxide films on the clay surfaces (Van Houten, 1973; Maynard, 1983; Mücke and Agthe, 1988; Siehl and Thein, 1989; Young and Taylor, 1989; Petranek and van Houten, 1997; Pichler and Veizer, 1999; Mucke, 2000; Mücke and Farshad, 2005). Once deposited, the iron can be released from clays or organic matter into pore water if pH- Eh conditions are appropriate, and then re-precipitated to form iron minerals.

1.3. Iron ore deposits in Egypt

Iron ores occur in Egypt in two forms: Precambrian banded iron formations (BIFs) and Phanerozoic ironstone deposits. Distribution of the two iron ore types is shown in Figure 1.2.

1.3.1. Banded iron formations (BIFs)

BIFs occur in 13 different localities in the north and central Eastern Desert of Egypt, from Safaga in the north to Marsa Alam to the south (Fig. 1.2). Um Anab and Wadi Karim are nice examples of banded iron formation in that region where the BIF conformably alternates with Neoproterozoic arc metavolcanic rocks, which comprise metabasalts and mafic to intermediate metapyroclastic rocks (Basta et al., 2011). According to these authors, the BIFs are of Algoma type iron associated with volcanic arcs. Another example for the BIF in the Eastern Desert is the Abu Marwat BIF, which has been interpreted as a result of the interaction between volcanically derived fluids and seawater (Botros, 1991). The fluids were capable of leaching iron, silica, carbonate gold and others from basalt and andesite in the early stages of island arc vulcanicity.

Other examples of BIFs are Um Nar, Um Ghamis, El Dabbah, Um Shadad, Abu Diwan and Gabal El Hadid deposits (Fig. 1.2). The BIF band usually ranges in thickness from few centimeters up to 5 meters with an average thickness of 1.5 m. In most cases, the BIF occurs as strongly folded and faulted bands with different folding and faulting patterns and exhibits oxide facies composed of alternating iron-rich and silica-rich bands. Carbonate and sulfide facies also do occur.

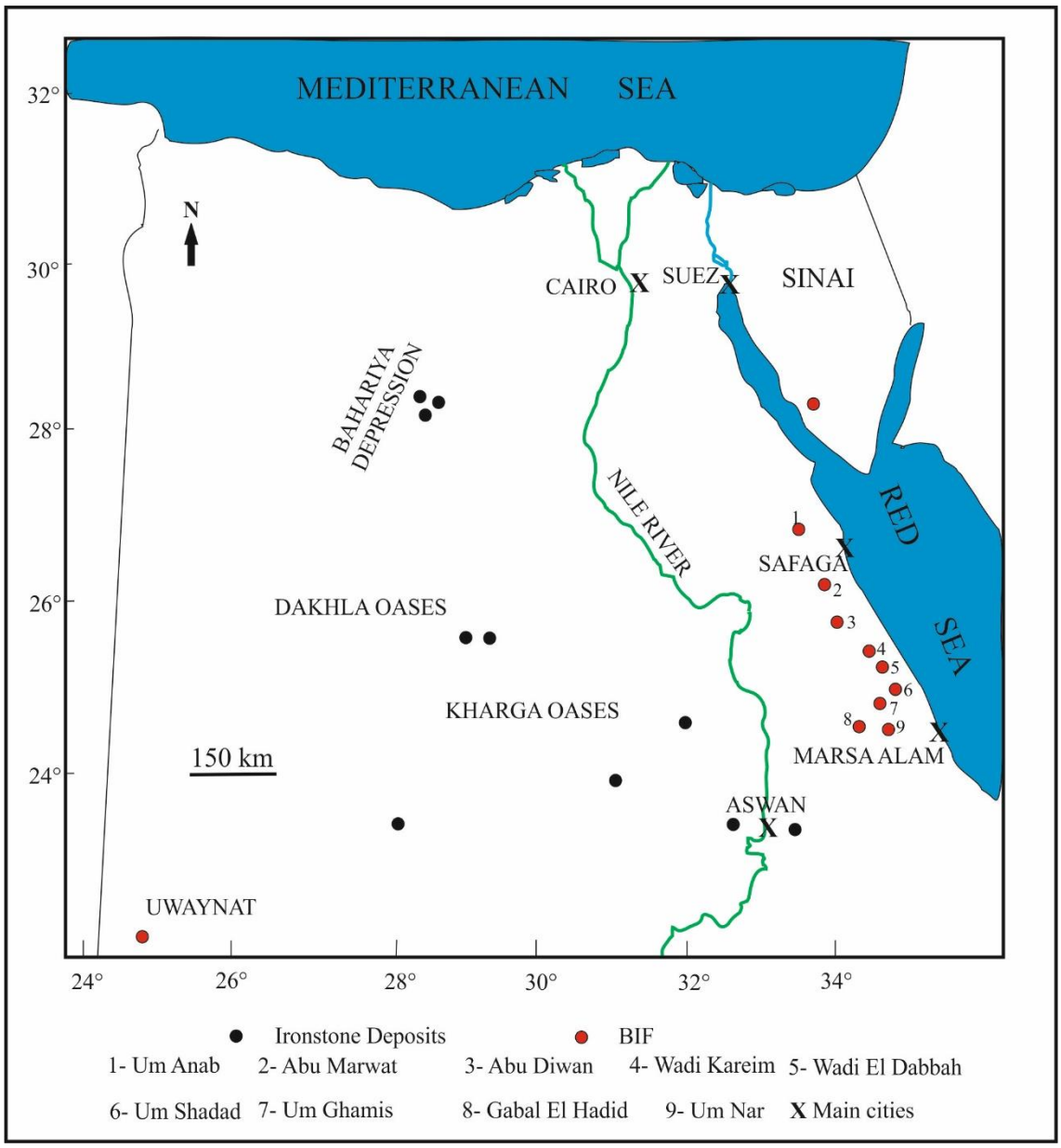

Figure 1.2. Distribution of the iron ore deposits in Egypt with indication of the main localities (after Abouzeid and Khalid, 2011).

Besides the localities in the Eastern Desert, the BIFs occur to the south of the Western Desert, in the area between the Egyptian- Libyan borders to the west of Gabal Kamel and extend outside Egypt in the Libyan and Sudanese territories that are considered to be of Lake Superior type (Khattab et al., 2002). The banded iron formation of this area occurs as thin bands (5-10 m) within amphibolite and quartzo-felsphathic gneisses (Khalid and Diaf, 1996). Economically, the banded iron formation of the south Western Desert of Egypt (at Gabal Kamel) is less important due to the intrusion of huge granitic bodies that cut the extension of the ore.

1.3.2. Phanerozoic ironstones

Phanerozoic ironstones occur irregularly distributed in several localities (Fig. 1.2). Aswan iron ore and Bahariya ironstones are the two main exploited areas for feeding the steel industry in Egypt. The ironstone deposits of Aswan area correspond to the oolitic type. They were the main supply of iron ores for the Egyptian iron and steel industry from its establishment in 1956 until 1972, when they were replaced by the iron ore exploited in Bahariya. The ore is of bedded oolitic type and occurs in the form of two bands interbedded with ferruginous sandstone and clay capping Precambrian rocks. The thickness of the bands varies from 0.2 to 3.5 m. The reserves were estimated between 121-135 million tones with average content of 46.8% Fe (Attia, 1955). The ironstone deposits of the Aswan area are included in a shallow marine succession deposited during the Coniacian-Santonian southward shift of the Tethyan paleoshoreline. This event occurs intercalated between two regressive phases during which fluvial facies accumulated (Klitzsch, 1986). The Aswan ironstone is formed of oolitic (oolitic sandy, true oolitic, lean oolitic), non-oolitic (green laminated, red and black sheeted, muddy banded and lenticular) deposits as well as storm generated reworked ironstone conglomerate (Bhattacharyya, 1989). The iron-bearing minerals of the Aswan deposits are mainly hematite, chamosite, kaolinite, goethite, quartz and other constituents like pyrite and siderite; the latter minerals occur pseudomophously replaced by goethite and hematite (Mücke, 2000).

The second main locality showing Phanerozoic ironstone occurrences is our case study area in the Bahariya region (Fig. 1.2). In this area located in the central Western Desert, there is a variety of ironstone occurrences including the economic Cenozoic ironstone deposits of El Gedida, Ghorabi and El Harra (El Akkad and Issawi, 1963; Basta and Amer, 1969; El Sharkawi et al., 1984; El Aref et al., 1999; Dabous, 2002; El Aref et al., 2006a, b; Baioumy et al., 2013; Salama et al., 2014, and references therein) (Fig. 1.3). The ironstones of Bahariya area played a significant role in the geomorphological evolution of the region as they precluded extensive erosion of the outcropping sedimentary formations and resulted in a prominent landscape feature (Afify et al., 2015a, b). Economic iron ores reach up to 270 million metric tons of estimated iron ore resources with an average of 47.6% Fe (Said, 1990). The iron-bearing minerals occur as thin ironstone beds and concretions in Cenomanian siliciclastic rocks (Tanner and Khalifa, 2010; Afify et al., 2015a) and/or capping Cenomanian rocks in the hillocks exposed in the depression. Likewise, ironstone occurs as big ore bodies associated with Eocene carbonate rocks (Baioumy et al., 2013; Afify et al., 2015b, 2016, and references therein) (Fig. 1.3).

Currently, the only iron ore under exploitation in the Bahariya Depression is El Gedida mine, which shows little or no overburden. Nearby areas such as Ghorabi, Nasser, El Heiz, and El Harra are of low-grade ores and of high silica content (El Akkad and Issawi, 1963; Afify et al., 2015b).

When mining started in the El Gedida area in 1972, the minable reserves were estimated accurately by 135 Mt, with an estimated ore production of 3 to 3.5 Mt per year. The mining method is by open pit and the main iron ore processing plant is located at El Gedida. The plant consists simply of crushing equipment (jaw and cone crushers) designed to reduce the run-of-mine ore to the maximum size required by the sinter plant at Helwan, near Cairo, which means waste of energy and high operational costs. The raw ore is transported by train with all its gangue content from the mine to the steel plant for a distance of over 300 km. It could have been more beneficial if the ore is concentrated in the mine

site, i.e., raising the iron content of the ore from 52 % Fe to 65 % Fe, by using modern techniques of flotation, flocculation/flotation, high intensity magnetic separation, and magnetic roasting followed by low intensity magnetic separation (Abouzeid and Khalid, 2011). This will overcome all the above drawbacks of using the mined ore as it is.

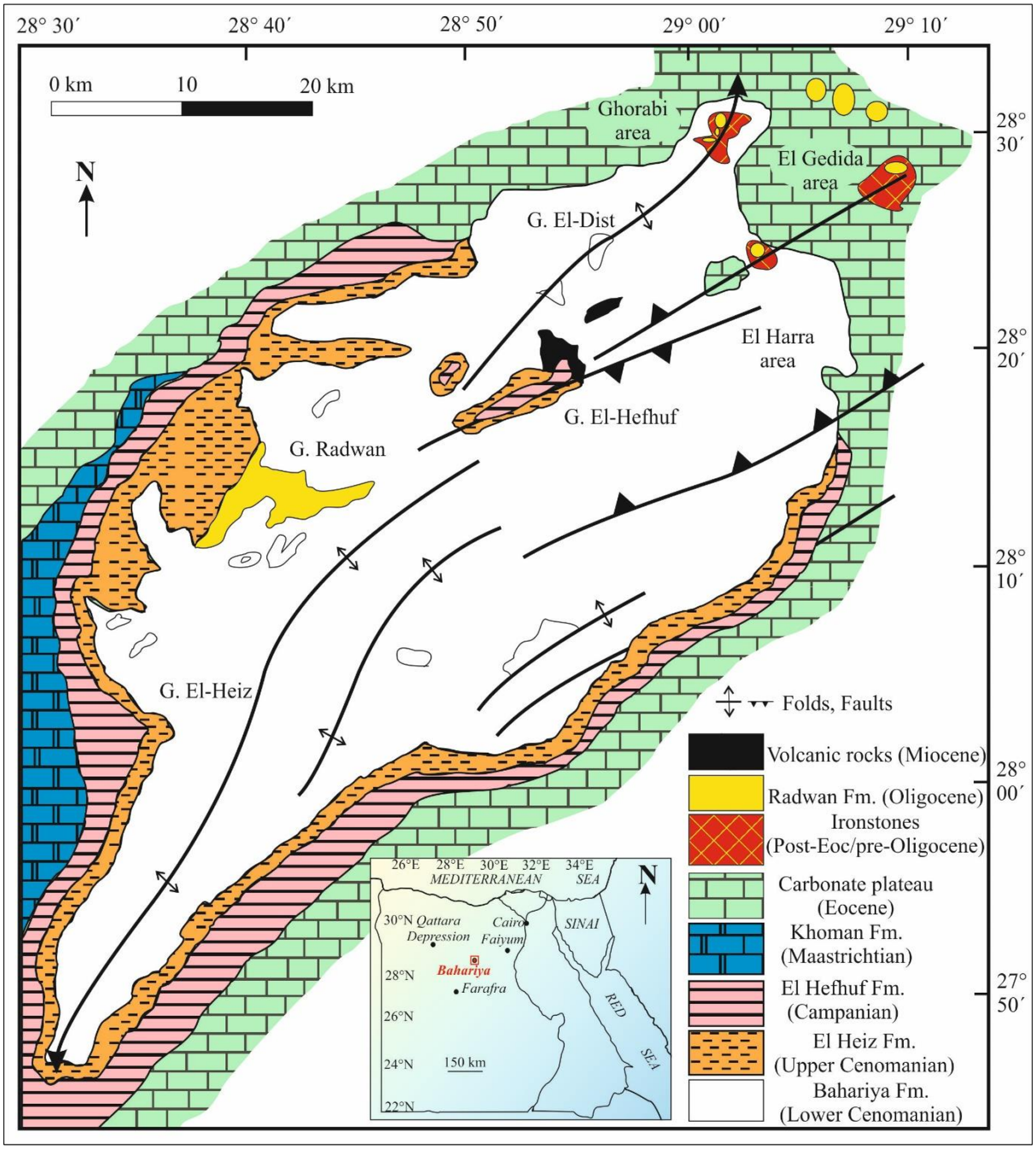

Figure 1.3. Geologic map of the Bahariya Depression showing the main stratigraphic units (modified after Said and Issawi, 1964).

The ironstones of the Bahariya area display a variety of occurrences, e.g., concretionary, massive, stromatolite-like, pisolithic, colloidal, reiniform aggregates, coating boxwork, oncolitic-like, brecciated, leisegang rings and bands, geode and brecciated fabrics (Afify et al., 2015a, b, 2016). The origin, mechanism of formation, timing and sources of these ironstone deposits has been a matter of debate. This can be summarized as follows:

Basta and Amer (1969) suggested that the iron ore of El Gedida mine area was formed by slow but intense metasomatic replacement of the lower Middle Eocene limestone with partial replacement of the uppermost part of the Bahariya Formation and the lower member of the Radwan Formation (Oligocene). The mineralization was structurally controlled and the iron solutions derived from volcanic processes. Basta and Amer (1969) concluded that the ore deposits formed after the Oligocene.

Helba et al. (2001) subdivided the ironstones of El Harra and El Gedida mine areas into four units. From bottom to top, the succession is composed of lower variegated mud- ironstone followed upward by ooidal, oncoidal and nummulitic ironstone, upper variegated mud- ironstone and uppermost nummulitic ironstone.

Dabous (2002) concluded that the economic ironstone deposits of the Bahariya area are not lateritic. Their formation related to mixing of warm ascending groundwater leaching iron from the underlying Nubia aquifers and descending water with iron leached from the overlying Upper Eocene-Lower Oligocene glauconitic clays.

El Aref et al. (2006a, b) subdivided the ironstone at Gebel Ghorabi mine into two ironstone sequences, separated by an intra- Eocene paleokarst unconformity. The lower sequence comprises four ironstone facies (lagoonal- tidal flat, lagoonal fossiliferous, shallow subtidal- intertidal nummulitic ooidal- oncoidal ironstone, and shallow subtidal nummulitic ironstone). The upper sequence is composed of green mudstone facies followed upward by a peritidal ironstone sequence formed of shallow subtidal mudstone and subtidal-intertidal nummulitic bioclastic ironstone cycles. El Aref et al. (2006a, b) considered the ironstone facies as primary deposits.

Tanner and Khalifa (2010) studied the ferruginous facies of the Bahariya Formation and set up that the ferruginous sandstone beds locally weathered to form prominent iron crusts. The ferruginous horizons are composed of either unaltered sandstone with pervasive ferruginous matrix or distinct ironstone beds with massive, nodular, vesicular and pisolitic textures. Tanner and Khalifa (2010) interpreted the ironstone crusts as ferricretes, formed by iron accumulation that resulted from the oxidation and precipitation of soluble iron or colloids transported in the sediment load or by groundwater occurring at or below the water table.

Salama et al. (2012, 2013, 2014) subdivided the ironstone of the Ghorabi deposit into three main facies (manganiferous mud and fossiliferous ironstone, microbially- mediated ironstone which includes stromatolitic and nummulitic- ooidal oncoidal ironstone, and lateritic ironstone as a result of subaerial weathering processes). The authors concluded that the ironstones deposited primarily in a marine setting and their formation was enhanced by microbial activity. They related the formation of the ironstone to global warming during the early Paleogene, closely associated with eustatic sea-level changes.

Baioumy et al. (2013, 2014) supported sources and mechanisms of iron and manganese formations that in our opinion are contradictory. They postulated formation of supergenetic ore deposits (most probably from the Naqb limestone host rock) and hydrogenous iron mixed with iron of hydrothermal origin (seawater precipitation to hydrothermal exhalite).

II

Objectives and methodology

2.1. Objectives
2.2. Materials and methods
2.2.1. Fieldwork and geological mapping
2.2.2. Sampling and sample preparation
2.2.3. Petrography and high resolution textural analyses
2.2.4. Mineralogy
2.2.4.1. Bulk mineralogy
2.2.4.2. Clay mineralogy
2.2.5. Geochemistry
2.2.5.1. Major and trace elements geochemistry
2.2.5.2. Rare earth elements and yttrium geochemistry
2.2.5.3. Carbon and oxygen isotope geochemistry
2.2.5.4. Sulfur and oxygen isotope geochemistry
2.2.5.5. Fluid inclusions microthermometry

2.1. Objectives

The main target of this research is to provide new insight on the geology, mineralogy and genesis of the several types of ironstone deposits that occur in different stratigraphic units cropping out in the northern part of the Bahariya Depression. One type of ironstone occurs in the Cenomanian Bahariya Formation, forming thin beds and concretions. A second type is represented by big ore bodies apparently hosted in Eocene rocks at three mine areas of El Gedida, Ghorabi-Nasser and El Harra (Fig. 1.3). The two

ironstone types will be referred to as the Upper Cretaceous ironstone crusts and concretions in the Cenomanian Bahariya Formation and the Eocene ironstone deposits hosted in the Eocene carbonates, respectively.

The main objectives of this work are to improve understanding on the following aspects:

1- Sedimentology of the host rocks for either the siliciclastic Bahariya Formation or the Eocene carbonates surrounding the ore deposits at the three mine areas. Determination of the depositional environments and diagenetic evolution of the host rocks could help in understanding the mechanisms of ironstone formation in the two ironstone types.
2- Effect of host rock mineral composition and facies on the textures, morphologies and distribution of the ore-bearing minerals.
3- Characterization of the mineralogy and geochemistry of the host rocks and the associated ironstones, including the gangue minerals, to clarify the type of fluids responsible for the formation of the ironstones.
4- Tectonics of the study area and its role on the genesis of the different ironstone types.
5- Age dating of the host rocks, especially those of the Eocene carbonates in order to determine the extent of gaps and unconformities between the Eocene rock units. Age dating of these carbonates could help in timing of the associated ironstones and consequently give light on the mechanisms and ironstone genesis.

The achievement of the aforementioned objectives will result in

a) Comparison between ironstone formation under different geological conditions and/or varied geological settings depending on varied host rocks. The comparison is carried out in terms of mineralogy, petrology and geochemistry of the two ironstone types.
b) Proposal of a genetic model for the different ironstone types present in the northern part of the Bahariya Depression. The model should integrate the source of iron in the different rock units, the effect of tectonics and the lithology and diagenesis of the host rocks.

2.2. Materials and methods

2.2.1. Fieldwork and geological mapping

Fieldwork was focused on detailed description of the stratigraphic succession forming the northern part of the Bahariya Depression (Fig. 1.3). The stratigraphic description was carried out on the Bahariya, Naqb, Qazzun, El Hamra, Radwan formations and the overlying continental carbonates exposed on the plateau surface. Likewise, detailed field and laboratory studies of the associated ironstone deposits were performed. Three sections representing the Bahariya Formation were logged in the Ghorabi, El Harra and Gabal El-Dist areas. Seven sections from the ironstone succession exposed at the Ghorabi-Nasser area and two sections from its surrounding carbonates were studied. Two sections from the carbonate plateau and the adjacent ironstone deposits at the El Harra area were analyzed. Three sections from the ironstone succession at the El Gedida area and three sections from the surrounding carbonates to the east and north of the study area were studied. Location and distribution of the studied sections are shown in chapters 3, 4 and 5. Fieldwork and geological mapping were supported by analysis of satellite imagery, digital topographic models and maps, and remote sensing data using ASTER images.

2.2.2. Sampling and sample preparation

About 220 samples of carbonate rocks, ironstones, sandstones, siltstones and claystones and other rock materials were collected through three fieldtrips during seasons 2012-2014. Field observations and lithostratigraphic logging and sampling were complemented by collecting samples of fossil specimens, especially larger benthic foraminifers (*Nummulites*) from the Eocene stratigraphic succession. All the rock samples were housed at the Petrology and Geochemistry Department, Faculty of Geological Sciences, Complutense University of Madrid (UCM) for petrological, mineralogical and geochemical investigations.

The soft Eocene samples with isolated *Nummulites* were disaggregated in a solution of Na_2CO_3, H_2O_2 and water and later sieved through apertures of 1.0, 0.5 and 0.25 mm and prepared for biostratigraphic analysis. The

Nummulites samples were housed at the Stratigraphy, Paleontology and Marine Geosciences Department, University of Barcelona.

2.2.3. Petrography and high resolution textural analyses

Detailed petrographic, mineralogical and geochemical characterization of the different rock types was achieved in the present study. All the lithified samples were prepared as polished thin sections and polished slabs. Petrographic characteristics were determined using an Olympus BX51 optical microscope with white light and ultraviolet fluorescent light sources as well as a Nikon reflected light microscope. Fluorescent ultraviolet light was used to identify the presence of organic matter. Distinction of carbonate minerals was facilitated by staining of the samples with alizarin red-potassium ferricyanide (Lindholm and Finkelman, 1972). For high-resolution textural and morphometric analyses, fresh broken pieces were studied using scanning electron microscopy (SEM). SEM study was carried out using a JEOL JSM-820 and JEOL JSM-6400 operating at 20 kV and equipped with an energy dispersive X-ray microanalyzer (SEM-EDAX). Likewise, carbon-coated thin sections were prepared for backscattered images (BSE) and secondary images (SE) on a JEOL Superprobe JXA 8900-M wavelength dispersive electron microprobe analyzer (WDS-EMPA). The petrography on thin sections and polished slabs was carried out at the Petrology and Geochemistry, Stratigraphy, and Crystallography and Mineralogy departments of the Faculty of Geological Sciences, Complutense University of Madrid. SEM and EMPA analyses were carried out in the CAI Técnicas Geológicas of the Faculty of Geological Sciences, and the Centro Nacional de Microscopía Electrónica (CNME), UCM.

2.2.4. Mineralogy

2.2.4.1. Bulk mineralogy

Mineral compositions of all of the collected samples were determined by XRD analyses. Small parts of the samples were crushed mechanically to less than 100 μm and prepared for X-ray diffraction to determine the bulk mineralogy. This was achieved using a Philips PW-1710 diffractometer and a Bruker D8 Advance diffractometer operating under monochromatic Cu Kα

radiation (λ= 1.54060 Å) at 40kv and 30 mA. XRD analysis was performed following the method of Chung (1974) using EVA Bruker software. XRD was achieved at the Petrology and Geochemistry Department and the CAI of Técnicas Geológicas, Faculty of Geological Sciences, UCM.

2.2.4.2. Clay mineralogy

The quantitative mineralogical composition of all of the samples was determined in two steps, the first being the identification and estimation of the percentages of all minerals including percentage of phyllosilicates (bulk mineralogy, described above); the second step dealt with identification and estimate of the relative proportions of each phyllosilicate species (for fractions less than 2 μm). Thirty grams of the samples rich in clays (20-30%) were crushed, mixed with distilled water and disaggregated using an ultrasonic bath to completely disperse the clays. Washing of the samples by distilled water and a high-speed super centrifuge was made to remove the evaporite minerals by dialysis. The carbonate-rich samples were reacted by HCl (10%) to remove carbonate minerals. The < 2 μm size fraction was extracted manually, following the Stokes' law.

Three oriented thin films: air-dried (AD), ethylene glycolated (EG) and thermal treated (TT) oriented mounts were then prepared for every sample by repeated pipetting of the clay suspension onto glass slides. The ethylene glycolated oriented mounts were kept in ethylene vapor heated at 60 ºC for twenty-four hours whereas the thermal treated mounts where heated for 550 ºC for three hours. X-ray diffraction (XRD) patterns were obtained using a Bruker D8 Advance diffractometer and Cu Kα radiation. This analysis was carried out at the CAI of Técnicas Geológicas, Faculty of Geological Sciences, UCM.

2.2.5. Geochemistry

2.2.5.1. Major and trace elements geochemistry

Major oxides (in wt.%) and trace elements (in ppm) geochemical analyses of bulk samples were carried out where variable samples of ironstones, carbonates and other materials were mechanically crushed in an agate mortar and pestle to powder. Fused discs were prepared for energy dispersive X-ray fluorescence (ED-XRF) using a Bruker

S2 RANGER X-ray fluorescence spectrometer with X-Flash Silicon Drift Detector to study major and trace elements geochemistry. Loss on ignition (L.O.I.) was obtained by heating 1g of powdered sample at 1000 °C for 1 h. These analyses were done at the CAI Técnicas Geológicas of the Faculty of Geological Sciences, UCM.

Elemental analyses (in wt.%) and chemical composition determination of minerals either in the ironstones or their host rocks were carried out on carbon-coated polished thin sections using a JEOL Superprobe JXA 8900-M wavelength dispersive electron microprobe analyzer (WDS-EMPA) equipped with four crystal spectrometers and beam diameter between 2 to 5 µm to minimize damage from the electron beam. EMPA was performed at the CNME, UCM.

2.2.5.2. Rare earth elements and yttrium geochemistry

The behavior of the rare earth elements and yttrium (REY), as a part from the trace elements geochemistry, during scavenging by Fe and Mn oxyhydroxides is sufficiently well understood from many studies of natural and experimental systems to design discrimination diagrams not only based on statistics but on a combination of process understanding and knowledge about element sources (Bau et al., 2014). REY have been used as geochemical probes because of their coherent behavior during geochemical processes and because of their predictable fractionation. Accordingly, rare earth elements and yttrium (REY) geochemical analyses were carried out on different ironstone samples using inductively coupled plasma/mass spectrometry (ICP/MS) following an established analytical protocol and using international certified reference material for quality control. The analysis was achieved after digestion of 0.25 g of selected sample powder with HNO_3, HF and $HClO_4$ in a capped Teflon-lined vessel, evaporation to dryness and subsequent dissolution in 25 ml of 4% vol of HCl.

The smoothness of a shale normalized REY pattern is a simple but reliable criterion to test the quality of a chemical analysis and to eliminate questionable data sets (Bau et al., 2014; Hein et al., 2016). Thus, REY patterns (yttrium was inserted between Dy and Ho according to its ionic radius) are

normalized to post-Archean Australian Shale (PAAS: Mcleannan, 1989) to detect resemblance in the different types of the studied ironstones. Rare earth elements are mainly in trivalent state except two elements; i.e. europium and cerium, which mostly exist as Eu^{+2} and Ce^{+4}, respectively. Discrimination between light-REE (LREE; La, Ce, Pr, and Nd), middle- REE (MREE; Eu, Gd, Tb, and Dy), and heavy-REE (HREE; Er, Tm, Yb, and Lu) is achieved when plotted together with Sm, Ho, and Y in spidergrams. Different discrimination diagrams are also plotted, e.g., Ce/Ce* anomaly against Nd concentration and Y_{SN}/Ho_{SN} values. Anomalies of Ce, Eu, La, Gd and Y were also calculated. The Eu, Ce, Pr, Gd and La anomalies, where shale normalized (SN), are calculated as:

$Eu/Eu^* = 2Eu_{SN}/(Sm_{SN}+Gd_{SN})$, $Ce/Ce^* = 2Ce_{SN}/(La_N+Pr_{SN})$, $Pr/Pr^* = 2Pr_{SN}/(Ce_{SN}+Nd_{SN})$, $La/La^* = La_{SN}/(3Pr_{SN}-2Nd_{SN})$, $Gd/Gd^* = Gd_{SN}/(0.33Sm_{SN}+0.67Tb_{SN})$.

2.2.5.3. Carbon and oxygen isotope geochemistry

Carbon and oxygen isotopic compositions for carbonates, especially dolomite and ankerite minerals, were reported using standard δ notation in units of ‰ relative to V-PDB standard (the Vienna Pee Dee Belemnite standard). Carbon and oxygen stable isotope analyses were performed on carbonate-rich ironstone samples from the lower and upper members of the Cenomanian Bahariya Formation as well as from the dolomites of the Lower Eocene Naqb Formation. Sampling using micro-drilling techniques was attempted to obtain the exact carbonate minerals (dolomite and ankerite) required for the analyses after detailed petrographic and mineralogical investigations. Separation of dolomite and ankerite from samples collected in the Bahariya Formation was often difficult, thus the term dolomite/ankerite is used for these mineral phases. The $\delta^{13}C$ and $\delta^{18}O$ values were measured on CO_2 released from differential dissolution of 10–20 mg of washed sample in 100% H_3PO_4. Some contamination between calcite and dolomite/ankerite carbonates could occur during drilling and extraction processes. Accordingly, the samples were subjected to the sequential separation between the dolomite/ ankerite and calcite. Calcite was removed as CO_2 after 4 hours of

reaction at 25 °C. For dolomite, CO_2 was extracted after an additional 24 hours step at 70 °C. This analysis was carried out at the Laboratory of Stable Isotopes (SIDI), Faculty of Sciences, Autónoma University of Madrid.

2.2.5.4. Sulfur and oxygen isotope geochemistry

Sulfur and oxygen isotope analyses were achieved on the sulfate minerals associated with the Eocene ironstones, e.g., barite, jarosite and alunite. Eleven purified barite samples as well as two jarosite samples and one alunite sample were selected for S, O isotopes (δ^{34}S-CDT and δ^{18}O-SMOW (SO_4)) to elucidate the origin of the mineralizing fluids. Isotope ratios were determined using Elemental Analyzer-Isotope Ratio Mass Spectrometer (EA-IRMS) (Delta+XL) and Temperature Conversion-Elemental Analyzer (TC/EA) (Delta+XL). All results reported in the usual permit notation relative to IAEA standards. The analysis was achieved at the Isotope Science Laboratory, Department of Geosciences, University of Calgary, Canada.

2.2.5.5. Fluid inclusions micro-thermometry

Fluid inclusions studies were achieved on the barite and some quartz crystals associated with the Eocene ironstones at the Ghorabi, El Harra and El Gedida areas. 80–120-µm-thick, doubly polished thin sections were prepared. In order to minimize sample heating and fluid inclusion stretching during sample preparation, a low-speed saw was used for cutting rock samples. Conventional fluid inclusions petrography and microthermometry were performed on a Linkam FTIR 600 heating–cooling stage mounted on a polarization microscope with a video camera attached to a screen. Standardization was carried out at temperatures of −56.6, 0 and 385 °C using quartz wafers containing synthetic H_2O and H_2O–CO_2 fluid inclusions. The analyses using this technique were performed at the Stratigraphy Department of the Faculty of Geological Sciences, UCM.

III

Geologic setting of the Bahariya Depression

3.1. Stratigraphy
3.1.1. Paleozoic
3.1.2. Mesozoic
3.1.2.1. Jurassic and Lower Cretaceous
3.1.2.2. Upper Cretaceous outcropping succession
3.1.2.2.1. The Bahariya Formation
3.1.2.2.2. The El Heiz Formation
3.1.2.2.3. The El Hefhuf Formation
3.1.2.2.4. The Khoman Formation
3.1.3. Cenozoic outcropping succession
3.1.3.1. The Naqb Formation
3.1.3.2. The Qazzun Formation
3.1.3.3. The El Hamra Formation
3.1.3.4. The Radwan Formation
3.1.3.5. The continental carbonate unit
3.1.4. Volcanic-subvolcanic rocks
3.2. Tectonic setting

3.1. Stratigraphy

The Bahariya Depression is located nearby the central part of the Western Desert of Egypt, about 370 km southwest of Cairo (Fig. 1.2) covering an area of about 1800 km^2 with greatest length 94 km and greatest width 42 km (Fig. 1.3). The depression is located between latitudes 27º 48′ and 28º 31′ N and longitudes 28º 30′ and 29º 15′ E. It is characterized by large oval or elliptical shape oriented towards the northeast (Fig. 1.3). The northern part of the depression is represented topographically by a limestone plateau

surrounding the depression which is dissected by valleys and covered by isolated conical hills (Fig. 3.1). The Bahariya Depression is formed by a thick outcrop succession of Upper Cretaceous – Lower Cenozoic sedimentary deposits, locally capped by Miocene volcanic rocks (Fig. 3.1). The outcrop succession of the area comprises, from bottom to top, the Lower Cenomanian Bahariya Formation, the Upper Cenomanian El Heiz Formation, the Campanian El Hefhuf Formation, and Maastrichtian Khoman Chalk Formation. These are unconformably overlain by the Eocene Naqb, Qazzun and El Hamra formations. The Cretaceous – Eocene succession is unconformably overlain by the Oligocene Radwan Formation. Continental carbonate deposits of yet not clearly defined age are capping the Eocene carbonates in the northern part of the depression (Fig. 3.1); this stratigraphic unit is provisionally referred to as ´´post-Eocene continental carbonate unit´´. The succession cropping out in the Bahariya Depression overlies a thick subsurface succession mostly formed of Lower Cretaceous, Jurassic and Paleozoic sedimentary rocks that unconformably overlie the Precambrian basement. A simplified section showing the subsurface stratigraphic succession of the Bahariya-1 well drilled by the Devon Energy Egypt Companies (see Fig. 3.1 for location) is given in Figure 3.2 whereas the outcrop stratigraphic succession is shown in Figure 3.3. A brief description of the subsurface and outcrop successions of the Bahariya area is shown in the following subchapters.

3.1.1. Paleozoic

The exploratory well (Bahariya-1 well; Fig. 3.1) drilled by Devon Energy Egypt Companies intersected a thick succession of Lower Cretaceous, Jurassic and Paleozoic sedimentary rocks. The Paleozoic section measures 1024 m and comprises two units: lower unit (Shifah Formation) and upper unit (Safi Formation) (Fig. 3.2). The 436 m thick lower unit is Middle Cambrian in age and consists of clastic rocks with abundant shale beds overlying the basement rocks. The upper unit is of Permo-Carboniferous age and consists of sandstone with some shale beds at the top; thickness of the unit reaches up to 588 m (Fig. 3.2).

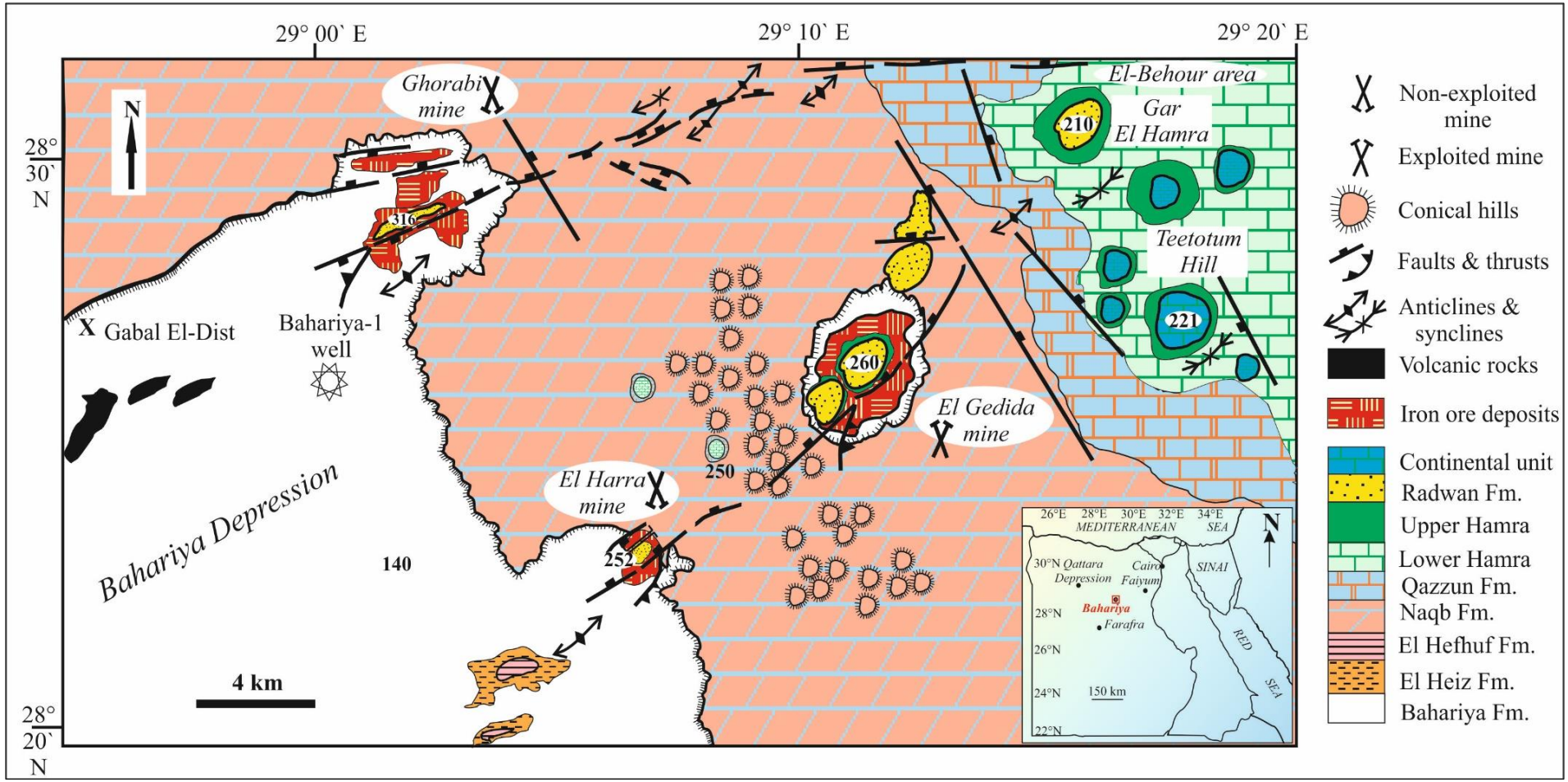

Figure 3.1. Geologic map showing the outcrop succession of the northern part of the Bahariya Depression (modified after Said and Issawi, 1964). Mapping was performed by using satellite images and detailed fieldwork.

3.1.2. Mesozoic

3.1.2.1. Jurassic and Lower Cretaceous

The Mesozoic succession in the subsurface section consists of Jurassic and Lower Cretaceous sedimentary rocks (Fig. 3.2). The Jurassic succession starts with the Lower Jurassic Ras Qattara Formation (137 m) that unconformably overlies the Safi Formation. The Ras Qattara Formation consists of non-marine clastic rocks and followed upwards by the clastic rocks of the Middle Jurassic Khatatba Formation (228.5 m). The marine transgression that terminated the Jurassic cycle in the north Western Desert is represented by a carbonate rock unit, the Masajid Formation (Sultan and Halim, 1988). The Masajid Formation was either not deposited or eroded in the Bahariya area where the Khatatba Formation is overlain unconformably by the Early Cretaceous Alam El Bueib Member of the Burg El Arab Formation (91.5 m). The latter consists of shallow marine deposits and massive fluvial sandstone bodies and is overlain unconformably by the continental to shoreline clastic deposits of the Kharita Member of the Burg El Arab Formation (286.5 m) (Fig. 3.2). This stratigraphic unit is overlain by the fluviomarine deposits of the Bahariya Formation.

The Jurassic Khatatba Formation is considered to be the source rock for most of the hydrocarbon field in the north Western Desert where it is characterized by organic-rich sedimentary rocks (Moretti et al., 2010), whereas the Cretaceous sandstone deposits, especially those of the Cenomanian Bahariya Formation and the Turonian Abu Roash Formation, represent the main reservoir for many oil fields in the north Western Desert (Bagge and Keeley, 1994; Rossi et al., 2002; Moretti et al., 2010). Ferroan dolomite, siderite and pyrite are present in the clastic rocks of the Khatatba Formation and other subsurface rock units as observed in oil wells in the north Western Desert (Rossi et al., 2001, 2002). The siderite crystals show several growth stages and the Fe-dolomite was pervasive in the upper part of the Khatatba Formation. These carbonate minerals were affected by dissolution, probably during the Late Cretaceous (Rossi et al., 2001).

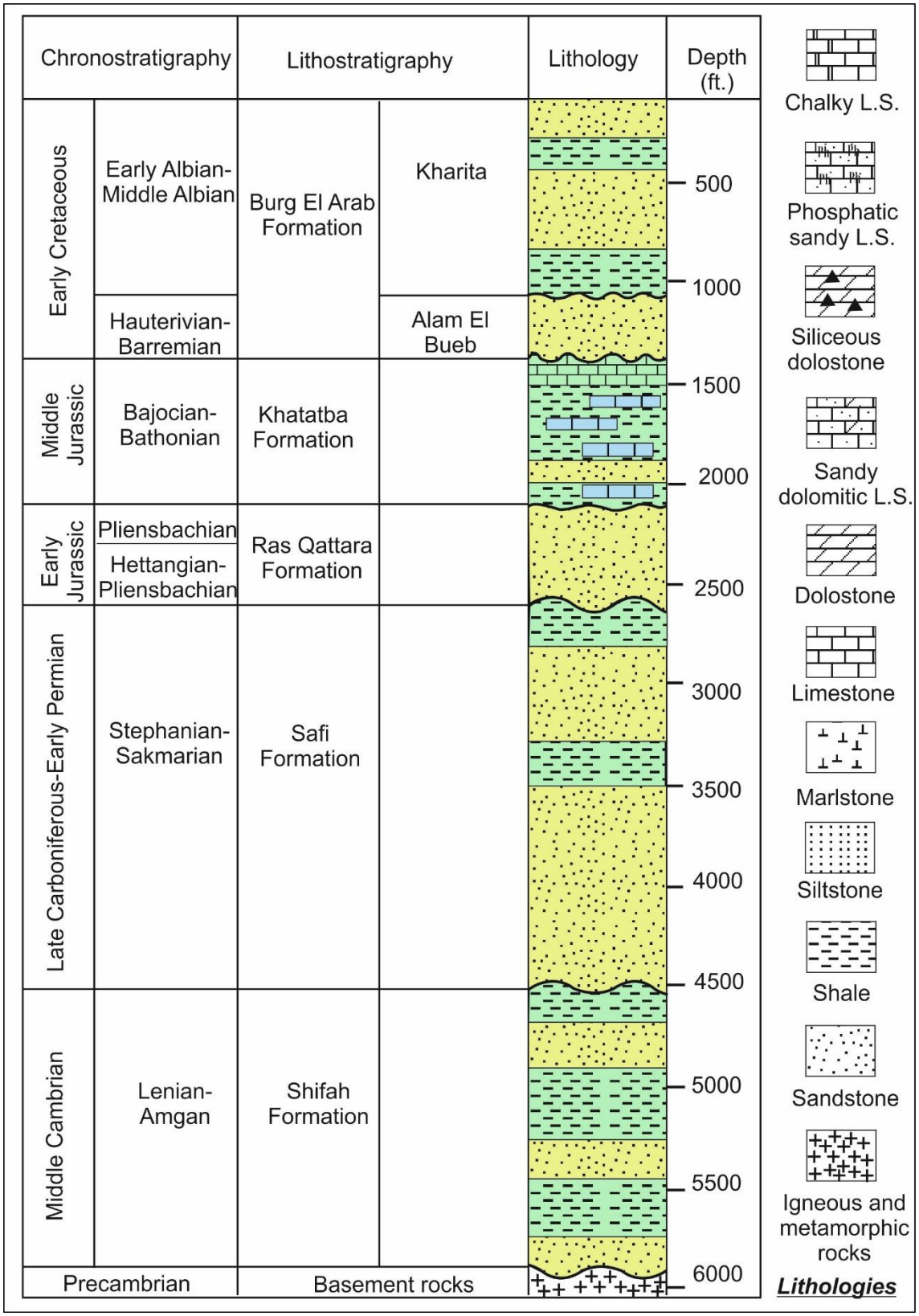

Figure 3.2. Simplified section of the subsurface rock units recorded in the Bahariya-1 exploratory well drilled in the northern part of the Bahariya Depression by Devon Energy Egypt Companies.

3.1.2.2. Upper Cretaceous outcropping succession

The exposed rocks of the Bahariya Depression and its surrounding plateau range in age from Cenomanian to Middle Miocene. They are of sedimentary origin except for basalt flows, dolerite sills and dykes. From bottom to top, the Mesozoic stratigraphic succession exposed in the Bahariya area consists of the Bahariya, El Heiz, El Hefhuf, and Khoman Chalk formations (Fig. 3.3).

3.1.2.2.1. The Bahariya Formation

The outcrop succession of the Bahariya area starts with the Lower Cenomanian Bahariya Formation (Said, 1962) although its lower boundary is not exposed. The maximum measured thickness of the formation reaches up to 170 m at Gabal El-Dist (Fig. 3.4A). The rock unit is composed of clastic sedimentary deposits (sandstones, siltstones, claystones and shales) with subordinate carbonates, mainly representative of fluviomarine facies (Fig. 3.3) (Afify et al., 2015a). It is subdivided into three units, lower, middle and upper units (Soliman and Khalifa, 1993): ironstone crusts and concretions are abundant in its lower and upper units (Afify et al., 2015a). To the north of the depression, the Bahariya Formation is unconformably overlain by the Lower Eocene Naqb Formation whereas it is overlain conformably by the El Heiz Formation to the south (Fig. 1.3).

The shallow marine and transitional facies of the Bahariya Formation represent a gradual transgression following the initial regressive period of sedimentation of the Kharita Formation during the Cretaceous. The Bahariya Formation is considered to be a potential source rock for hydrocarbons in north Western Desert where organic-rich clastic horizons are dominant (Moretti et al., 2010). These organic-rich beds are clearly observed in the studied outcrops of the northern Bahariya Depression (Afify et al., 2015a). Additional description of the fluviomarine Bahariya Formation is presented in chapter 4.

3.1.2.2.2. The El Heiz Formation

The Upper Cenomanian, El Heiz Formation (El Akkad and Issawi, 1963), consists of clastic rocks with occasional

carbonate interbeds. These deposits are mainly formed of marly shale, sandy clays, calcareous sandstone, brownish limestone and sandy dolomitic limestone that were deposited in fluviomarine environments. The thickness of the El Heiz Formation reaches up to 40 m to the south of the depression and decreases up to 12 m to the north, where it is overlain unconformably by the Naqb Formation (El Akkad and Issawi, 1963). The sedimentary deposits of the El Heiz Formation were accumulated at higher water depth than those of the Bahariya Formation (El Akkad and Issawi, 1963; Moustafa et al., 2003).

3.1.2.2.3. The El Hefhuf Formation

The El Heiz Formation is followed upwardly by the Campanian El Hefhuf Formation (El Akkad and Issawi, 1963). It consists of cherty cavernous dolostone with chert nodules at the base, which passes upward into brown limestone, marl, shale, cross-bedded sandstone, and phosphatic and dolomitic sandy limestone. It measures up to 170 m thick to the south of the Bahariya Depression (Fig. 3.3).

3.1.2.2.4. The Khoman Chalk Formation

The succeeding Maastrichtian Khoman Chalk Formation (El Akkad and Issawi, 1963) is mainly represented by massive white chalk and chalky limestone (Fig. 3.4B) measuring up to 45 m. It overlies conformably the El Hefhuf Formation on both sides of the depression and extends southward with increasing thickness.

3.1.3. Cenozoic outcropping succession

The Cenozoic outcrop succession of the Bahariya area is well exposed to the northern part of the depression forming a plateau of carbonate Eocene rocks surrounding the depression (Fig. 3.1). The Eocene stratigraphy of the northern Bahariya area was subdivided by Said and Issawi (1964) into three rock units: the Naqb, Qazzun and El Hamra formations (from bottom to top). The Eocene carbonates are overlain unconformably by the sandstones of the Oligocene Radwan Formation. In low-lying areas of the plateau, the Eocene formations are unconformably overlain by continental carbonates that accordingly are considered post-Eocene, tentatively

dated as Oligocene-Miocene (Afify et al., 2016). Miocene basaltic and doleritic extrusions are recorded in the northern part of the Bahariya area.

Big ore bodies of economic ironstones are encountered in the Eocene succession at three areas in the northern part of the region (Fig. 3.1). These ore deposits occur mainly along two major fault systems in three mines: Ghorabi, El Harra and El Gedida areas (Afify et al., 2015b, 2016, and references therein). More details about the sedimentology, mineralogy and geochemistry of the Eocene rock units as well as their hosted ironstones are described in detail in chapter 5. A brief description of the Cenozoic outcropping succession in the Bahariya area is as follows.

3.1.3.1. The Naqb Formation

The Naqb Formation is well exposed as a scarp face above the slope-forming Bahariya Formation and form the base of the plateau surface (Fig. 3.1). The maximum thickness of this rock unit studied by Said and Issawi (1964) reaches up to 68 m thick. Lithologically, the Naqb Formation is mainly dolomitized, rugged, irregularly bedded and partly siliceous. It was subdivided by Afify et al. (2015b, 2016) into two carbonate sequences; lower sequence and upper sequence separated by a paleokarst.

3.1.3.2. The Qazzun Formation

The Qazzun Formation is well exposed to the north and east of the study area (Fig. 3.1) and consists mainly of bright, white chalky nummulitic limestone (Fig. 3.4C) reaching up to 32.5 m-thick at Gar El Hamra section (type section). In outcrop, the Qazzun Formation., is easily recognizable from its underlying and overlying Eocene rock units (Naqb and El Hamra formations, respectively) due to its distinct chalky lithology and clean white color. The boundary between the Qazzun and the Naqb Formation is characterized by presence of highly silicified nodular limestone forming concretions (Fig. 3.4D and E). These geomorphologic fabrics are well-preserved on the plateau surface that was resistant to abrasion because of strong silicification.

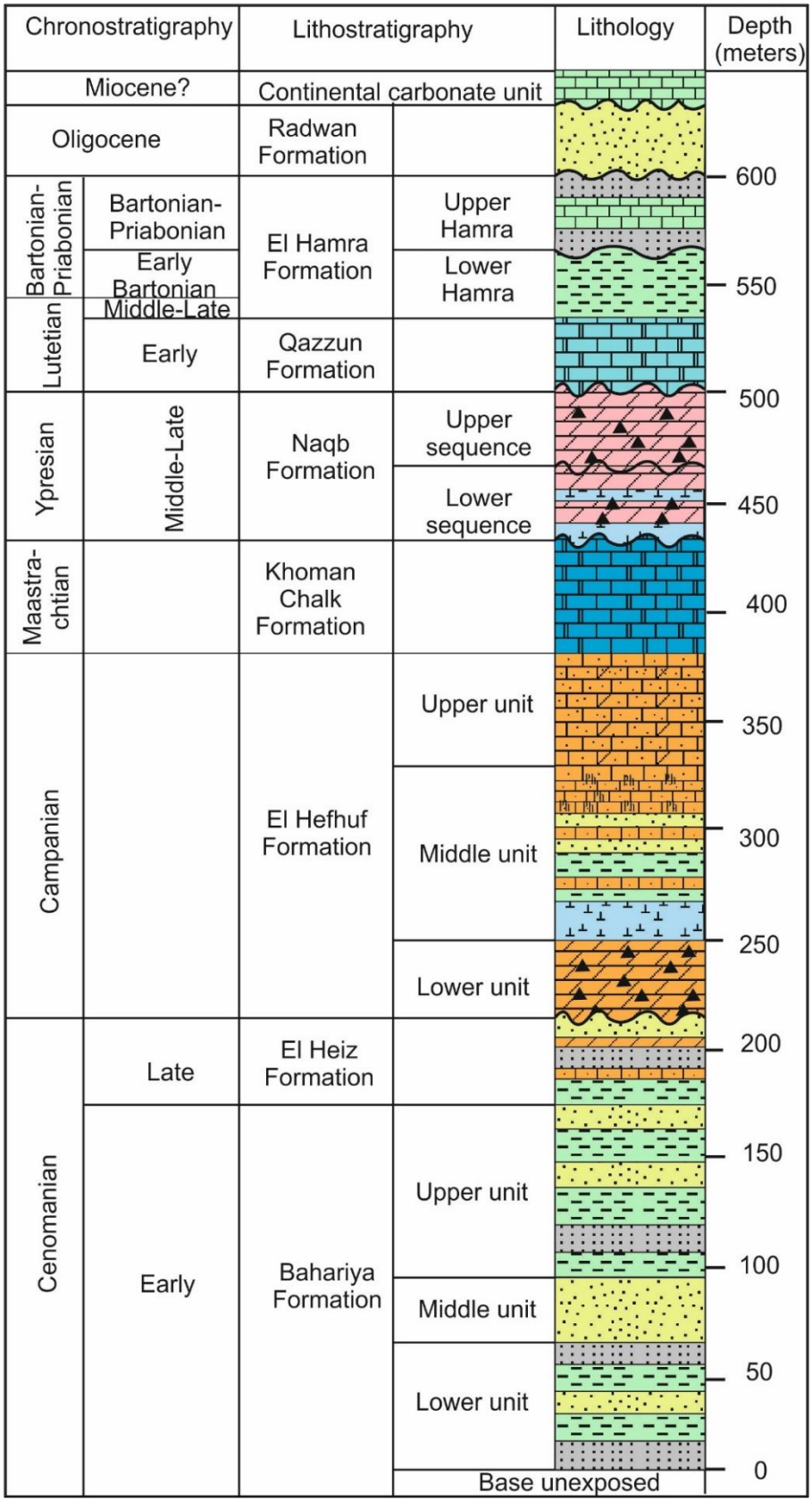

Figure 3.3. Simplified composite section showing the stratigraphic succession cropping out in the Bahariya area (data after Soliman and Khalifa, 1993; Issawi et al., 2009; Afify et al., 2015a, b, 2016).

3.1.3.3. The El Hamra Formation

The Qazzun Formation is followed upwardly by El Hamra Formation that was lithologically subdivided by Issawi et al. (2009) and Afify et al. (2016) into Lower and Upper Hamra. The El Hamra Formation is composed of soft to slightly indurated, fossil-rich limestone with few marlstone intercalations (Fig. 3.4F). Toward the north of the Bahariya Depression, thickness of El Hamra Formation increases concomitantly reaching up to 65 m-thick, with dominance of fossiliferous-rich clays/sandy clays.

3.1.3.4. The Radwan Formation

The horizontally bedded Radwan Formation (El Akkad and Issawi, 1963) consists of sandstone (mainly quartzarenite) and subordinate siltstone. It forms caps ranging from 1 m to 40 m in thickness as seen in its type locality at Gabal Radwan (see Fig. 1.3 for location). It measures up to 25 m of upwardly coarse-grained slightly cross-bedded to graded-bedded sandstone in the northern part of the Bahariya Depression (Fig. 3.4G). Few detrital barite crystals are observed in the lower part of the Radwan Formation around the mine areas. The Radwan Formation was deposited in the Bahariya area along the main faults affecting the depression and the plateau surface where it was clearly observed in low-lying structurally-controlled areas (Figs. 1.3 and 3.1). The sandstones were affected by staining and red pigmentation by iron from washing of the underlying units by the fluvial system.

3.1.3.5. The continental carbonate unit

This horizontally-bedded unit is reported for the first time in the northern part of the Bahariya area (Fig. 3.1). It occurs as isolated hills, preferentially preserved in the Eocene synclines to the eastern and northeastern part of the study area (Afify et al., 2016). It is well exposed at the Teetotum hill to the east of El Gedida mine (Fig. 3.1). It measures up to 20 m-thick and consists of massive, irregularly bedded limestone (Fig. 3.4H). It is characterized by occurrence of massive pisolithic and micritic limestones with scarce small gastropods and rhizoliths representative of lacustrine-palustrine environments. This

carbonate succession may be equivalent to the clastic-carbonate unit present in the adjacent Farafra Depression (Sanz-Montero et al., 2013). A detailed study of these continental deposits will be undertaken as a future research work in the Bahariya region.

3.1.4. Volcanic and subvolcanic rocks

In the northern part of the Bahariya Depression (e.g., Gebel El Hefhuf), Miocene basaltic and doleritic extrusions are recognized. The types of volcanic rocks in this region can be divided into three main varieties, mainly amygdaloidal basalt which is the oldest extruded lava followed by intruded dolerite (Meneisy and El Kalioubi, 1975). Later on, another period of vulcanicity took place and porphyritic olivine basalt was extruded covering the amygdaloidal basalt in Gebel El Hefhuf and the small basalt hill nearby. As a result, the porphyritic olivine basalt prevented the layer of amygdaloidal basalt from erosion while absence of porphyritic basalt in Gebel Mayesra and Mandisha (Fig. 3.4I) caused the lower layer of amygdaloidal basaltic rocks to be deeply weathered. Columnar flood basalt sheets cover the Cenomanian Bahariya Formation at Gebel Mandisha area. The Mandisha basalts (Fig. 3.4I) occurred nearby the iron ore mines (28° 54' 02" E and 28° 22' 06" N). The volcanic-subvolcanic activity took place during the Oligocene – Miocene, when the Gulf of Suez and Red Sea rift began to open (Meneisy, 1990; Afify et al., 2015b, 2016). The variation in types of rock and alteration indicate that the formation of the volcanic rocks in this area took place at several times and long periods of vulcanicity, mostly throughout the Oligocene and Miocene.

Significant hot springs arise in the northern part of the Bahariya Depression, with temperatures ranging from 30 to 55 °C (El Shazly et al., 1991). These hot springs are rich in iron and sulfur. The deep aquifers in the area studied show high Fe^{2+} and H_2S as well (Korany, 1995). Some iron-rich geyser deposits (Fig. 3.4J) were found in the northern part of the depression; they are mainly represented by goethitic and limonitic iron deposits and are in the vicinity of the magmatic intrusions. These hot springs and geyser deposits as well as the high heat fluxes are mostly related to the magmatic and volcanic activity that affected the area.

Figure 3.4. A) Type section of the Bahariya Fm. (Gabal El-Dist). B) Massive chalk and chalky limestones in mushroom structures (Khoman Chalk Fm., White Desert between the Bahariya and Farafra areas). C) Residual hills of chalky limestone (Qazzun Fm., northern Bahariya plateau). D) and E) Melon-like silicified limestone on the plateau surface to the north of Bahariya. F) Outcrop view of bedded limestone with claystone intercalations forming the El Hamra Fm. G) Hill of sandstone forming the Radwan Fm. at the northern part of the Bahariya area. H) Outcrop view of the continental carbonate unit overlying the El Hamra Fm. I) Outcrop view of the columnar basalts of Mandisha at the northern Bahariya Depression. J) Geyser deposit of reddish limonitic ironstone (measuring 2 m-thick) in the vicinity of the volcanic rocks.

3.2. Tectonic setting

The Bahariya area is a large oval NE-oriented depression in the north central part of Egypt which represents a part of the Syrian Arc system. It lies on the same line with Abu Roach and Farafra areas all as a part of the major structural Laramide highs and also with the same direction of north Sinai fold belts (Moustafa et al., 2003). The Bahariya basin was deformed by four tectonic phases during the early Mesozoic, Late Cretaceous, post-Middle Eocene and Middle Miocene respectively (Moustafa et al., 2003). Three of these structural phases affected the exposed rock units of the Bahariya area where the deep seated normal faults of the early Mesozoic deformation were reactivated in the Late Cretaceous and post Eocene by oblique slip faults and en-echelon folds (Moustafa et al., 2003; Afify et al., 2015b; 2016). The Late Cretaceous and post Eocene deformation phases resulted in the formation of the Bahariya swell where its crest was eroded continuously forming the depression (Figs. 1.3 and 3.1). The different structure features reported in the northern part of the Bahariya area was supported by satellite imagery and detailed fieldwork.

The Late Cretaceous deformation was dated as post-Campanian and pre-Maastachtian as the El Hefhuf Formation was tilted and its topmost part was eroded in the southern part of the Bahariya Depression (Moustafa et al., 2003). As well it is unconformably overlain by the horizontally-bedded Khoman Chalk Formation. This deformation phase is generally considered to be pre-Eocene where the Upper Cretaceous sediments are overlain by the Eocene sediments with angular unconformity to the north of the depression. This structural deformation is characterized by NE-oriented folds, ENE right-lateral strike-slip faults, NE reverse faults, WNW right-lateral strike-slip faults and NW normal faults and thrusts affecting the Upper sediments but not the overlying Eocene sediments (Moustafa et al., 2003). During the Late Cretaceous-Middle Eocene, the Alpine tectonic movement occurred and most of the Western Desert hydrocarbon traps were formed (Rossi et al., 2002).

The post-Middle Eocene deformation phase is represented by oblique slip movement with right-lateral wrenching. It is represented by several folds and monoclines that have right-stepped, en-echelon configuration (Moustafa et al., 2003). This phase of deformation occurred during the Late Eocene-Pre-Oligocene and mostly in the Priabonian (Afify et al., 2016). This deformation phase affected the Eocene succession, where the ironstones replaced these Eocene units at three main areas along two major fault systems (Afify et al., 2015b, 2016). As well, the Eocene succession was deformed by E-W, ENE, NW-SE normal and strike-slip faults (Fig. 3.1) (Afify et al., 2016). Some of these faults affected the Oligocene Radwan Formation in the northern part of the depression and considered to be of Miocene time.

The last phase of deformation affected the Bahariya area was extensional and occurred during the Middle Miocene that was accompanied by igneous activity. This tectonic movement resulted in the formation of several doloretic intrusions and basaltic extrusions in the form of sills, dykes, laccolith and lava flows. The direction of the extension was NNE-SSW with the intrusion of WNW feeder dykes, sills and laccolith within the Cretaceous units. This phase of deformation is contemporaneous with that in other parts of Egypt and most probably related to the Gulf of Suez-Red Sea rifting (Meneisy, 1990; Abd El-Aziz et al., 1998; Afify et al., 2015b, 2016).

The tectonic phases recorded in the Bahariya region can be correlated with the regional Mesozoic and Cenozoic tectonic and magmatic events reported by Guiraud et al. (1992) and Guiraud (1998) in west and central Africa as well as in north African Tethyan margin due to the break-up of Gondwana and the opening of the Atlantic Ocean. The similar events are those of the Late Cretaceous compressive event, intra-Eocene compressive event, Late Eocene compressive event, Neogene igneous activity; Moustafa et al., 2003; Afify et al., 2015b, 2016).

IV

Ironstone crusts hosted in Cenomanian clastic rocks

4.1. Diagenetic origin of ironstone crusts in the Lower Cenomanian Bahariya Formation, Bahariya Depression, Western Desert, Egypt
4.1.1. The article
4.1.2. Conclusions from the article
4.2. Additional data
4.2.1. Clay mineralogy
4.2.2. Carbon and oxygen isotope analyses of host carbonate rocks
4.2.3. Major and trace elements geochemistry
4.2.4. Rare earth elements and yttrium (REY) geochemistry
4.3. Discussion and conclusions on the genesis of the Upper Cretaceous ironstones of the Bahariya area

4. Ironstone crusts hosted in Cenomanian clastic rocks

This chapter is centered on iron-rich rocks associated with clastic sediments present in the Cenomanian Bahariya Formation. Full understanding of the ironstones of the Bahariya Formation requires not only a clear description and interpretation of the sedimentary facies but also the determination of the paragenetic mineral sequence forming the ironstones and their host siliciclastic rocks. In this purpose, detailed sedimentological, petrological and geochemical analyses were carried out on samples collected from different ironstone crusts and concretions as well as samples from the host rock Bahariya Formation at three sections located in the northern part of the Bahariya Depression. The studied ironstone crusts are thin, up to 1-meter-thick and are encountered in both the lower and upper units of the Bahariya Formation. Main results of the comprehensive study of the ironstone hosted in the Cretaceous Bahariya Formation were reported in a paper by Afify et al. (2015a) where a new model for the

formation of the ferruginous beds was suggested (section 4.1).

The article deals with one of the objectives of the present PhD work: it contains detailed description of the main ironstone crusts associated with the clastic rocks of the Lower Cenomanian Bahariya Formation. The work deals with the stratigraphy and sedimentology of the Bahariya Formation (the host rock) with detailed description of the main lithofacies and interpretation of the paleoenvironments in which this rock unit was accumulated. The mineralogy, petrography and geochemistry of the ironstones were studied in detail. Taking in mind previous literature either on the area or from general models stated for ironstone formation, this work argues and proposes a diagenetic model for the formation of the ironstone crusts in clastic rocks. The model describes the flow mechanism and possible source of the iron-rich fluids forming the crusts.

In addition to data reported by Afify et al. (2015a), complementary mineralogical and geochemical analyses are shown in section 4.2. The analyses included: clay mineralogy, carbon and oxygen stable isotope compositions of the associated carbonate minerals, especially those present in the ironstone crusts and concretions, major and trace elements geochemistry as well as rare earth elements and yttrium contents in the ironstone rocks. Results on the mineralogy and geochemistry are followed by interpretation integrating the mechanism of ironstones formation and the timing and source of ironstones in the Bahariya Formation (see section 4.3).

4.1. Diagenetic origin of ironstone crusts in the Lower Cenomanian Bahariya Formation, Bahariya Depression, Western Desert, Egypt

A.M. Afify, M.E. Sanz-Montero, J.P. Calvo, H.A. Wanas

Article published in:

***Journal of African Earth Sciences*, volume 101(2015), pages 333–349.**

doi:10.1016/j.jafrearsci.2014.10.005

4.1.1. The article
4.1.2. Conclusions from the article

4.1.1. The article

Journal of African Earth Sciences 101 (2015) 333–349

Contents lists available at ScienceDirect

Journal of African Earth Sciences

journal homepage: www.elsevier.com/locate/jafrearsci

Diagenetic origin of ironstone crusts in the Lower Cenomanian Bahariya Formation, Bahariya Depression, Western Desert, Egypt

A.M. Afify [a,*], M.E. Sanz-Montero [a], J.P. Calvo [a], H.A. Wanas [b]

[a] Department of Petrology and Geochemistry, Faculty of Geological Sciences, Complutense University, Madrid, C/José Antonio Nováis, 2, 28040 Madrid, Spain
[b] Geology Department, Faculty of Science, Menoufia University, Shebin El-Kom, Egypt

ARTICLE INFO

Article history:
Received 8 May 2014
Received in revised form 6 October 2014
Accepted 7 October 2014
Available online 23 October 2014

Keywords:
Ironstone crusts
Late Cretaceous
Bahariya Formation
Egypt
Iron-rich carbonates
Selective replacement

ABSTRACT

In this paper, a new interpretation of the ironstone crusts of the Bahariya Formation as late diagenetic products is provided. The siliciclastic Lower Cenomanian Bahariya Formation outcropping in the northern part of the Bahariya Depression (Western Desert, Egypt) is subdivided into three informal units that are mainly composed of thinly laminated siltstone, cross-bedded and massive sandstone, fossiliferous sandstone/sandy limestone and variegated shale. Abundant ironstone crusts occur preferentially within its lower and upper units but are absent in the middle unit. The ironstone crusts show selective replacement of carbonate components, including calcretes, by iron oxyhydroxides. More permeable parts of the terrigenous beds such as burrow traces, subaerial exposure surfaces, concretionary features and soft-sediment deformation structures led to heterogeneous distribution of the iron oxyhydroxides.

A variety of diagenetic minerals, where goethite and hematite are the main end-products, were characterized by mineralogical analysis (XRD), petrography and SEM observation, and geochemical determinations (EMPA). Other diagenetic minerals include Fe-dolomite/ankerite, siderite, manganese minerals, barite, silica, illite/smectite mixed-layer, and bitumen. These minerals are interpreted to be formed in different diagenetic stages. Some minerals, especially those formed during eodiagenesis, show features indicative of biogenic activity. During burial, dolomite and ankerite replaced preferentially the depositional carbonates and infilled secondary porosity as well. Also during mesodiagenesis, the decomposition of organic matter resulted in the formation of bitumen and created reducing conditions favorable for the mobilization of iron-rich fluids in divalent stage. Telodiagenesis of the Cenomanian Bahariya deposits took place during the Turonian–Santonian uplift of the region. This resulted in partial or total dissolution of Fe-dolomite and ankerite which was concomitant to iron oxyhydroxide precipitation upon mixing with shallow oxygenated water.

Circulation of reducing iron-rich fluids through fractures and inter and intrastratal discontinuities is proposed as an alternative model to explain the controversial source of iron for the ironstone crusts of the Bahariya Formation. The origin of iron-rich fluids is probably related to the basement rocks. The provided model relates the fluid movements through fractures and discontinuities with the preferential replacement of carbonates. This combination of processes is consistent with the heterogeneous geometries and the wide distribution of the ironstones.

1. Introduction

The northern part of the Bahariya Depression in the Western Desert of Egypt shows a variety of ironstone occurrences including the presence of economic Cenozoic ironstone deposits in El Gedida, Ghorabi and El Harra areas (Akkad and Issawi, 1963; Basta and Amer, 1969; El Sharkawi et al., 1984; El Aref et al., 1999, 2006a,b; Dabous, 2002; Salama et al., 2012; Baioumy et al., 2013). These ironstones constitute a prominent landscape feature that has played a significant role in the geomorphological evolution of the region as they preclude extensive erosion of the outcropping sedimentary formations.

The continental to shallow marine deposits of the Lower Cenomanian Bahariya Formation contain abundant ironstone crusts whose origin has been matter of debate. The transformation of ilmenite to rutile was described as an important source of iron for the ironstone caps forming isolated hills in the Bahariya Depression (Mücke and Agthe, 1988). The ironstone crusts were interpreted as resulting from hematitization and/or oxidation of glauconite by lat-

* Corresponding author.
E-mail address: adelmady@ucm.es (A.M. Afify).

http://dx.doi.org/10.1016/j.jafrearsci.2014.10.005
1464-343X/

4.1.2. Conclusions from the article

The ironstone crusts are prominent throughout the lower and upper members of the Cenomanian Bahariya Formation though they are absent in the middle member. The stratigraphic formation is mostly composed of siliciclastic rocks, i.e. cross-bedded and massive sandstone, siltstone, variegated shale and fossiliferous sandstone/sandy limestone. Dark bituminous-rich sandstones occur in the middle member of the formation. The ironstone crusts and concretions show preferential occurrences and selective replacement of carbonate components, including calcretes, by iron oxyhydroxides. More permeable parts of the terrigenous beds such as burrow traces, subaerial exposure surfaces, concretionary features and soft-sediment deformation structures led to heterogeneous distribution of the iron oxyhydroxides.

A variety of diagenetic minerals that formed throughout eo-, meso-, and telodiagenetic stages were recorded after field sedimentological work, XRD mineral determinations, standard petrography and SEM and electron microprobe (EMPA) analyses. New mineral phases formed during early diagenesis, i.e. siderite, barite, Mn-minerals and goethite coatings, are volumetrically less important than those produced during burial and telodiagenetic stages. These latter diagenetic products comprise Fe-dolomite/ankerite, bitumen, silica/ feldspar overgrowths and high amount (up to 65%) of iron oxyhydroxides. During burial, dolomite and ankerite replaced preferentially the depositional carbonates such as micrite, bioclasts and several calcrete fabrics as well as infilled secondary porosity. Those carbonate minerals were not previously reported in the literature about the Bahariya ironstones. Also during diagenesis, decomposition of organic matter resulted in the formation of bitumen and created reducing conditions favourable for the mobilization of iron-rich fluids in divalent stage.

Telodiagenesis of the Cenomanian Bahariya deposits took place during the Late Cretaceous deformation phases that affected the Bahariya area. Uplift resulted in partial to total dissolution of the Fe-dolomites and subsequent precipitation of iron oxyhydroxides. The preservation of large centers and clear rims with no

collapse features of the Fe-dolomites implies alteration by solution. Fe-dolomite and ankerite dissolution was concomitant to iron oxyhydroxide precipitation upon mixing with shallow oxygenated water.

Source of iron for the ironstone crusts of the Bahariya Formation has been a matter of debate and various formative sources have been proposed (Mesaed, 2006; Catuneanu et al., 2006; Tanner and Khalifa, 2010). These include alteration of clay minerals and heavy minerals, extensive weathering of older rocks and further transport of iron in solution or as colloid, whether in the sediment load or by groundwater inflow, etcetera. Circulation of reducing iron-rich fluids through fractures and inter and intrastratal discontinuities is proposed as an alternative model. The origin of iron-rich fluids probably related to the underlying formations of Paleozoic, Jurassic or earlier Cretaceous.

4.2. Additional Data

4.2.1. Clay mineralogy
4.2.2. Carbon and oxygen isotope analyses of host carbonate rocks
4.2.3. Major and trace elements geochemistry
4.2.4. Rare earth elements and yttrium (REY) geochemistry

4.2.1. Clay mineralogy

The mineralogy of the clays associated with the ironstone crusts occurring in the Bahariya Formation in the northern part of the depression was studied in three sections (the Ghorabi, El Harra and Gabal El-Dist) by Afify et al. (2015a). The recorded clay minerals within the ironstone crusts were mainly smectite, illite/smectite (I/S) mixed-layers and subordinate kaolinite. In that paper, slight illitization of smectite in the ironstone crusts was interpreted as due to low burial temperature or most likely shallow burial depth. On this basis, we continued with the study of clays in the host rock at the three studied sections to complete the diagenetic history in the Bahariya Formation.

Thirty clay-rich additional samples of nearly similar lithology and stratigraphic position were collected from the lower and upper units of the Bahariya Formation at the three previously studied sections. The identification of the studied clay minerals was performed according to Moore and Reynolds (1989). The semi-quantitative estimate for every phase of the recorded clay minerals (including mixed-layers) was measured using the reflective power and peak-position method (Table 4.2.1). XRD study of the <2 µm fraction in oriented mounts revealed that the clay mineral phases are mainly smectite (iron-rich, di-octahedral), I/S mixed-layers and subordinate kaolinite. Palygorskite and sepiolite only occur in a few samples.

Mineral	Reflection	d(Å)	°2θ(CuKα)	Reflective power
Kaolinite	(001)	7.1	12.45	2
Illite	(001)	10	8.83	1
Palygorskite	(001)	10.4	8.5	0.67
Sepiolite	(001)	12.8	6.9	1
Smectite + EG	(001)	17	5.2	4
I/S + EG	(001)	10-15	8.83-6.2	1-4

Table 4.2.1. Spacing (d), position (°2θ) and reflective power for the main clay minerals recorded in our case study (after Moore and Reynolds; 1989).

Interstratification process occurs mainly at the Ghorabi and El Harra sections where illite co-exists with the smectite in a mixed-layer. The amount of illite in illite/smectite (I/S) mixed-layers and their interstratification order were expressed using the Reichweite (R) terminology (Reynolds, 1980) (Table 4.2.2). Amounts of illite in I/S mixed-layers varies in the studied samples, but increase to the top of the Ghorabi and El Harra sections (Table 4.2.3, Fig. 4.2.1).

% Illite	R (Reichweite)	001/002	
		d(Å)	°2θ(Cu Kα)
10	0	8.58	10.31
20	0	8.67	10.20
30	0	8.77	10.09
40	0	8.89	9.95
50	0	9.05	9.77
60	1	9.22	9.59
70	1	9.40	9.41
80	1	9.64	9.17
90	3	9.82	9.01

Table 4.2.2. Position of the useful reflection for estimating percent of illite in illite/smectite mixed-layers (after Moore and Reynolds; 1989).

The interstratified I/S mixed-layers are clarified by the comparison of the air-dried (AD) and ethylene glycolated (EG) diffractograms. As well, the thermal treated (TT) diffractograms at 550 °C of this group of minerals destroy any intermediate reflection, resulting in a diffractogram of illite type (Fig. 4.2.1). Ordered I/S mixed-layers occur towards the top of the Bahariya Formation in the Ghorabi and El Harra sections (Fig. 4.2.1).

In contrast, illite associated with smectite does not occur at Gabal El-Dist (Fig. 4.2.1). Discrete smectite and R0 I/S appeared in samples collected from Gabal El-Dist, whereas R0, R1 and R3 I/S mixed-layers occur at the Ghorabi and El Harra sections (Table 4.2.3). Occurrence of R1 and R1-R3 I/S mixed-layers were characterized by variable basal reflection (001) situated mostly between 12 and 14 Å in the ethylene glycolated diffractograms (Fig. 4.2.1).

In short, transformation of smectite to illite was recorded mainly in the Ghorabi and El Harra sections increasing to the top of the succession forming R1 and R3 as the last step (Fig. 4.2.1). In Gabal El-Dist section, the absence of R1 and R3 point out a less developed illitization process where high percentages of smectite coexist (Fig. 4.2.1).

Increasing depth	Sample	Smectite	R0 I/S	R1-R3 I/S	Kaolinite	I% in I/S*
	Gh-A	-	-	23.22%	76.78%	70-80%
	Gh-B	-	73.38%	26.62%	-	70%
	Gh-C	66.25%	-	-	33.75%	-
	Hr-A	-	65.98%	34.02%	-	50-60%
	Hr-B	-	100%	-	-	25%
	Hr-C	-	90%	-	10%	10%
	D-A	86%	-	-	14%	-
	D-B	88%	-	-	12%	-
	D-C	-	86%	-	14%	5-10%

Table 4.2.3. Percentage of illite in I/S mixed-layers as well as other associated clay minerals after solvation with ethylene glycol in the clay-rich samples of the three studied sections (El Harra section: Hr, Ghorabi section: Gh, Gabal El-Dist section: D). (* When two types of mixed-layers coexist in the same sample, the percentage of illite indicates the average between them).

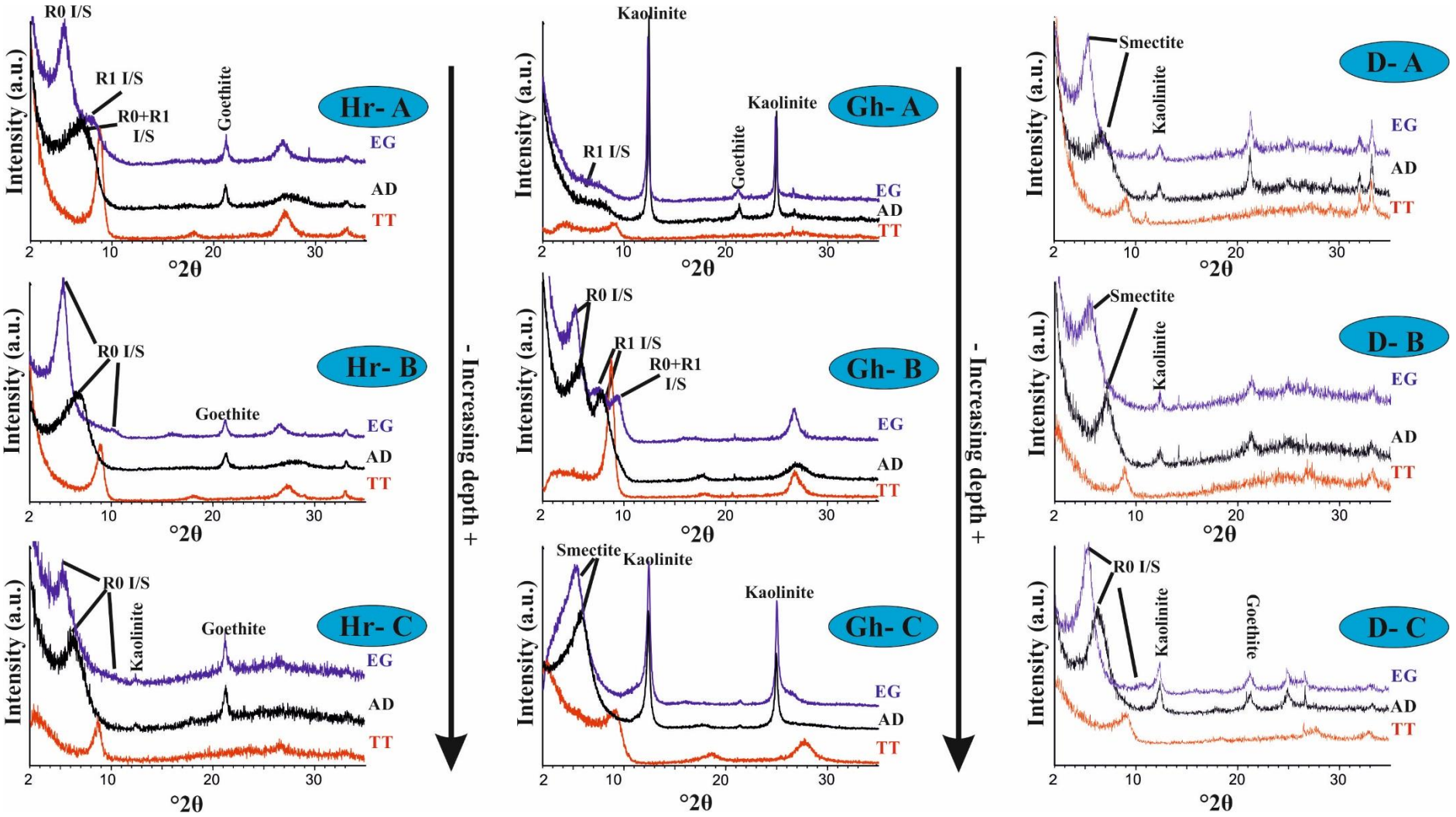

Figure 4.2.1. Air-dried (AD), ethylene glycolated (EG) and thermal-treated (TT) diffractograms showing the clay mineralogy and mixed-layered illite/smectite (I/S) variations with depth in the Bahariya Formation at three outcrops (El Harra section: Hr, Ghorabi section: Gh, Gabal El-Dist section: D).

4.2.2. Carbon and oxygen isotope analyses of host carbonate rocks

Petrography, mineralogy and elemental analyses of the carbonate minerals associated with the ironstone rocks of the Cenomanian Bahariya Formation were described in detail by Afify et al. (2015a). Moreover, studying of carbon and oxygen stable isotopes of carbonate minerals, especially those of the dolomite and ankerite, associated with the ironstone crusts is critical as they represent the main host minerals for the iron oxyhydroxides (Afify et al., 2015a). Carbon and oxygen stable isotope analyses were performed on eight carbonate-rich ironstone samples from the lower and upper members of the Bahariya Formation. Distribution of these samples is shown in Figure 2 of Afify et al. (2015a) and the stable isotope values are listed in Table 4.2.4. Sampling was carried out using micro-drilling techniques that allowed collecting the exact amount required for the analyses of dolomite and ankerite. Even though, some contamination between dolomite/ankerite and calcite could occur during drilling and extraction processes. Accordingly, the samples were subjected to the sequential separation between the dolomite/ankerite and calcite when isotope geochemistry was performed (see methodology of carbon and oxygen stable isotopes; chapter 2).

Sample	$\delta^{13}C_{V\text{-}PDB}$‰	$\delta^{18}O_{V\text{-}PDB}$‰
Dist 5	-6.10	-9.35
Dist 4	-5.34	-5.79
Dist 3	-7.22	-8.52
Ghorabi 13	-3.51	-10.33
Ghorabi 9	-1.18	-8.05
Ghorabi 7	-0.54	-4.90
Hr10	-3.59	-10.09
Hr3	-0.76	-1.74

Table 4.2.4. Stable isotopic composition of the dolomite/ankerite minerals in the Bahariya Formation at Gabal El-Dist, Ghorabi and El Harra sections.

The $\delta^{13}C$ and $\delta^{18}O$ values of the dolomite/ankerite minerals are cross-plotted in Figure 4.2.2. The $\delta^{13}C$ values of the carbonate minerals show wide range between -7.22‰ and -0.54‰ V-PDB. The more negative carbon

isotopic values were recorded in samples from the Gabal El-Dist section (see Figure 2 of Afify et al. (2015a) for samples location). The $\delta^{18}O$ values ranges from -10.33‰ to -1.74‰ V-PDB. Slight positive correlation between carbon and oxygen isotope compositions is recognized (Fig. 4.2.2).

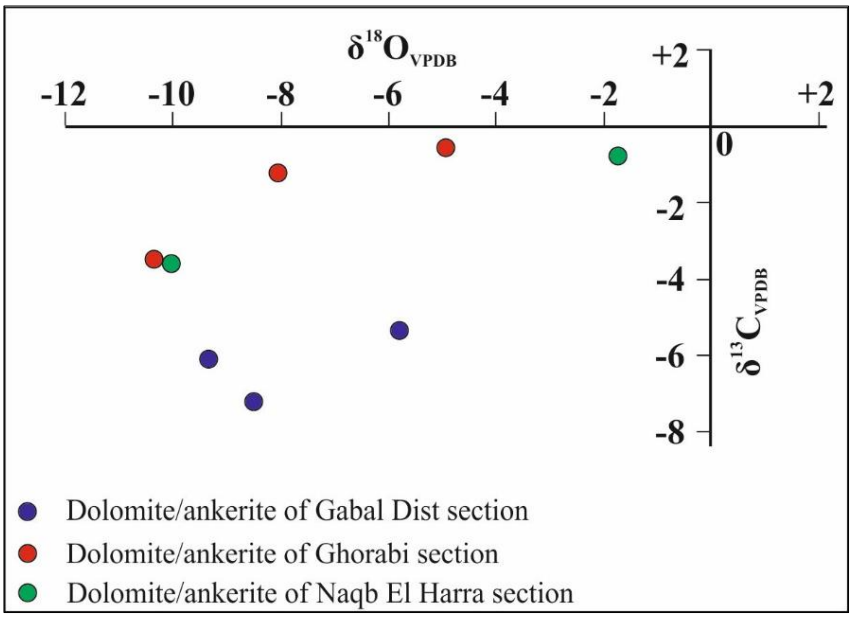

Figure 4.2.2. Cross-plot showing the stable isotopic values of the dolomite/ankerite minerals in the Bahariya Formation at Gabal El-Dist, Ghorabi and El Harra sections.

4.2.3. Major and trace elements geochemistry

Major and trace elements geochemical analyses of samples collected from the iron-rich and carbonate-rich ironstone crusts of the Bahariya Formation were performed by X-ray florescence (XRF) and electron microprobe (EMP) and were supported by scanning electron microscope equipped with energy dispersive X-ray spectrometry (SEM-EDX). The obtained geochemical data of the samples are given in Tables 4.2.5 and 4.2.6; distribution and location of the samples are shown in Figure 2 of Afify et al. (2015a).

Samples	Dist1	Dist4	Dist5	Gh8	Gh14	Gh15	Hr1	Hr6
Oxides/elements	Ironstone crusts of the Bahariya Formation							
Major oxides (wt.%)								
SiO_2	11.95	2.43	5.34	19.30	9.83	8.57	21.86	11.15
Na_2O	0.77	0.86	0.80	0.91	1.95	1.46	7.78	2.58
MgO	8.47	1.58	1.47	1.23	0.32	0.75	0.37	0.29
Al_2O_3	3.01	3.41	3.45	5.60	7.58	7.89	5.05	5.33
P_2O_5	0.64	0.49	0.46	0.64	0.10	bdl	0.26	bdl
K_2O	0.36	0.10	0.77	0.92	0.48	0.68	0.58	0.27
CaO	12.43	1.73	10.31	1.43	0.19	0.27	0.08	0.09
TiO_2	0.25	0.22	0.10	0.36	0.49	0.43	0.42	0.31
MnO	0.86	1.85	1.52	0.54	0.72	2.25	1.32	0.28
Fe_2O_3	30.80	73.26	62.81	57.96	63.48	60.58	54.41	54.96
Trace elements (ppm)								
Cr	bdl	bdl	bdl	bdl	bdl	bdl	bdl	bdl
Ni	146.9	488.5	421.6	356.5	477.1	429.0	180.1	33.9
Cu	9.0	8.1	10.8	17.6	29.4	14.0	15.7	14.5
Zn	10.8	bdl	7.2	52.1	111.7	bdl	28.7	30.9
As	14.5	3.0	16.0	3.0	5.1	3.0	4.8	8.9
Rb	74	296	223	228	259	239	72	34
Sr	184	233	322	181	164	339	47	155
Zr	333	136	98	359	162	84	349	1065
Nb	3.8	6.9	4.8	4.5	11.6	18.4	4.2	25.3
Pb	62	346	237	208	271	260	79	48
S	1162	1972	626	1343	309	464	1264	1660
REE (ppm)								
Sc	5.8	3.9	10.0	12	12	9.3	6.2	7.4
Y	59	29	31	78	41	14	47	17
La	55	27	25	57	24	27	47	13
Ce	121	55	53	127	52	33	110	25
Pr	16	7.1	6.8	18	7.1	4.6	14	3,3
Nd	65	28	28	74	30	17	58	13,2
Sm	13	5.5	6.0	16	7.1	3.0	13	2,8
Eu	3.2	1.3	1.5	3.8	2.0	0.70	2.9	0.57
Gd	13.0	5.8	6.1	17	9.1	2.8	11.4	2.9
Tb	1.8	0.83	0.88	2.4	1.4	0.43	1.6	0.45
Dy	10.1	4.7	5.4	14	8.4	2.8	9.3	2.9
Ho	2.1	1.07	1.23	3.1	1.8	0.67	2.0	0.69
Er	5.5	2.9	3.5	8.3	4.9	2.1	5.4	2.1
Tm	0.63	0.36	0.45	1.00	0.61	0.29	0.66	0.29
Yb	4.0	2.3	3.1	6.4	3.9	2.1	4.5	2.1
Lu	0.49	0.29	0,42	0.84	0.53	0.31	0.59	0.31
ΣREE	310.82	142.15	141.38	348.84	152.84	96.8	280.35	69.61
LREE	286.2	129.7	126.4	312.8	131.3	88.1	256.3	60.77
HREE	24.62	12.45	14.98	36.04	21.54	8.7	24.05	8.84
ΔEu	1.155	1.077	1.162	1.078	1.146	1.136	1.122	0.937
ΔCe	0.935	0.915	0.935	0.904	0.912	0.675	0.982	0.880
ΔPr	1.054	1.060	1.033	1.079	1.046	1.137	1.025	1.063
ΔLa	0.899	0.930	0.994	0.853	0.978	1.262	0.922	0.994
Y_{SN}/Ho_{SN}	1.03	0.995	0.925	0.924	0.836	0.767	0.863	0.904
ΔGd	1.197	1.191	1.170	1.204	1.195	1.091	1.134	1.119

*bdl: below detection limit

Table 4.2.5. Major, trace and rare earth element values from ironstone crusts in the Bahariya Formation, determined by XRF and ICP/MS analyses. Anomalies of Ce, Eu, Pr and other ratios are Post Archean Australian Shale (PAAS) normalized (see Figure 2 of Afify et al. (2015a) for samples location).

The whole-rock compositions of the ironstone samples using XRF are given in Table 4.2.5 whereas the ratios between the major oxides are plotted in

Figure 4.2.3. The ironstones show enrichment in Fe_2O_3 reaching up to 73 wt.% whilst the MnO content is very low and reaches up to 2 wt.%. Samples rich in SiO_2 and Al_2O_3 are related to the clays that occur associated with the iron bearing minerals. The clay-rich samples are characterized by low manganese content, this indicating that Mn is not related to the composition of the clays (Fig. 4.2.3). The whole-rock chemical analyses show relative enrichment of terrigenous elements related to presence of clays and quartz, i.e. Al_2O_3 (up to 7.89 wt.%), SiO_2 (up to 21.86 wt.%) and Na_2O (up to 7.78 wt.%). CaO and MgO contents increase in carbonate-rich ironstone samples reaching up to 12 wt.% and 8.5 wt.% respectively (Fig. 4.2.3). The bulk composition of the ironstones shows low trace element contents (Zn, Ni and Sr reach up to 112 ppm, 489 ppm and 339 ppm maximum values, respectively) and relative enrichment in terrigenous elements, e.g., Zr content reaches up to 1065 ppm (Table 4.2.5).

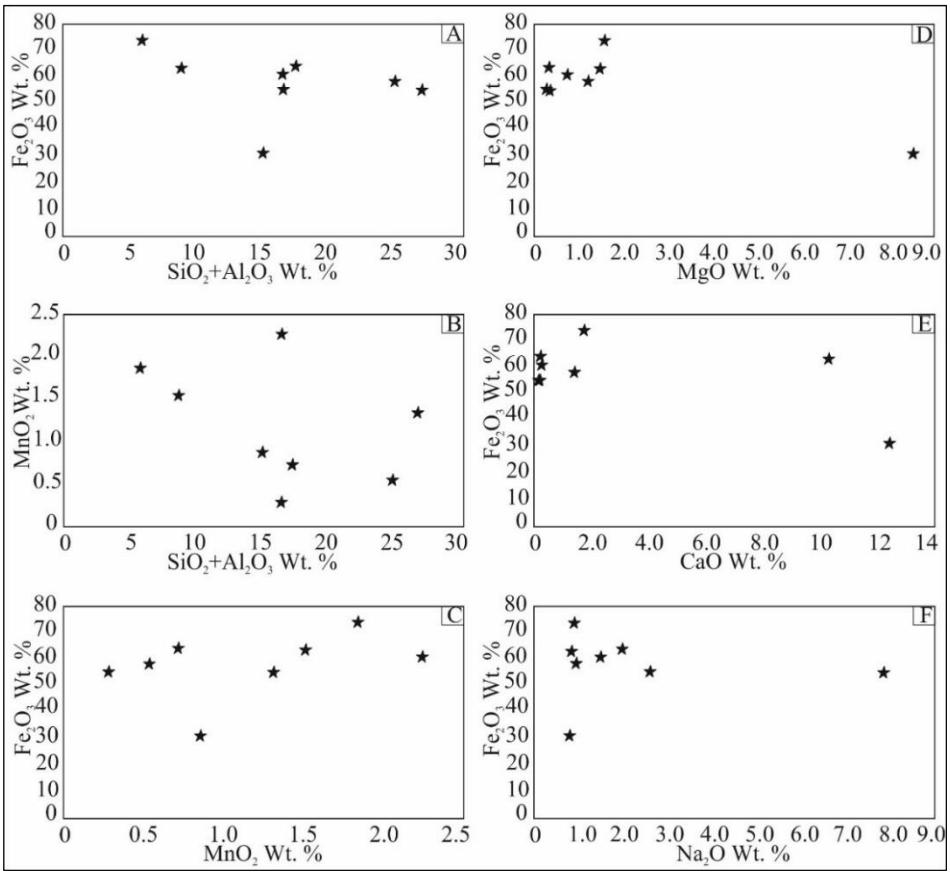

Figure 4.2.3. Graphics showing the bivariate relationships between major oxides in the ironstones of the Bahariya formation. The values were determined by X-ray fluorescence.

Data obtained after electron microprobe analysis (EMPA) of the separated iron oxyhydroxides and associated manganese and carbonate minerals are given in Table 4.2.6. Values of major oxides determined in the ferromanganese and carbonate minerals are plotted in Figure 4.2.4. Fe_2O_3 in the iron oxyhydroxides reaches up to 78 wt.% whilst MnO reaches up to 2.2 wt.%, and MgO and CaO are up to 4.8 wt.% and 2.8 wt.% respectively. SiO_2 and Al_2O_3 contents reach up to 4 wt.% and 2 wt.% respectively, whilst P_2O_5 does not exceeds 0.6 wt.% (Table 4.2.6). The element composition of the iron oxyhydroxides indicates goethite and hematite that show slight contamination of silica, alumina and sodium, which is mainly from the clay matrix. MgO and CaO content are mostly from the replaced carbonate minerals where their content decreases in the expense of Fe_2O_3 in the ferromanganese minerals. The manganese content is very low in both iron oxyhydroxides and iron-rich carbonates (Fig. 4.2.4).

Oxides	SiO_2	Al_2O_3	FeO	MnO	MgO	CaO	Na_2O	K_2O	TiO_2	P_2O_5	SO_3	BaO	ZnO
Points													
1	**1.90**	**0.15**	**72.54**	**0.27**	**0.18**	**0.07**	**0.12**	**bdl**	**0.001**	**0.33**	**0.07**	**0.07**	**0.17**
2	**2.70**	**0.32**	**68.10**	**0.84**	**2.10**	**0.45**	**bdl**	**bdl**	**0.006**	**0.15**	**0.57**	**0.8**	**bdl**
3	**2.272**	**bdl**	**73.05**	**0.361**	**0.111**	**0.049**	**0.032**	**bdl**	**0.01**	**0.24**	**0.01**	**0.124**	**0.08**
4	**4.11**	**0.19**	**68.34**	**0.51**	**1.10**	**0.18**	**0.19**	**0.02**	**0.02**	**0.60**	**0.14**	**0.01**	**0.002**
5	**2.95**	**0.47**	**64.53**	**1.46**	**0.50**	**0.40**	**0.41**	**0.10**	**0.01**	**0.54**	**0.32**	**0.05**	**0.10**
6	**2.73**	**2.10**	**60.92**	**0.43**	**2.11**	**0.09**	**0.08**	**bdl**	**bdl**	**0.47**	**0.21**	**0.07**	**0.13**
7	**0.28**	**0.07**	**78.30**	**0.17**	**0.13**	**0.13**	**0.25**	**0.03**	**0.01**	**0.12**	**0.59**	**0.04**	**0.18**
8	**3.098**	**0.861**	**55.76**	**2.2**	**4.816**	**2.793**	**0.069**	**0.014**	**bdl**	**0.154**	**0.94**	**0.36**	**0.003**
9	**0.16**	**0.32**	**0.83**	**58.16**	**1.11**	**0.88**	**0.69**	**0.82**	**bdl**	**0.24**	**0.88**	**21.01**	**0.03**
10	**bdl**	**0.589**	**0.236**	**42.42**	**0.122**	**0.474**	**0.306**	**0.307**	**bdl**	**bdl**	**10.6**	**21.62**	**0.002**
11	**0.028**	**0.638**	**0.280**	**44.92**	**0.164**	**0.486**	**0.366**	**0.419**	**bdl**	**bdl**	**8.53**	**21.01**	**0.003**
12	**0.164**	**0.323**	**0.832**	**58.16**	**1.109**	**0.883**	**0.685**	**0.822**	**0.005**	**0.10**	**0.88**	**8.03**	**0.10**
13	**0.164**	**0.390**	**0.600**	**50.44**	**0.15**	**0.29**	**0.200**	**0.261**	**0.007**	**bdl**	**0.09**	**11.19**	**0.005**
14	**0.089**	**0.473**	**0.614**	**50.95**	**0.21**	**0.32**	**0.281**	**0.290**	**0.006**	**0.10**	**0.16**	**11.53**	**0.007**
15	**0.628**	**0.315**	**1.261**	**43.46**	**0.368**	**0.489**	**0.469**	**0.293**	**0.01**	**0.3**	**0.08**	**9.176**	**0.15**
16	**0.180**	**0.224**	**0.394**	**56.57**	**1.072**	**0.794**	**1.062**	**0.951**	**bdl**	**bdl**	**0.12**	**6.934**	**bdl**
17	**bdl**	**0.008**	**4.122**	**0.843**	**20.20**	**29.47**	**bdl**	**0.023**	**0.02**	**0.1**	**bdl**	**bdl**	**0.05**
18	**0.487**	**0.056**	**14.29**	**0.395**	**16.34**	**26.59**	**0.069**	**0.036**	**bdl**	**0.3**	**0.09**	**0.04**	**0.01**
19	**1.10**	**0.81**	**11.01**	**0.36**	**11.29**	**12.32**	**0.14**	**0.05**	**0.003**	**0.30**	**0.59**	**bdl**	**bdl**
20	**bdl**	**bdl**	**3.86**	**0.82**	**21.59**	**30.63**	**0.22**	**0.02**	**bdl**	**0.12**	**0.35**	**bdl**	**0.01**
21	**bdl**	**0.04**	**4.61**	**0.84**	**20.61**	**31.04**	**0.14**	**0.04**	**bdl**	**0.32**	**0.37**	**0.02**	**0.05**
22	**bdl**	**bdl**	**3.58**	**1.01**	**20.18**	**31.46**	**0.09**	**0.02**	**0.01**	**0.45**	**0.22**	**0.02**	**bdl**

*bdl: below detection limit

Table 4.2.6. Major and trace element values (in wt.%) of selected iron-rich (1 – 8), manganese-rich (9 – 16) and carbonate-rich (17 – 22) minerals from ironstone crusts in the Bahariya Formation, determined by electron microprobe analyses (EMPA).

Point analyses of the carbonate minerals revealed that they correspond mainly to iron-rich dolomite and ankerite (Table 4.2.6; Fig. 4.2.4). CaO and MgO content ranges between 21.32 wt.% and 31.46 wt.% for CaO and 11.29 wt.% and 21.59 wt.% for MgO. The iron content (Fe_2O_3) in the ferroan dolomite and ankerite minerals ranges between 3.58 wt.% and 14.29 wt.%. The manganese minerals are associated with micron-sized barite crystals and contain up to 58.16 wt.% MnO, 1.26 wt.% Fe_2O_3, 1.1 wt.% MgO, 0.9 wt.% CaO and 1 wt.% Na_2O. They are Ba-rich (mean 8.5 wt.% of BaO); this content reaches up to 21.6% where contaminated with barite.

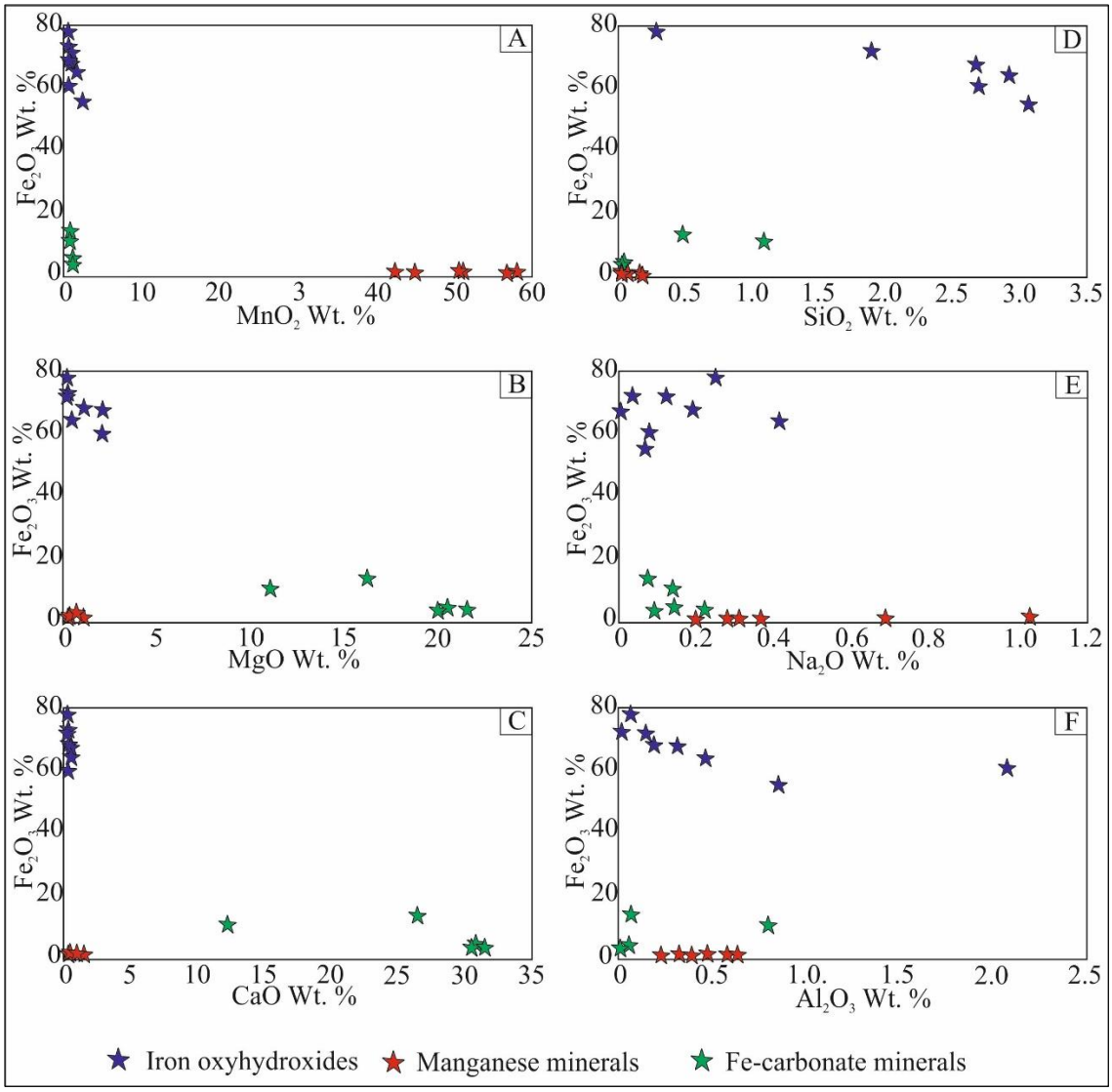

Figure 4.2.4. Discrimination diagrams showing correlation between major oxides in the three main minerals forming the ironstone crusts; values were determined by using electron microprobe analysis.

4.2.4. Rare earth elements and yttrium (REY) geochemistry

Variations in rare earth elements and yttrium (REY) content are potential predictors for evaluating both provenance and origin of the ore fluids (Bau et al., 2014; Hein et al., 2016), especially if they are combined with variations in mineralogy and other geochemical insight. Normalized REE distribution patterns of chemical sediments can be interpreted in terms of fluid compositions, types of precursor minerals and/or physical and chemical conditions of mineralization processes as the REE are not easily fractionated during sedimentation (Mclennan, 1989). REY geochemical analyses were carried out using inductively coupled plasma/mass spectrometry (ICP/MS) on eight samples of ironstone crusts. REY values are shown in Table 4.2.5 and plotted in Figure 4.2.5, normalized to Post Archean Australian Shale (PAAS; McLennan, 1989). ΣREE, LREE (light rare earth elements), HREE (heavy rare earth elements), Ce/Ce*, Eu/Eu*, Y_{SN}/Ho_{SN}, Gd/Gd* ratios are also shown in Table 4.2.5.

The total REE contents show wide range between 69.61 ppm and 348.84 ppm (Table 4.2.5). They show enrichment of light rare earth elements (LREE) when compared with the heavy rare earth elements (HREE). The pattern geometry and values of the analyzed ironstone samples display similar characteristics of flat spidergrams when normalized to PAAS (Fig. 4.2.5). All the samples show slight negative Ce anomaly. However, a negative Ce anomaly might be misinterpreted as a positive La anomaly (Bau and Dulski, 1996) due to the enhanced stability of La, and thus its enrichment, in solution (Bolhar et al., 2004). Discrimination between these two anomalies can be stated by the Ce/Ce* and Pr/Pr* values (Bau and Dulski, 1996). A combination of Ce/Ce* < 1 and Pr/Pr* ≤ 1 would indicate a positive La anomaly. Moreover, the negative Ce anomaly can be confirmed by the positive Pr anomaly determined in the studied ironstone samples of the Bahariya Formation. In addition, the ironstone crusts show a rather small positive Eu and Gd anomalies (Fig. 4.2.5). Because of its very similar ionic radius to Ho^{3+}, Y^{3+} can be inserted into REE patterns between isovalent Dy^{3+} and Ho^{3+} (Bau, 1996). When inserted between Dy and Ho, yttrium (Y) mostly shows negative anomaly close to unity (Table 4.2.5).

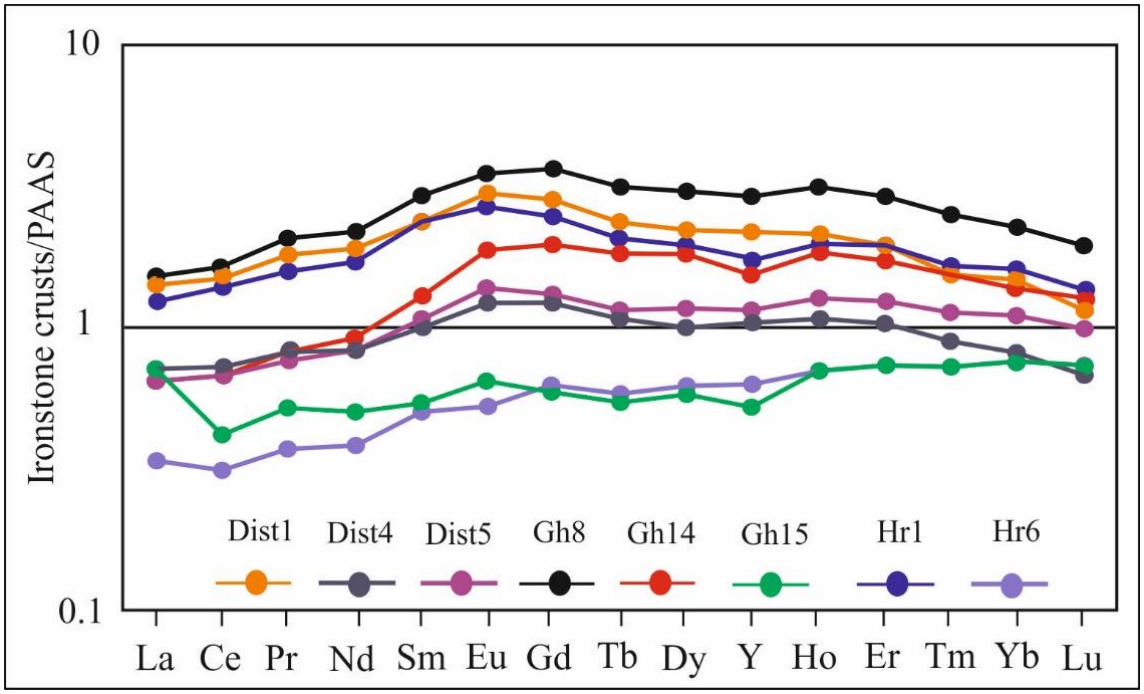

Figure 4.2.5. PAAS-normalized REY distribution patterns for the ironstone crusts in the Bahariya Formation at the three studied sections (see Figure 2 of Afify et al. (2015a) for samples location).

Since Ce, Nd and Y produce the most significant anomalies in patterns of REY partition coefficients and normalized REY concentrations (Bau et al., 2014), graphs of Ce anomaly *versus* Nd concentrations and Ce *versus* Y anomaly are plotted in Figure 4.2.6. Graphs of Ce anomaly *versus* Nd concentration and Ce anomaly *versus* Y anomaly effectively discriminate between different models of ironstone formations, regardless of their diverse mineralogical composition (Bau et al., 2014). These two simple and user-friendly, strong diagrams are based on the REY signature of a precipitate, because the REY are known for their coherent behavior in natural environments. According to data published by Bau et al. (2014) and Hein et al. (2016), we can differentiate between the three main genetic models for ironstones: hydrogenetic, diagenetic and hydrothermal.

Graphs of Ce anomaly against Nd concentration and Ce anomaly against Y anomaly are plotted in Figure 4.2.6. In a bivariate diagram of Ce/Ce* ratio against the Nd concentration (Fig. 4.2.6 A), the studied ironstone crusts show negative to no Ce anomaly.

Concerning Nd concentration, they show enrichment and fall in the 10-100 ppm range; the ironstone crusts mostly show a slight trend of increasing Nd concentration with increasing Ce/Ce* ratio. With regard to Ce-REE and Y-REE relationships, they are relevant because Ce and Y produce the most significant anomalies in patterns of REY partition coefficients and normalized REY concentrations (Bau et al., 2014). In a bivariate diagram of Ce anomaly against Y_{SN}/Ho_{SN} values, all samples show negative Y_{SN} values or close to unity ($Y_{SN}/Ho_{SN} \leq 1$) and negative Ce anomaly (Fig. 4.2.6 B).

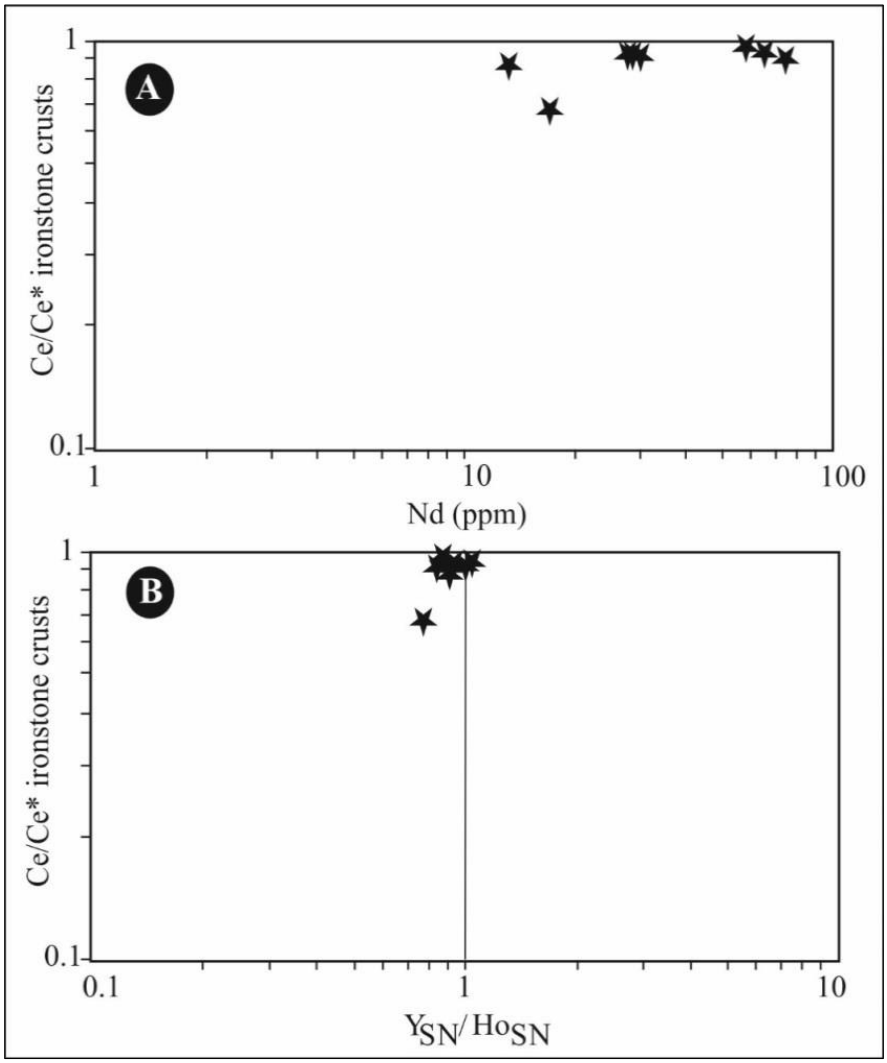

Figure 4.2.6. A. Graph of Ce/Ce* *vs.* Nd concentration for the ironstone crusts studied in the Bahariya Formation. B. A cross plot of Ce anomaly *vs.* Y_{SN} anomaly for the ironstone crusts (SN: normalized to PAAS).

4.3. Discussion and conclusions on the genesis of the Upper Cretaceous ironstones of the Bahariya area

The interpretation of the origin of ironstone beds occurring in the Cretaceous Bahariya Formation improved by using the above supplementary data. The study of the stable isotopic composition of the carbonate minerals (dolomite/ankerite) that represent the main host minerals for the iron-bearing rocks contributes to understanding the type of fluids and timing of the process involved in the formation of the iron-rich materials. Negative $\delta^{13}C$ values of the dolomite/ ankerite cements (-0.76 to -7.22‰ VPDB) suggest that marine carbon, mainly derived from depositional components, was the dominant carbon source for the carbonate minerals (Tucker and Wright, 1990; Mazzullo, 2000). Moreover, the occurrence of bitumen associated with the lower and upper units of the Bahariya Formation (Afify et al., 2015a) point to an organic carbon as a possible source of these carbonate minerals in burial diagenesis (Irwin et al., 1977). Organic matter oxidation and thermal decarboxylation during burial can be suggested as a source of carbon especially in samples showing more negative $\delta^{13}C$ values (e.g. -7.22‰ VPDB) associated with the bituminous-rich horizons (Mansburg et al., 2008).

The negative $\delta^{18}O_{VPDB}$ values ranging from -1.74 to -10.09‰ VPDB of both dolomite and ankerite suggest precipitation from deep burial conditions, i.e. higher temperature from pore water that have undergone some rock-water interaction (Land, 1980; Veizer, 1983; Suchecki and Hubert, 1984). Likewise, the Sr, Na low content and the Fe, Mn high content of the dolomite/ankerite cements could reflect meteoric diagenesis and suboxic to anoxic pore-water (Land, 1983). Sources of Mg^{+2}, Fe^{+2} and Mn^{+2} during burial were probably related to the transformation of iron oxyhydroxides and clays (Hendry et al., 2000) that formed during eodiagenetic and meso-diagenetic stages, respectively. The presence of these cations in solution upon thermal decarboxylation is inferred to have stabilized ankerite and Fe-dolomite (Hendry et al., 2000). The

absence of positive correlation and variability in the obtained data of carbon and oxygen stable isotopic composition along with their formation through fractures (Afify et al., 2015a) reflect the different phases of dolomite and ankerite formation under variable geochemical conditions.

Likewise, the high Fe (means > 1000 ppm?) and/or high Mn (means > 50 ppm?) content indicates that the pore waters were reducing and that a significant source of Fe and/or Mn was present (Budd, 1997).

In summary, precipitation of these carbonate minerals from intra-formational fluids was affected by dissolution of biogenic carbonates and thermal decomposition of organic carbon. Mixing of organic and inorganic carbon sources as well as the dominance of reduced fluids is suggested to be the more reliable genetic model for Fe-dolomite and ankerite formation. This model is further coherent with the migration and accumulation of hydrocarbons in the Bahariya and north Western Desert basins during Upper Cretaceous (Rossi et al., 2001, 2002; Metwalli and Pigott, 2005; Moretti et al., 2010).

Passing from the mechanism of formation of dolomite and ankerite host minerals to the hosted ironstones, the geochemical attributes, including whole-rock composition, elemental analyses and REY values of these ironstone crusts, support a diagenetic model for their formation. Replacement of the carbonate minerals, identified as relics by element analysis of the ferromanganese minerals was the main mechanism related to activity of iron-rich fluids. The slight enrichment of detrital-derived trace elements in the bulk composition of the ironstone crusts could suggest a hydrogenetic origin (Bau et al., 2014; Hein et al., 2016) of these crusts, though these trace elements are mainly present where the ironstones are associated with clays and detrital minerals, which could also indicate a terrigenous source (Hein et al., 2016). Nevertheless, point analyses of the ferromanganese minerals are indicative of depletion in detrital-derived trace elements, which is clearly in opposition to the hydrogenetic origin and the terrigenous source; contrary it suggests a hydrothermal or diagenetic origin (Nicholson, 1992; Hein et al., 2008; Bekker et al., 2010).

The total REE content of the ironstone crusts widely range from 69.61 ppm to 348.84 ppm. These values fit well REE values (110 – 489 ppm) characteristic of diagenetically formed ironstone (Bau et al., 2014). They are clearly out of the range (1228 – 2282 ppm) shown by hydrogenetic ironstone and by hydrothermal ironstones (15 – 149 ppm) (Bau et al., 2014). Similar REY data were obtained from ferromanganese nodules interpreted as diagenetic from the Peru Basin (Von Stackelberg, 1997). In agreement with the latter authors, diagenetic Fe–Mn ironstones display negative Y anomalies and negative Ce anomalies, which match the results obtained by analyses of the ironstone crusts in Bahariya (negative Ce anomalies, negative Y anomalies and intermediate Nd concentrations, between 10 and 100 ppm). Accordingly, the REY values support a diagenetic origin of iron formation within the clastic rocks after replacement of the carbonate minerals, thus confirming previous statement by Afify et al. (2015a).

Ce is a rare earth element that is due to redox reactions is observed in aqueous solutions and their precipitates (Bau et al., 1996). Ce anomaly results from oxidation of trivalent Ce to Ce^{4+} and subsequent decoupling of Ce from the other REEs due to formation of less soluble Ce^{4+} species and/or preferential adsorption of Ce^{4+} species on particle surfaces. In an oxidative environment, Ce^{3+} change to the less soluble Ce^{4+} and thus it removes from the solution by suspended particles, resulting in a negative Ce anomaly relative to its neighbor elements (Bau and Dulski, 1996; Bolhar et al., 2004). A marked Ce depletion is evident for the distribution patterns of dissolved rare earth elements under oxic conditions, whereas no depletion or even Ce enrichment occur in anoxic settings. Negative Ce anomalies suggest suboxic conditions wherein aqueous Ce^{3+} is depleted (Kakuwa and Matsumoto 2006). Thus, the presence of a negative Ce anomaly in the studied ironstones is attributed to oxidize surface where the iron-rich reducing fluids were mixed with oxidized meteoric water or passed to oxidizing conditions.

The small positive Eu anomaly of the Cretaceous ironstones could be a signature inherited from hydrothermal solutions that lost their positive Eu anomaly, due to a relatively high oxygen level (Klinkhammer et al.,

1983). Accordingly, a hydrothermal genetic model for these crusts is ruled out. This is justified by the discrimination diagrams about Ce/Ce* against Nd concentration and Y_{SN} anomaly. The studied samples do not show large positive Ce or any significant Y anomalies, i.e. Ce/Ce* and Y_{SN}/Ho_{SN} ratios are mostly close to unity, supporting diagenetic origin and excluding the hydrothermal origin of these deposits (Bolhar et al., 2004; Bau et al., 2014).

In summary, the ironstone crusts and concretions hosted in the clastic rocks of the Lower Cenomanian Bahariya Formation are interpreted as late diagenetic in origin after replacement of the mesodiagenetic iron-rich carbonates. They formed by reducing iron-rich basinal fluids that moved through fractures, discontinuities and permeable rocks. Uplifting of the Bahariya area during the Late Cretaceous caused mixing of reduced and meteoric waters in an oxidizing environment. Source of the iron-rich basinal fluids was mostly from underlying rocks. For instance, the Jurassic Khatatba Formation, which is characterized by noticeable presence of siderite, ferroan-dolomite and pyrite were affected by dissolution during Late Cretaceous (Rossi et al., 2001, 2002). Migration of oil from the Khatatba Formation and other possible sources, e.g., the Lower Cretaceous Alam El Bueb and Kharita formations, and the Upper Cretaceous Bahariya and Abu Roash formations, occurred in the north Western Desert during the Late Cretaceous. The oil migration was coincident with tectonic inversion and folding of the Syrian Arc system (Metwalli and Pigott, 2005). Such process could enhance the reducing conditions through which iron-rich solutions moved and support the model proposed by Afify et al. (2015a) for the diagenetic origin of these rocks during Upper Cretaceous tectonic deformation affected the area.

The studied clay mineralogy associated with the ironstone crusts show slight illitization indicative of shallow burial depth during mesodiagenesis (Afify et al., 2015a). Even though, the supplementary data dealing with clay mineralogy of the clastic host rock shows changes in the clay mineral assemblages up in the sections. These changes can be interpreted as a result of local increase in temperature, probably related to

faults, at the top of the Bahariya succession. This upward evolution of clays is not recognized at the Gabal El-Dist. Conclusions derived from the clay mineral assemblages and their relationship with eventual influence of hydrothermalism at the Ghorabi and El Harra areas will be discussed in more detail in chapter 5.

V

Ironstone mineralization hosted in Eocene carbonates

5.1. Nummulite biostratigraphy of the Eocene succession in the Bahariya Depression, Egypt: Implications for timing of iron mineralization (Article)
- **5.1.1.** ***The article***
- ***5.1.2.*** ***Conclusions from the article***

5.2. Ironstone deposits hosted in Eocene carbonates from Bahariya (Egypt) –New perspective on cherty ironstone occurrences (Article)
- ***5.2.1.*** ***The article***
- ***5.2.2.*** ***Conclusions from the article***

5.3. Additional data
- ***5.3.1.*** ***Mineralogy and petrology***
- ***5.3.2.*** ***Major and trace elements geochemistry***
- ***5.3.3.*** ***Rare earth elements and yttrium (REY) geochemistry***
- ***5.3.4.*** ***Sulfur and oxygen isotope geochemistry***
- ***5.3.5.*** ***Fluid inclusions geochemistry***

5.4. Discussion and interpretation of the Eocene ore-bearing minerals
- ***5.4.1.*** ***Ferromanganese minerals and quartz***
- ***5.4.2.*** ***Phosphates***
- ***5.4.3.*** ***Sulfate minerals***
- ***5.4.4.*** ***Clay minerals – clays as geothermal indicators***

5. Ironstone mineralization hosted in Eocene carbonates

The ironstone deposits of the northern part of the Bahariya Depression occur as big ore bodies in three mining areas: El Gedida, El Harra and Ghorabi, which are related to two major fault systems. The ore deposits are stratigraphically equivalent to the

surrounding Eocene carbonates (Fig. 3.1).

Due to the scarcity of Phanerozoic cherty ironstones, the Bahariya ore deposits provide a relative modern analogue for the banded iron formations (BIFs) that were abundant worldwide during the Precambrian. Thus, the Eocene succession is ideal for examination of the petrological and geochemical changes that occurred during the formation of cherty ironstones. Accordingly, the main chronostratigraphic, sedimentological, petrological, geochemical and diagenetic features shown by both the carbonates and the associated ore deposits were studied and the results published in two articles.

As the existing chronostratigraphic framework of the area was controversial, the first article (section 5.1) revises the stratigraphic attribution of the three Eocene stratigraphic units, i.e. Naqb, Qazzun and El Hamra formations, based on larger benthic foraminifers. The updated biostratigraphic and sedimentological schemes provided in the paper are critical to precise the timing of the mineralization. In addition, the dating of the ironstone strongly supports a post-depositional formation model for the ironstone.

Linking the mineralogy and geochemistry of the cherty ironstone deposits with the sedimentology of the associated carbonate rocks as well as with the tectonics and magmatism of the area, the second article (section 5.2) provides new insight into the origin of the cherty iron ore deposits in relation to hydrothermal processes. A paragenetic sequence, including the main processes and minerals, passing from the host carbonate rocks to the ore deposits is included in the article.

In addition, section 5.3 deals with unpublished results. These mainly deal with the geochemical characterization of the ore deposits and their associated minerals. All published and new data are placed together in the integrative model of formation presented in section 5.4.

5.1. Nummulite biostratigraphy of the Eocene succession in the Bahariya Depression, Egypt: Implications for timing of iron mineralization

A.M. Afify, J. Serra-Kiel, M.E. Sanz-Montero, J.P. Calvo, E.S. Sallam

Article published in:

***Journal of African Earth Sciences*, volume 120(2016), pages 44–55.**

doi:10.1016/j.jafrearsci.2016.04.016

5.1.1. The article
5.1.2. Conclusions from the article

5.1.1. The article

Journal of African Earth Sciences 120 (2016) 44–55

Contents lists available at ScienceDirect

Journal of African Earth Sciences

journal homepage: www.elsevier.com/locate/jafrearsci

Nummulite biostratigraphy of the Eocene succession in the Bahariya Depression, Egypt: Implications for timing of iron mineralization

A.M. Afify [a, b, *], J. Serra-Kiel [c], M.E. Sanz-Montero [a], J.P. Calvo [a], E.S. Sallam [b]

[a] Petrology and Geochemistry Department, Faculty of Geological Sciences, Complutense University, Madrid, C/ José Antonio Nováis, 2, 28040 Madrid, Spain
[b] Geology Department, Faculty of Science, Benha University, 13518 Benha, Egypt
[c] Stratigraphy, Paleontology and Marine Geosciences Department, University of Barcelona, C/ Martí i Franquès, s/n, 08028 Barcelona, Spain

ARTICLE INFO

Article history:
Received 2 February 2016
Received in revised form
14 April 2016
Accepted 19 April 2016
Available online 21 April 2016

Keywords:
Nummulites
Eocene carbonates
Ironstone
Chronostratigraphy
Western Desert
Central Egypt

ABSTRACT

In the northern part of the Bahariya Depression (Western Desert, Egypt) the Eocene carbonate succession, unconformably overlying the Cretaceous deposits, consists of three main stratigraphic units; the Naqb, Qazzun and El Hamra formations. The Eocene carbonates are relevant as they locally host a large economic iron mineralization. This work revises the stratigraphic attribution of the Eocene formations on the basis of larger benthic foraminifers from both carbonate and ironstone beds. Eight *Nummulites* species spanning the late Ypresian – early Bartonian (SBZ12 to SBZ17) were identified, thus refining the chronostratigraphic framework of the Eocene in that region of Central Egypt. Moreover, additional sedimentological insight of the Eocene carbonate rocks is presented. The carbonate deposits mainly represent shallow marine facies characteristic of inner to mid ramp settings; though deposits interpreted as intertidal to supratidal are locally recognized.

Dating of *Nummulites* assemblages from the youngest ironstone beds in the mines as early Bartonian provides crucial information on the timing of the hydrothermal and meteoric water processes resulting in the formation of the iron ore mineralization. The new data strongly support a post-depositional, structurally-controlled formation model for the ironstone mineralization of the Bahariya Depression.

1. Introduction

The Bahariya Depression is located near the central part of the Western Desert of Egypt (Fig. 1) where it shows elliptical geometry surrounded by a carbonate plateau mainly formed of Eocene rock units in its northern part. The Eocene stratigraphy, especially of the Middle to Upper Eocene formations in the Bahariya region has been a matter of dispute (Issawi et al., 2009). This was probably due to the lithostratigraphic variations and facies changes of the Eocene formations with respect to their equivalents outside the region as well as lack of agreement about the stratigraphic discontinuities between the exposed rock units in the area. Three Eocene rock units, the Naqb, Qazzun and El Hamra formations, were described exclusively for the Bahariya Depression by Said and Issawi (1964). These deposits have economic significance since they represent the host rock of the only ironstone mineralization currently exploited for steel industry in Egypt. Moreover, these ore deposits are unique along the Caenozoic palaeo-Tethyan shorelines in North Africa and South Europe (Salama et al., 2014) and can be interpreted as an analog for banded iron formations (BIFs) (Afify et al., 2015a,b). The origin of these deposits has also been a matter of scientific discussion for long time (e.g., El Shazly, 1962; El Akkad and Issawi, 1963; Said and Issawi, 1964; Basta and Amer, 1969; Dabous, 2002; Salama et al., 2013, 2014; Baioumy et al., 2014; Afify et al., 2014, 2015a,b). Despite this fact no much work was focused on the facies architecture and evolutionary pattern of the Eocene host rocks and their relation with the iron mineralization. Likewise, there is lack of detailed chronostratigraphic framework of the Eocene formations. In the classical papers on the geology of the region, e.g., Said and Issawi (1964), the age of the Naqb Formation was loosely attributed to the early Middle Eocene whereas the same rock unit was dated as upper Ypresian (middle Ilerdian-Cuisian) by Boukhary et al. (2011) on the basis of larger benthic foraminifera. The Qazzun Formation was attributed to the upper Middle Eocene without detailed biostratigraphic basis (Said and Issawi, 1964). This was also the case for El Hamra Formation,

* Corresponding author. Petrology and Geochemistry Department, Faculty of Geological Sciences, Complutense University, Madrid, C/ José Antonio Nováis, 2, 28040 Madrid, Spain.
E-mail address: adelmady@ucm.es (A.M. Afify).

http://dx.doi.org/10.1016/j.jafrearsci.2016.04.016
1464-343X/

5.1.2. Conclusions from the article

The Eocene stratigraphic succession exposed at the northern Bahariya study area consists of three rock units, the Naqb, Qazzun and El Hamra formations that mainly represent shallow marine facies characteristic of inner to mid ramp settings; though deposits interpreted as intertidal to supratidal are locally recognized. The Naqb Formation comprises two sedimentary sequences. The lower sequence is characterized by inner- to mid- ramp facies that passed upwardly into the intertidal-supratidal facies of the upper sequence. The carbonate facies of the Qazzun Formation reflects shallow water, high-energy conditions in a middle ramp setting whereas the carbonate and terrigenous facies of the El Hamra Formation are indicative of deep to shallow subtidal environments. The dominance of nummulite-rich banks in the lower unit of the El Hamra Formation reflects deep subtidal environments. The deposits of this unit represent shallowing upward conditions with dominance of oyster and gastropod banks. In the upper unit, occurrence of fossiliferous banks increases in combination with dominant glauconitic shallow marine facies.

The ore deposits retain largely many stratigraphic and sedimentary features of the associated carbonates, i.e. thickness, bedding, lateral and vertical sequential arrangement and fossil content, which provides strong evidence for the replacement of carbonates by Fe-Mn minerals and associated minerals.

Eight *Nummulites* species spanning the late Ypresian – early Bartonian (SBZ12 to SBZ17) were identified from the Eocene carbonate and ironstone rocks, thus updating the framework of the Eocene succession in that region of central Egypt.

The new biostratigraphic data allow to precise the chronology of the ore-forming processes as the ferruginized fossil assemblages indicate that their host carbonates span late Ypresian – early Bartonian. Therefore, the formation of the ore deposits can be dated later than early Bartonian, most probably during the Priabonian and before the Oligocene, which is supported by the fact that neither the Priabonian glauconitic claystones (upper unit of the El Hamra Formation) nor the Oligocene sandstones show iron replacement.

5.2. Ironstone deposits hosted in Eocene carbonates from Bahariya (Egypt)–New perspective on cherty ironstone occurrences

A.M. Afify, M.E. Sanz-Montero, J.P. Calvo

Article published in:

***Sedimentary Geology*, volume 329(2015), pages 81–97.**

http://dx.doi.org/10.1016/j.sedgeo.2015.09.010

5.2.1. The article
5.2.2. Conclusions from the article

5.2.1. The article

Sedimentary Geology 329 (2015) 81–97

Contents lists available at ScienceDirect

Sedimentary Geology

journal homepage: www.elsevier.com/locate/sedgeo

Ironstone deposits hosted in Eocene carbonates from Bahariya (Egypt)—New perspective on cherty ironstone occurrences

A.M. Afify [a,b,*], M.E. Sanz-Montero [a], J.P. Calvo [a]

[a] Department of Petrology and Geochemistry, Faculty of Geological Sciences, Complutense University, Madrid, C/ José Antonio Nováis, 2, 28040 Madrid, Spain
[b] Department of Geology, Faculty of Science, Benha University, 13518 Benha, Egypt

ARTICLE INFO

Article history:
Received 3 August 2015
Received in revised form 17 September 2015
Accepted 18 September 2015
Available online 26 September 2015

Editor: Dr. B. Jones

Keywords:
Cherty ironstone
Dolomitization
Tectonic constraints
Hydrothermalism
Eocene carbonates
Egypt

ABSTRACT

This paper gives new insight into the genesis of cherty ironstone deposits. The research was centered on well-exposed, unique cherty ironstone mineralization associated with Eocene carbonates from the northern part of the Bahariya Depression (Egypt). The economically important ironstones occur in the Naqb Formation (Early Eocene), which is mainly formed of shallow marine carbonate deposits. Periods of lowstand sea-level caused extensive early dissolution (karstification) of the depositional carbonates and dolomitization associated with mixing zones of fresh and marine pore-water. In faulted areas, the Eocene carbonate deposits were transformed into cherty ironstone with preservation of the precursor carbonate sedimentary features, i.e. skeletal and non-skeletal grain types, thickness, bedding, lateral and vertical sequential arrangement, and karst profiles. The ore deposits are composed of iron oxyhydroxides, mainly hematite and goethite, chert in the form of micro- to macro-quartz and chalcedony, various manganese minerals, barite, and a number of subordinate sulfate and clay minerals. Detailed petrographic analysis shows that quartz and iron oxides were coetaneous and selectively replaced carbonates, the coarse dolomite crystals having been preferentially transformed into quartz whereas the microcrystalline carbonates were replaced by the iron oxyhydroxides.
A number of petrographic, sedimentological and structural features including the presence of hydrothermal-mediated minerals (e.g., jacobsite), the geochemistry of the ore minerals as well as the structure-controlled location of the mineralization suggest a hydrothermal source for the ore-bearing fluids circulating through major faults and reflect their proximity to centers of magmatism. The proposed formation model can contribute to better understanding of the genetic mechanisms of formation of banded iron formations (BIFs) that were abundant during the Precambrian.

1. Introduction

The Eocene strata in northern Bahariya contain ironstone deposits of economic significance, some of them reaching a large size (Fig. 1). Despite significant research on these deposits (El Shazly, 1962; El Akkad and Issawi, 1963; Basta and Amer, 1969, and references therein), their origin is still a matter of debate. More recent publications show different and contrasting hypotheses for the source and mechanisms of formation of the Bahariya ironstones. Dabous (2002) concluded that the Bahariya ironstone deposits are not lateritic and that their formation was related to mixing of warm ascending groundwater leaching iron from the underlying Nubia aquifers and descending water with iron leached from the overlying Upper Eocene–Lower Oligocene glauconitic clays. Salama et al. (2013, 2014) concluded that the Bahariya ironstones were deposited primarily in a marine setting and their formation was enhanced by microbial activity. They related the formation of the ironstone to global warming during the early Paleogene, closely associated with eustatic sea-level changes. Recent work by Baioumy et al. (2013, 2014) supports sources and mechanisms of iron and manganese formations that are contradictory: supergenetic ore deposits (most probably from the Naqb limestone host rock) or hydrogenous iron mixed with iron of hydrothermal origin (sea water precipitation to hydrothermal exhalite).

New insight based on field, petrographic, mineralogical and geochemical studies of the ironstone deposits in the northern part of the Bahariya Depression (Fig. 1) is provided in this paper. The similarities between the ironstones and carbonate host rocks as well as the close relationship between the ore mineral body and the regional tectonic structure led us to revisit the models proposed for the formation of ironstone deposits of Bahariya. Moreover, the scarcity of Phanerozoic, in particular Cenozoic cherty ironstone makes the Bahariya ore deposits an interesting case study to investigate some new perspectives about the formation constraints of these kinds of rocks. It can help also in understanding the mechanisms of older iron-rich deposits where chert is an important constituent. In the study area, iron is paired with quartz formation, this resulting in sedimentary structures that resemble

* Corresponding author at: Department of Petrology and Geochemistry, Faculty of Geological Sciences, Complutense University, Madrid, C/ José Antonio Nováis, 2, 28040 Madrid, Spain.
E-mail address: adelmady@ucm.es (A.M. Afify).

http://dx.doi.org/10.1016/j.sedgeo.2015.09.010
0037-0738/

5.2.2. Conclusions from the article

In this paper, we focus on the sedimentology and tectonic controls on the formation of cherty ironstones hosted in the Eocene carbonates, especially the carbonates of the Naqb Formation. The Naqb Formation deposited on a shallow-water platform where intertidal, shallow subtidal and oolitic shoal facies are recognized. This rock unit is composed of two carbonate sequences separated by a paleokarstic surface. The carbonate sequences underwent extensive diagenetic processes, the most important of which are micritization, fabric retentive dolomitization and karstification. Periods of lowstand sea level caused extensive early dissolution (karstification) of the depositional carbonates and dolomitization processes likely associated with mixing zones of fresh and marine pore-water.

The Naqb Formation was totally replaced and/or cemented spatially by iron-bearing minerals and/or quartz nearby the major faults that affected the area. With increasing distance to the faults, the mineralization occurs just along the major sedimentary discontinuities. Outside the faulted areas, the carbonates do not show replacement, although pigmentation and staining by iron is a prominent feature. The depositional (facies and structures) as well as the karstic features (dissolution, brecciation, etc.) shown by the carbonates are recognizable in the ore deposits. Quartz, manganese minerals, barite and others, are commonly associated with the iron mineral phases.

Quartz formed micro and meso crystalline mosaics and chalcedonite aggregates in secondary porosity (mainly in moldic pores) as well as in sedimentary discontinuities. Petrographic analysis reveals that quartz and iron oxides were coetaneous and selectively replaced carbonates. The coarse dolomite crystals transformed preferentially into quartz whereas iron minerals replaced the microcrystalline carbonates.

Based on these results, a new post-depositional hydrothermal model is provided to elucidate the genetic mechanisms of the cherty ironstones. The ironstone deposits were interpreted as a replacement product due to dissolution of specialized rocks (dolomites) followed by precipitation of iron minerals and silica through structural and sedimentological

discontinuities. The formation of these deposits resulted from abundant silica and iron-rich fluids under acidic conditions mixed with meteoric oxidizing water. The proposed formation model can contribute to better understanding of the genetic mechanisms of formation of the Precambrian banded iron formations (BIFs).

5.3. Additional data

5.3.1. Mineralogy and petrology
5.3.2. Major and trace elements geochemistry
5.3.3. Rare earth elements and yttrium (REY) geochemistry
5.3.4. Sulfur and oxygen isotope geochemistry
5.3.5. Fluid inclusions geochemistry

5.3.1. Mineralogy and petrology

Ferromanganese minerals, quartz, phosphates, sulfates and clay minerals are dominant in the ore deposits. Those minerals preserve the main structures and microfacies of the associated carbonates.

Ferromanganese minerals: Goethite and hematite are the main components of the ironstone rocks. As seen under SEM (Fig. 5.3.1), they show a variety of morphologies mainly, tabular, platy, rosette-like, acicular, fibrous fibro-radiating, tubular, cubic, amorphous, shrub, and some show bacterial-like morphologies (filaments, globules and cocci and bacilli) and mostly of colloidal and reiniform aggregates (Fig. 5.3.1A–J). Likewise, they preserve the dolomite morphology of the precursor Naqb Formation whereas hematite was recorded mostly preserving pyrite pseudomorphs at El Gedida area (Fig. 5.3.1E, F). Meanwhile, the manganese minerals are dominant in the lowermost part of the ironstone succession (Afify et al., 2015b). They consist mainly of pyrolusite, jacobsite, psilomelane, romanechite, and todorokite (see chemical formula in Table 1.1). Mn-bearing minerals mostly occur as pore-filling crystals showing different morphologies, e.g., acicular, platy, amorphous and flakey (Fig. 5.3.1K, L).

Morphology of the ferromanganese minerals modified depending on the nature and type of the host rocks. The Fe-Mn minerals are well crystalline in the lower part of the ironstone succession forming tabular and platy textures, whereas they are acicular, micro-globular and amorphous where associated with quartz. The fibro-radiating fibrous, rosette-like and globular types occur in the highly karstified parts of the Naqb Formation at the Ghorabi and El Harra areas. The tubular morphologies form the pisolithic fabrics. Details about these ferromanganese minerals were described in a previous paper by Afify et al. (2015b).

Silica: The term silica is used here for the quartz mineral present in the ore deposits as amorphous silica, micro-quartz, mega-quartz and or chalcedony. Except for the occurrence of the decimeter-sized silica boulders and concretions, detailed description about the silica and its distribution was included in Afify et al. (2015b). The boulders (up to 50 cm in diameter: see Fig. 3.4D, E), are found isolated on the plateau surface along the major faults, thus nearby the mine areas. They consist of microcrystalline quartz with dolomite relics.

Phosphate minerals: Apatite-fluorapatite crystals occur as well-crystallized hexagonal prisms associated with filamentous goethite in secondary pores developed in a black hematitic type (Fig. 5.3.1M). These crystals occur only in the lower part of the ironstone succession at El Gedida mine.

Sulfate minerals: The main sulfate minerals associated with the iron mineralization are barite, jarosite, alunite, and subordinate gypsum and anhydrite. Barite occurs mainly through the faulted areas forming euhedral large crystals up to 5 cm in length, commonly showing concentric zoning (Fig. 5.3.2A–D). Barite occurs as poikilotopic cement, euhedral disseminated crystals, elongated parallel-bedded crystals and/or rosette-like crystals filling pores (Fig. 5.3.3A, B). Other type of barite forms up to 2 cm in size clusters of tabular crystals and/or elongated radial aggregates (Fig. 5.3.3B).

Alunite and jarosite sulfate minerals were recorded as irregular to lenticular bodies associated with amorphous silica and kaolinite below the pisolithic ironstones (upper part of the mineralization) at El Gedida (Fig. 5.3.2E, F). Few gypsum, anhydrite and some halite occur as recent pore filling evaporate minerals in the ore deposits.

Carbonate minerals: The carbonate minerals occurring in the ironstones are calcite and dolomite. Dolomite is present in the Naqb Formation as crystalline rhombic aggregates mainly replaced by iron and silica forming pseudomorphs and ghosts (Afify et al., 2015b). Likewise, big crystals (up to 700 µm) of calcite cements, arranged as speleothems, occur in the ironstone succession.

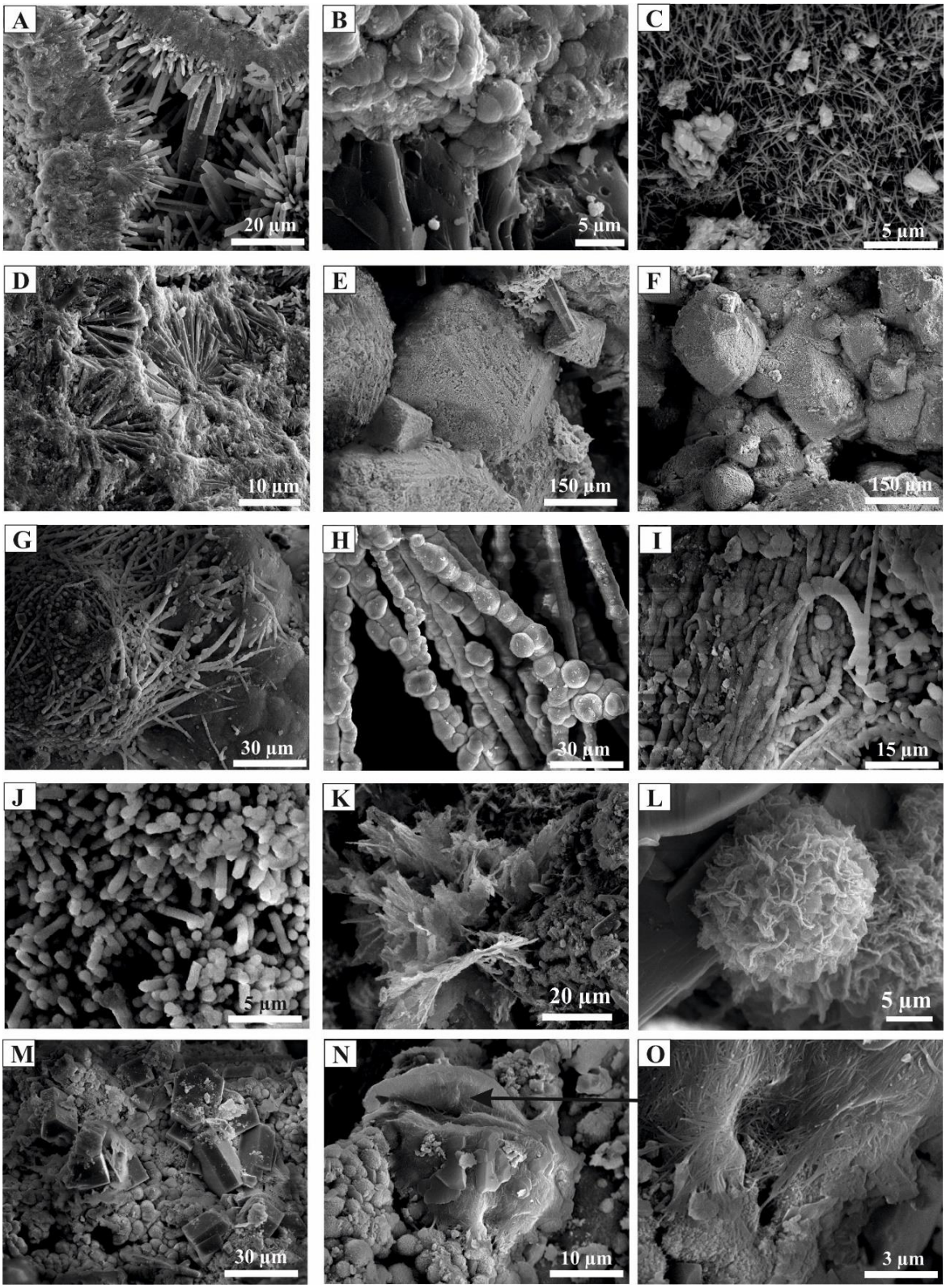

Figure 5.3.1. SEM photos of the iron-bearing minerals and their associated minerals showing a variety of morphologies and habits. A) Tabular, B) Globular, C) Acicular, D) Fibro-radiating iron oxyhydroxides. E), F) Pseudomorphs of iron oxyhydroxides mostly after pyrite cubic crystals, with few prismatic goethite, G), H), I) Filamentous-like goethite, J) Cocci and bacilli-like goethite, K), L) Flakey pore-filling todorokite and psilomelane, respectively, M) Well crystallized apatite crystals associated with micro-globular goethite, N), O) Pore-filling palygorskite (EDAX with Mg, Si and high amount of Al).

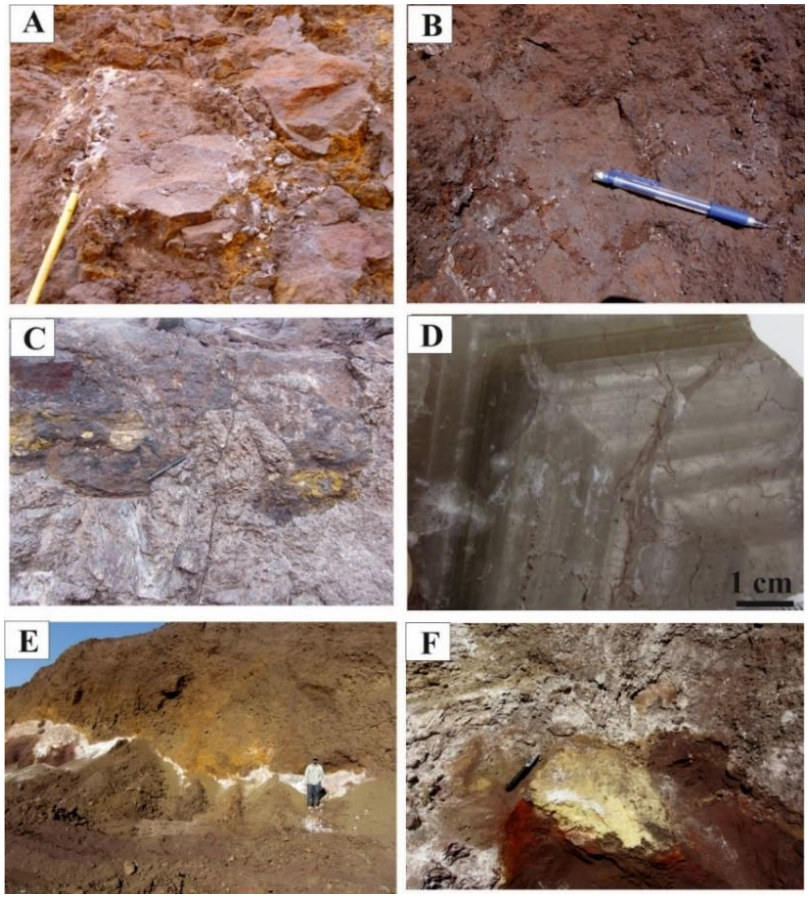

Figure 5.3.2. Outcrop views and petrography of sulfate minerals associated with the ironstone deposits where A) Fracture filling barite, B) Disseminated barite, and C) A cave in ironstone bed infilled with barite (lower part). D) Concentric zoned barite. E) Irregular thin bed composed of alunite, jarosite and amorphous silica underlying friable limonitic pisolithic ironstones. F) Lenticular body of yellow jarosite associated with scattered alunite within the iron oxyhydroxide groundmass at the El Gedida area.

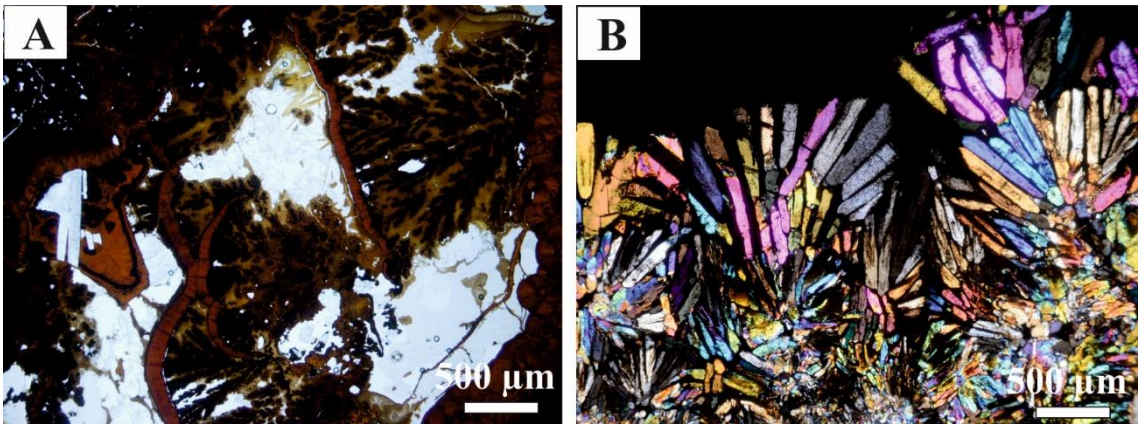

Figure 5.3.3. Photomicrographs of barite associated with the mineralization, A) Scattered and large poikilotopic barite crystals enclosing former minerals. B) Rosette-like radiating longitudinal barite crystals in the ironstone deposits (top of the photo represent the upward direction of the sample).

Clay minerals: The most abundant clays recorded using XRD, EMPA and SEM studies within the ironstones in the form of thin beds or rarely as pore-

filling minerals are smectite, illite/smectite (I/S) mixed-layers, kaolinite and palygorskite. Smectite and I/S mixed-layers were recorded mainly at the lower part of the ironstone succession (Fig. 5.3.4). The same clay association forms a thin clay bed at the paleokarst surface separating the lower and upper sequences of the Naqb Formation. Palygorskite, as pore-filling fibrous crystals (Fig. 5.3.1N, O), was found within El Gedida ironstones.

5.3.2. Major and trace elements geochemistry

The geochemical characterization of the ironstones was performed by X-ray fluorescence (Table 5.3.1) as well as by electron microprobe analyses (Table 5.3.2).

The whole-rock analyses show that the ironstone deposits are composed of up to 99 wt.% Fe_2O_3 and up to 8 wt.% MnO (Table 5.3.1). Manganese oxide increases in the lowermost part of the ironstone succession forming manganiferous ironstones (Fig. 5.3.5; Table 5.3.1). The silica content increases in the more porous (fossiliferous facies) reaching up to 76 wt.%. The studied ironstone samples show very low content of Al_2O_3, Na_2O and K_2O with the exception of bodies containing clay minerals (Table 5.3.1). SiO_2 and Al_2O_3 show negative correlation with Fe_2O_3 and MnO contents (Fig. 5.3.5) especially in the rocks displaying more abundant dissolution features, i.e. oolitic silicified ironstone. The ironstone samples are relatively rich in trace elements. Zn, Ni, Sr elements show the higher concentrations (1138.2 ppm, 719 ppm, 686 ppm maximum values respectively). These samples show depletion in detrital-derived elements, e.g., Zr, Nb, and likewise have low concentration of As and Cr (Table 5.3.1).

Table 5.3.2 shows the microprobe point analysis of five mineral groups: pure iron oxyhydroxides (e.g., goethite, hematite), Mn-rich iron oxyhydroxides (e.g., Mn-goethite), Mn, Mg-rich iron oxyhydroxides (e.g., Mn-, Mg-goethite), Fe, pure and Mg-rich manganese oxides (e.g., pyrolusite, manganite, jacobsite), and Ba-rich manganese oxides (e.g., romanechite, psilomelane, todorokite).

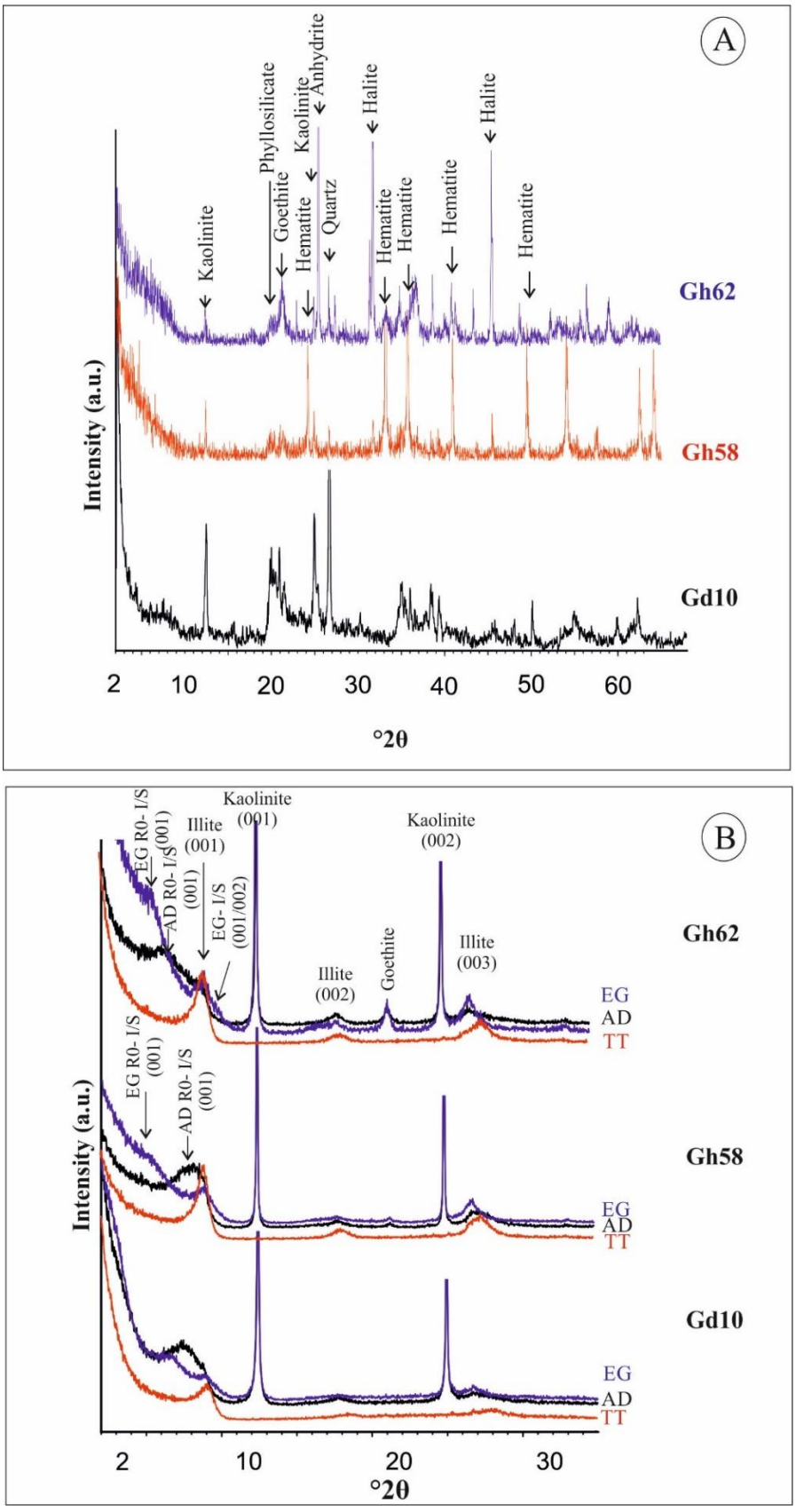

Figure 5.3.4. XRD diffractograms showing the bulk mineralogy of the clay-rich samples (A) and their clay mineralogy (B) in the Eocene ironstone deposits at the mine areas (Gh – Ghorabi samples, Gd – El Gedida samples).

Samples & Rock Types	Gh57	Gh74	Hr6	Gd5	Gd42	Gh61	Gh92	Hr7	Gh83	Gh65	Gh84	Gh89	Gh100	Gd12	Gd46	Gd62
Composition	Manganiferous ironstone					Oolitic, fossiliferous ironstone			Non-fossiliferous brecciated ironstone	Stromatolitic ironstone				Pisolitic and fossiliferous ironstone		
Major oxides (wt.%)																
SiO_2	bdl	bdl	bdl	bdl	0.97	19.28	51.08	75.65	bdl	bdl	bdl	bdl	bdl	bdl	bdl	62.52
Na_2O	1.14	0.99	1.04	0.95	0.89	1.02	0.89	0.82	0.94	1.24	0.87	0.88	0.92	0.84	1.44	1.55
MgO	0.66	0.52	0.40	0.38	0.38	0.68	0.39	0.38	0.48	0.54	0.40	0.55	0.52	0.40	0.32	0.29
Al_2O_3	2.56	2.58	2.69	2.51	2.76	2.49	2.49	2.49	2.49	2.62	2.71	3.04	4.22	3.43	2.60	2.49
P_2O_5	0.14	bdl	0.06	0.41	0.72	bdl	0.18	bdl	bdl	0.25	0.15	0.14	0.40	0.64	0.25	0.45
K_2O	bdl	bdl	bdl	bdl	0.42	bdl	bdl	bdl	0.09	bdl	bdl	bdl	0.03	bdl	bdl	bdl
CaO	bdl	0.03	bdl	bdl	bdl	0.70	0.73	bdl	0.33	22.20	0.40	1.24	0.51	bdl	0.02	2.65
TiO_2	0.11	0.05	0.07	0.10	bdl	0.03	0.01	0.04	0.39	0.16	0.07	0.73	0.36	bdl	0.63	0.20
MnO	6.81	6.86	2.38	1.34	0.59	3.40	0.38	0.34	7.66	0.43	0.85	0.67	0.73	0.50	4.48	0.20
Fe_2O_3	78.34	91.52	99.89	99.04	92.98	44.45	35.76	16.08	76.90	57.25	96.99	87.36	95.47	98.38	84.28	14.86
Trace elements (exclusive of REE and Y) (ppm)																
Cr	bdl	bdl	bdl	bdl	bdl	bdl	bdl	bdl	bdl	bdl	bdl	bdl	bdl	bdl	bdl	bdl
Ni	541.6	645.6	719.2	705.1	678.4	232.4	145.7	52.2	503.1	229.0	676.9	517.0	608.8	725.7	499.9	37.5
Cu	28	bdl	19.3	21.9	10.9	15.2	14.0	12.8	16.1	5.0	18.1	12.9	13.8	bdl	bdl	11.6
Zn	272.5	555.0	913.1	548.5	383.5	147.8	97.0	45.0	382.3	331.1	237.4	653.4	778.1	214.7	1138.2	148.1
As	3.0	3.0	45.3	4.9	25.6	7.6	20.4	24.1	4.6	8.7	3.0	10.4	12.6	39.3	49.5	13.2
Rb	312	393	473	492	439	127	81	16	299	147	488	399	459	486	361	15
Sr	293	304	414	219	198	150	82	21	335	197	230	221	305	504	224	686
Zr	bdl	bdl	bdl	bdl	bdl	bdl	bdl	bdl	bdl	30	bdl	bdl	bdl	bdl	bdl	78
Nb	6.0	9.7	7.7	8.3	3.8	6.6	6.6	3.8	3.8	3.8	5.1	3.8	17.4	3.8	7.7	9.2
Pb	434	510	492	521	410	167	81	74	414	20	504	419	457	444	420	15
S	669	397	1307	785	2092	621	2605	429	470	bdl	1496	2105	2113	586	436	bdl

*bdl: below detection limit

Table 5.3.1. Major oxides (in wt.%) and trace elements (in ppm) of selected bulk ironstone samples determined by XRF (Gh – Ghorabi mine samples, Gd – El Gedida mine samples, Hr – El Harra mine samples).

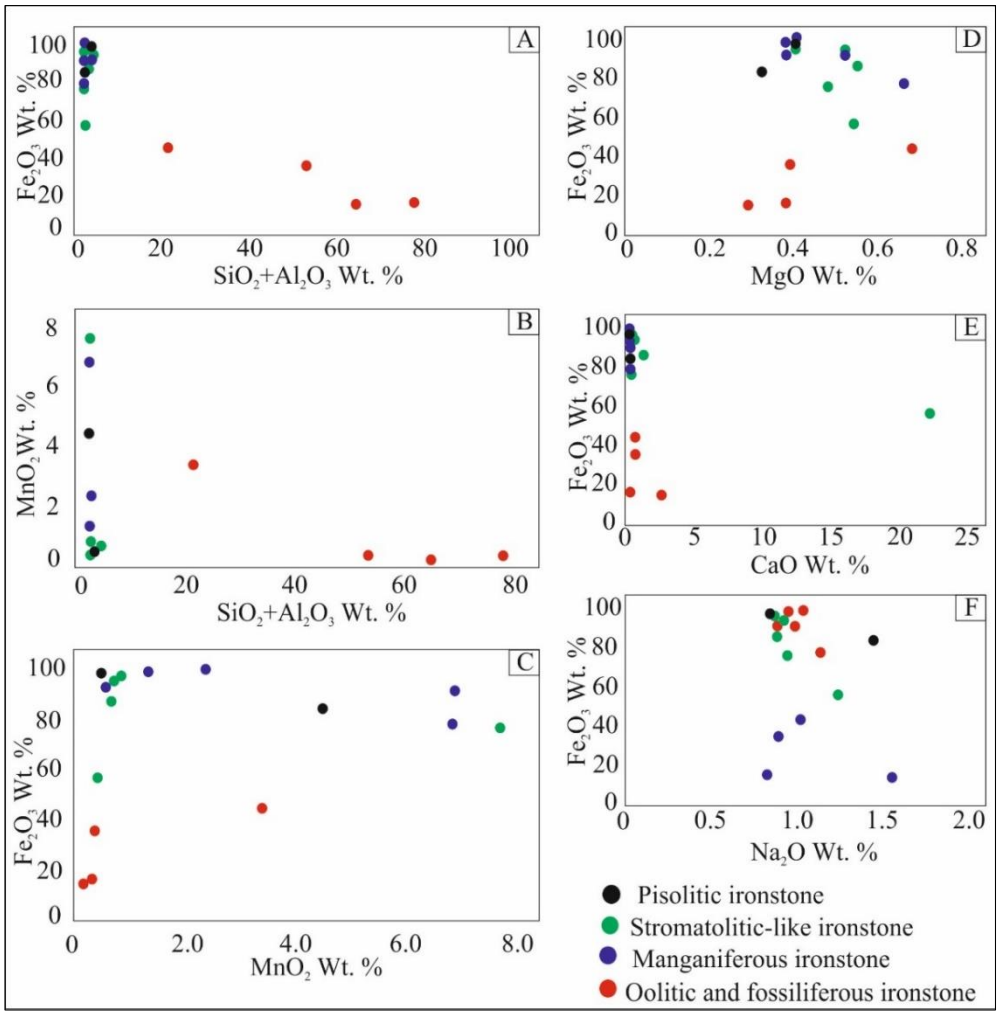

Figure 5.3.5. Bivariate graphs of major oxides in the different ironstone types (manganiferous ironstone, oolitic and fossiliferous ironstone, stromatolitic-like ironstone and pisolithic ironstone) determined by XRF analysis.

The three recognized groups of iron oxyhydroxides show variable ranges of Fe_2O_3 (36 - 83 wt.%), MnO (0.05 - 8.3 wt.%) and MgO (0 - 4 wt.%). The SiO_2 and Al_2O_3 contents do not exceed 5.4 wt.% and 2.5 wt.%, respectively (Fig. 5.3.6). Na_2O, K_2O and CaO contents do not exceed 1.3 wt.% and show the highest values where contaminated with clays and carbonates. Phosphorous content is very low and does not exceed 0.5 wt.%. Likewise, the manganese minerals contain up to 77 wt.% MnO, up to 40 wt.% Fe_2O_3, up to 12 wt.% MgO and up to10 wt.% BaO (Table 5.3.2). MgO shows positive correlation with MnO, especially in the lowermost part of the ironstone succession forming jacobsite and Mn-, Mg- goethite. In these minerals, Mn content increases on the expense of Fe content (Fig. 5.3.6).

Chemical composition		SiO_2	Al_2O_3	FeO	MnO	MgO	CaO	Na_2O	K_2O	TiO_2	P_2O_5	SO_3	BaO
Minerals	Points												
Iron oxyhydroxides	1	0.524	0.193	82.973	0.056	0.019	0.06	0.07	0.011	bdl	0.227	0.417	0.004
	2	0.106	0.041	80.468	1.591	0.373	0.089	0.017	bdl	0.023	0.070	0.672	0.039
	3	1.705	0.359	74.202	0.113	0.295	0.044	0.03	0.009	0.028	0.125	0.003	0.009
	4	1.089	1.38	70.051	0.122	0.33	0.108	0.156	0.016	0.041	2.317	bdl	0.074
	5	1.356	1.901	69.804	0.063	0.266	0.104	0.06	0.027	bdl	2.159	0.017	0.6
	6	1.155	1.067	57.533	0.073	0.283	0.035	0.059	0.02	0.211	0.894	0.211	bdl
	7	2.093	1.162	69.112	0.032	0.304	0.044	0.018	0.02	0.227	1.043	0.154	0.031
	8	4.765	2.523	66.703	0.103	3.269	0.313	0.098	0.015	0.318	0.893	0.123	0.023
	9	5.428	2.968	65.017	0.140	3.611	0.235	0.045	0.012	0.271	0.824	0.031	0.132
	10	1.663	1.195	67.382	0.174	0.329	0.033	0.105	0.04	0.234	0.959	0.210	bdl
Mn-rich iron oxyhydroxides	11	1.022	0.814	69.786	2.262	0.219	0.139	0.075	0.009	0.028	0.176	0.68	0.102
	12	1.229	1.078	68.319	2.153	0.208	0.149	0.029	bdl	0.041	0.191	0.641	0.217
	13	0.652	0.391	70.294	8.319	0.485	0.287	0.092	0.004	bdl	0.007	0.165	0.201
	14	0.984	0.437	72.893	3.218	0.404	0.203	0.032	0.012	0.024	0.486	0.251	0.114
	15	0.183	0.316	48.448	7.572	0.554	0.274	1.398	0.667	bdl	0.006	0.900	0.097
Mn, Mg-rich iron oxyhydroxides	16	0.004	bdl	38.89	4.942	10.47	0.704	0.084	bdl	0.037	0.093	0.032	0.251
	17	Bdl	0.001	37.279	4.577	11.426	1.296	0.047	0.021	0.033	0.025	0.008	0.247
	18	0.014	0.007	37.259	5.144	11.648	1.259	0.004	bdl	0.010	0.029	bdl	0.396
	19	0.098	0.058	36.242	5.291	13.548	1.408	0.011	0.001	bdl	0.026	0.020	0.030
	20	Bdl	Bdl	36.55	5.238	11.44	1.434	0.103	0.019	bdl	0.028	0.035	0.121
	21	Bdl	0.043	37.124	5.234	11.306	1.460	0.52	bdl	0.059	0.061	0.024	0.553
	22	0.567	0.823	52.472	23.62	0.246	0.242	0.092	0.01	0.033	0.012	0.143	0.113
Fe, Mg-rich manganese oxides	23	0.093	0.231	5.245	46.907	6.581	0.438	0.410	0.331	0.04	bdl	0.216	0.299
	24	0.009	1.007	1.602	50.357	8.169	0.214	0.190	0.277	0.031	bdl	0.124	0.189
	25	0.898	0.256	20.793	58.341	2.187	0.378	0.154	0.026	0.117	0.013	0.060	0.112
	26	0.531	0.414	1.844	76.998	0.071	0.381	0.079	0.023	0.005	0.035	0.027	0.084
Ba-rich ferromanganese oxides	27	0.486	0.565	23.686	47.412	0.263	0.312	0.359	0.627	0.449	0.230	0.265	8.607
	28	0.741	1.273	40.588	32.468	0.215	0.242	0.204	0.558	0.303	0.153	0.441	5.554
	29	0.577	3.745	41.888	26.861	0.319	0.291	0.383	0.445	0.237	0.145	0.507	3.889
	30	0.618	0.552	35.727	37.439	0.298	0.304	0.212	0.374	0.354	0.283	0.286	7.013
	31	0.099	1.039	3.259	64.956	0.833	0.578	0.586	1.170	0.473	0.151	0.101	9.552

*bdl: below detection limit

Table 5.3.2. Major element composition of selected ferromanganese minerals from different rock types using EMPA (in wt.%).

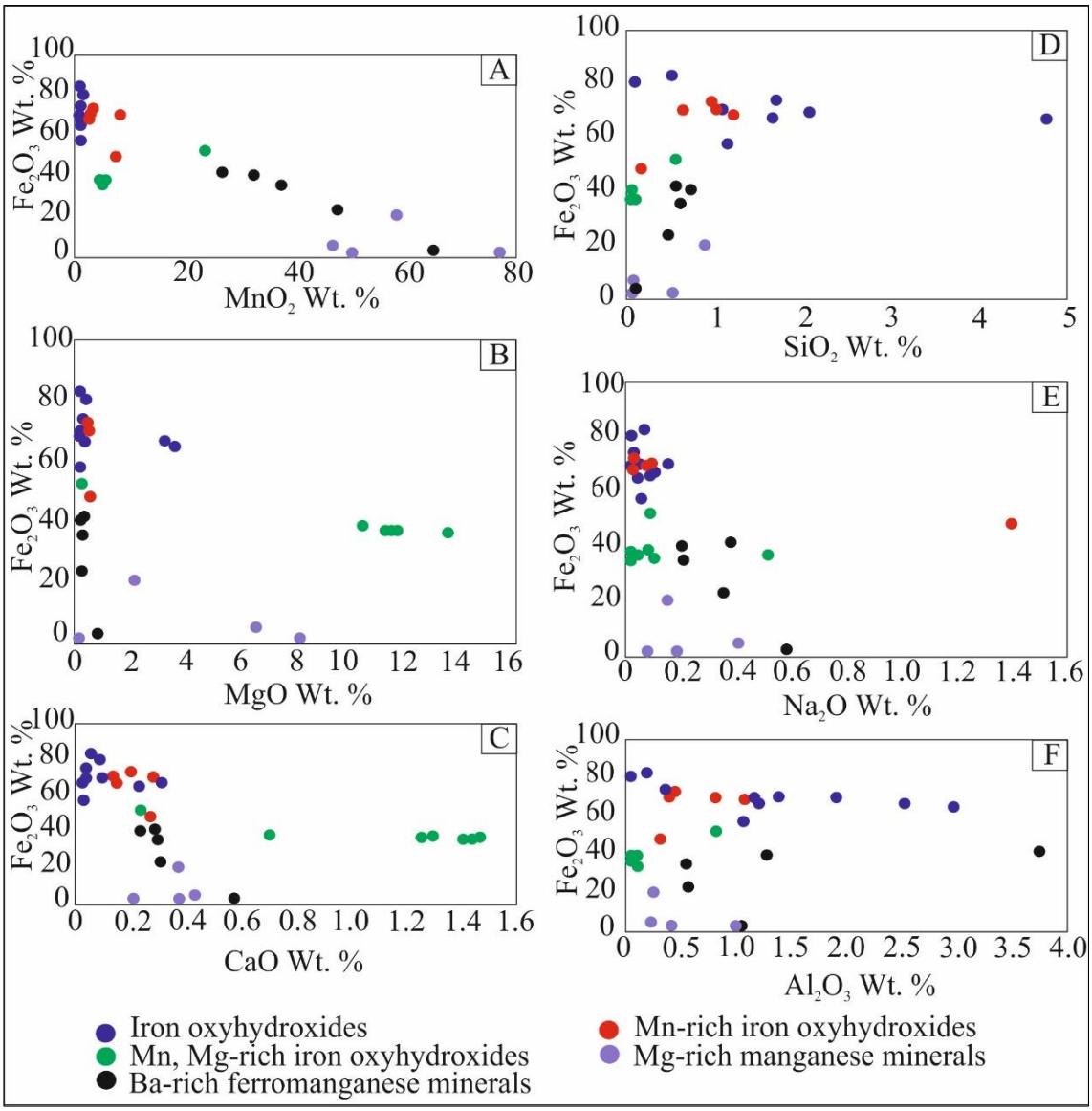

Figure 5.3.6. Correlation between the major oxides (determined by EMPA) in the five types of minerals present in the Eocene ironstones.

5.3.3. Rare earth elements and yttrium (REY) geochemistry

Rare earth elements and yttrium (REY) geochemical analyses were normalized to Post Archean Australian Shale (PAAS; McLennan, 1989). The distribution and abundance of rare earth elements and yttrium (REY) were studied in different ironstone rock types from the three mines. Results are shown in Table 5.3.3 and plotted in Figure 5.3.7. On the PAAS-normalized

spidergrams (Fig. 5.3.7), it is seen that the selected types of ironstone show different LREE (light rare earth elements) patterns. All the studied ironstone samples show enrichment in light rare earth elements (LREE) when compared with the heavy rare earth elements (HREE). The normalized REY patterns of the ironstone samples show an initial drop from La to Ce followed by a rise from the Ce minimum to the Eu maximum, then slight decrease towards a Lu minimum occurs in most of the samples (Fig. 5.3.7). The total concentration of REE in the ironstones is very low ranging between 1.96 ppm to 31.17 ppm (average 17.5 ppm) except in two samples in El Gedida (89.45, 60.67 ppm) and one sample from the Ghorabi (48.45 ppm) (Table 5.3.3). The higher concentrations (89.45, 60.67 ppm) occur in the manganiferous and pisolithic ironstone (lowermost part and topmost part of the ironstone succession) at the El Gedida area and in the stromatolitic-like ironstone at the Ghorabi area (48.45). The lower concentrations, ranging between 1.97 and 6.85 ppm, occur in the silicified ironstone samples (oolitic facies). Most of the samples show Ce depletion and some show evident in enrichment, e.g. Gh83.

Relationships between Ce-REE and Y-REE are relevant because Ce and Y produce the most significant anomalies in patterns of REY partition coefficients and normalized REY concentrations (Bau et al., 2014). Graphs showing Ce anomaly against Nd concentration and Ce anomaly against Y normalized values are included in Figure 5.3.8.

When represented in a bivariate diagram of Ce/Ce* ratio against the Nd concentration (Fig. 5.3.8A), all the samples are characterized by negative to no Ce anomaly. The Nd concentration is low (less than 10 ppm), with values in the range 0.39 to 8.2 except one sample where the Nd concentration reaches up to 13.0 ppm. In a bivariate diagram of Ce/Ce* ratio against Y_{SN}/Ho_{SN} ratio (Fig. 5.3.8B), the samples show mostly positive Y_{SN} anomaly ($Y_{SN}/Ho_{SN} \geq 1$) and negative Ce anomaly.

Samples & Rock Types	Gh57	Gh74	Hr6	Gd5	Gd42	Gh61	Gh92	Hr7	Gh83	Gh65	Gh84	Gh89	Gh100	Gd12	Gd46	Gd62
Composition	Manganiferous ironstone					Oolitic, fossiliferous ironstone			Non-fossiliferous brecciated ironstone	Stromatolitic ironstone				Pisolithic and fossiliferous ironstone		
	REE (ppm)															
Sc	1.0	0.35	1.3	0.27	1.6	0.41	0.24	1.5	0.44	0.55	1.0	0.46	4.8	2.4	1.0	2.2
Y	19	7.5	14	4.3	10.4	6.3	1.5	2.0	5.2	4.8	11	5.0	4.5	18	5.4	3.1
La	2.0	2.6	2.0	1.06	41	1.20	0.24	0.45	2.5	2.3	3.5	4.9	13	10.4	1.15	5.4
Ce	3.0	2.5	5.2	1.75	29	1.23	0.52	0.75	7.3	4.1	6.7	5.0	21	19	2.8	12.4
Pr	0.51	0.37	0.70	0.22	3.6	0.29	0.08	0.08	0.91	0.55	1.0	0.78	2.1	3.2	0.38	1.7
Nd	2.5	1.5	2.7	0.99	8.2	1.5	0.39	0.37	4.0	2.2	4.6	2.8	7.3	13.0	1.69	6.7
Sm	1.10	0.28	0.61	0.31	1.2	0.33	0.10	0.10	0.95	0.47	1.1	0.52	1.3	2.8	0.48	1.3
Eu	0.43	0.09	0.20	0.11	0.31	0.11	0.05	0.05	0.31	0.14	0.33	0.17	0.32	0.72	0.28	0.38
Gd	2.6	0.54	1.24	0.63	1.5	0.60	0.19	0.21	1,12	0.64	1.5	0.62	1.14	3.4	0.80	1.5
Tb	0.44	0.09	0.18	0.1	0.25	0.08	0.03	0.04	0.16	0.10	0.25	0.09	0.16	0.49	0.12	0.18
Dy	2.7	0.55	1.2	0.58	1.6	0.56	0.15	0.22	0.92	0.62	1.6	0.54	0.89	3.0	0.69	0.90
Ho	0.59	0.15	0.32	0.14	0.37	0.14	0.04	0.05	0.20	0.15	0.34	0.13	0.18	0.64	0.15	0.15
Er	1.43	0.37	0.83	0.33	1.03	0.41	0.08	0.15	0.47	0.38	0.86	0.32	0.46	1.8	0.36	0.30
Tm	0.18	0.05	0.09	0.04	0.16	0.06	0.02	0.02	0.06	0.05	0.10	0.05	0.07	0.26	0.05	0.05
Yb	1.07	0.23	0.46	0.20	1.07	0.31	0.06	0.10	0.35	0.32	0.54	0.22	0.46	1.7	0.24	0.18
Lu	0.14	0.03	0.08	0.03	0.16	0.03	0.01	0.01	0.04	0,04	0.07	0,03	0.07	0.26	0.03	0.03
ΣREE	18.69	9.35	15.81	6.49	89.45	6.85	1.96	2.60	19.29	12.06	22.49	16.17	48.45	60.67	9.22	31.17
LREE	12.14	7.88	12.65	5.07	84.81	5.26	1.57	2.01	17.09	10.4	18.73	14.79	46.16	52.52	7.58	29.38
HREE	6.55	1.47	3.16	1.42	4.64	1.59	0.39	0.59	2.20	1.66	3.76	1.38	2.29	8.15	1.64	1.79
ΔEu	1.053	1.002	0.985	1.066	1.067	1.082	1.575	1.468	1.395	1.168	1.175	1.388	1.238	1.080	2.009	1.265
ΔCe	0.685	0.571	0.993	0.835	0.492	0.482	0.852	0.904	1.089	0.841	0.822	0.580	0.913	0.752	0.962	0.933
ΔPr	1.037	1.108	1.094	0.974	1.345	1.100	1.005	0.891	0.983	1.070	1.030	1.215	0.993	1.165	1.012	1.090
ΔLa	2.031	1.829	0.667	1.698	1.452	3.131	1.506	2.201	0.894	1.055	1.340	1.285	1.203	0.850	1.024	0.776
Y_N/Ho_N	1.182	1.835	1.606	1.127	1.032	1.652	1.376	1.468	0.954	1.175	1.188	1.412	0.918	1.032	1.321	0.759

Table 5.3.3. REE content in different ironstone types recorded in the three mine areas using ICP/MS. The different anomalies are PAAS (Post Archean Australian Shale) normalized (Gh – Ghorabi mine samples, Gd – El Gedida mine samples, Hr – El Harra mine samples).

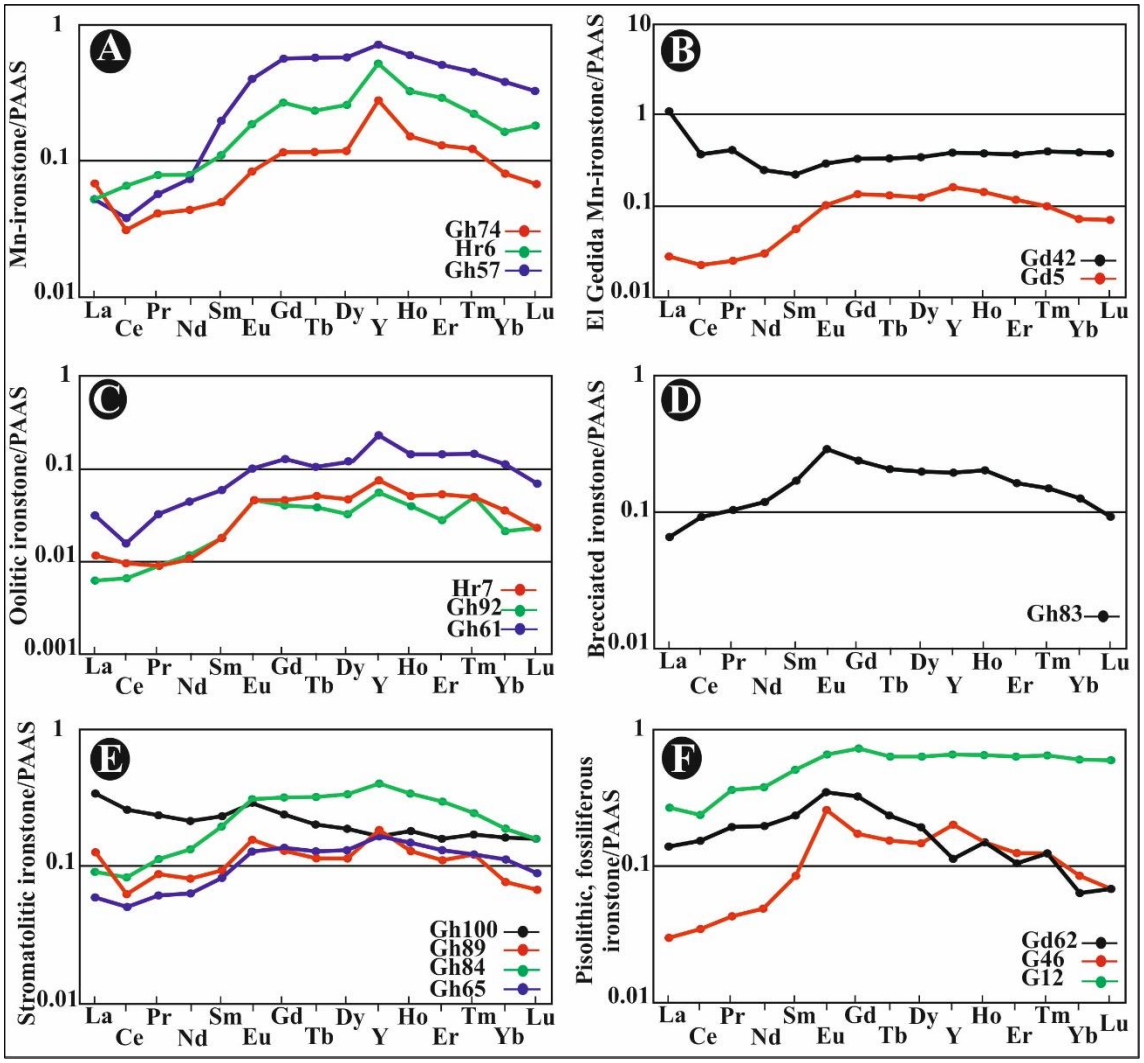

Figure 5.3.7. REY distribution patterns of six types of Eocene ironstones, PAAS-normalized (McLennan, 1989).

5.3.4. Sulfur and oxygen isotope geochemistry

Sulfur and oxygen isotope data ($\delta^{34}S$ and $\delta^{18}O$ (SO_4)) were obtained from barite, jarosite and alunite (Table 5.3.4). Six purified barite crystals selected for sulfur and oxygen isotope analyses displayed values of 12.1–21.1‰ for $\delta^{34}S$ and 13.66–17.14‰ for $\delta^{18}O$ (Fig. 5.3.9). Likewise, five drilled points in concentric zoned barite crystal were studied for sulfur and oxygen isotopes (Fig. 5.3.9). The isotope data of these white and dark zones (see Fig. 5.3.2 for structure of zoned barite) show slight similarities displaying values of 17.5–22.4‰ for $\delta^{34}S$ and 12.9–16.4‰ for $\delta^{18}O$. The sulfur and oxygen isotope

data of the barite crystals show positive correlation. The $\delta^{34}S$ values contrast markedly with isotopic composition values for two jarosite samples (-22.1‰ and -33.3‰) and one alunite sample (-16.8‰). The $\delta^{18}O$ values are 17.45‰ (alunite), 12.45‰ (jarosite), 5.40‰ (jarosite).

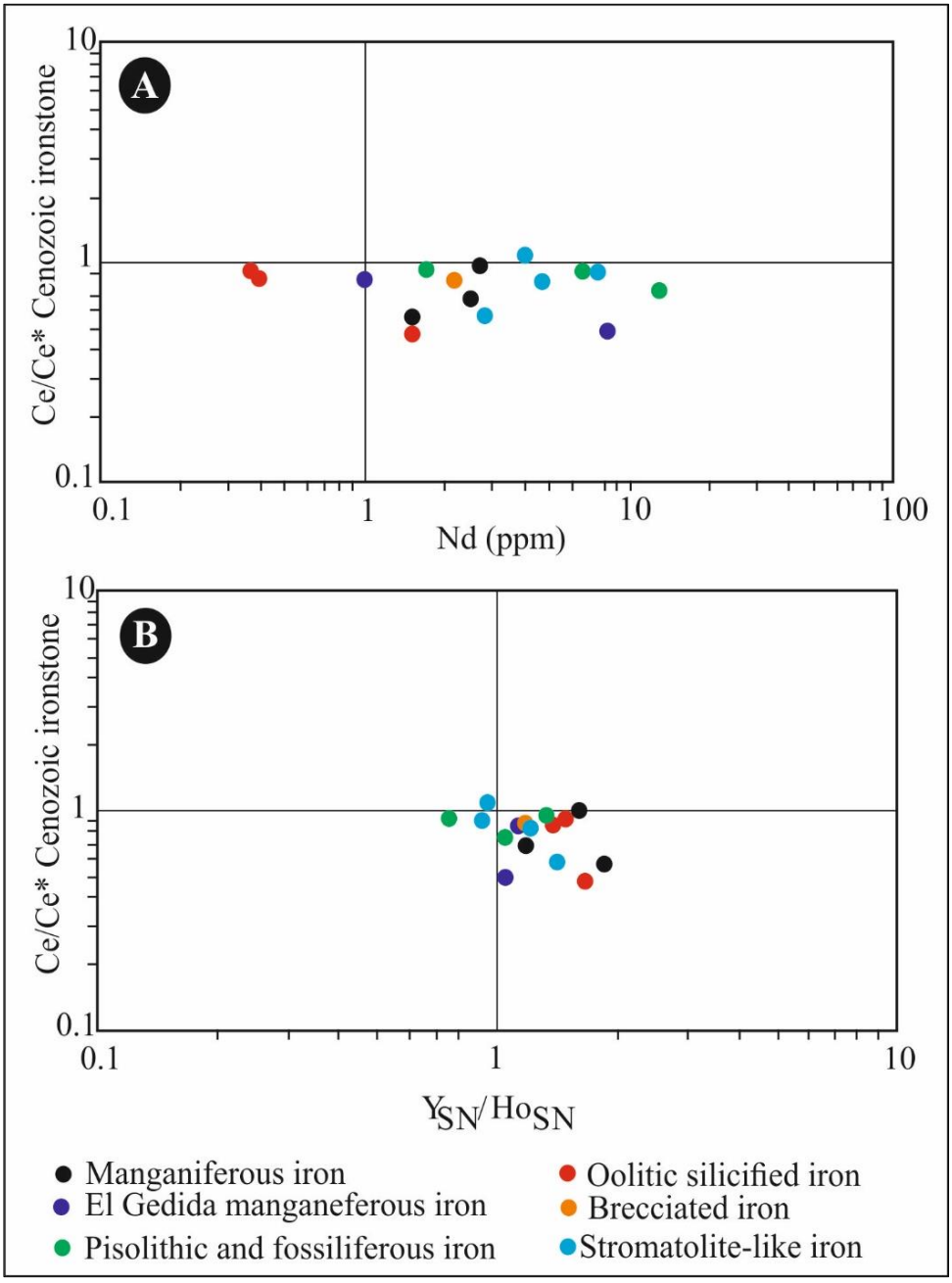

Figure 5.3.8. A) Graph showing Ce/Ce* *vs.* Nd concentrations and B) Discriminative diagram of Ce anomaly *vs.* Y_{SN} anomaly for the Eocene ironstones (SN: shale normalized).

Samples	$d^{34}S$ ‰	$d^{18}O_{BaSO_4}$‰
Barite 01	20.9	14.7
Barite 02	22.4	16.4
Barite 03	17.5	13.2
Barite 05	17.8	13.1
Barite 06	18.1	12.9
Barite Gh G	20.5	16.93
Barite Gh 72	16.8	13.66
Barite Gd G	15.4	15.85
Barite Gd 1	12.1	15.25
Barite Gd 3	19.8	17.14
Barite Gd 31	21.1	17.02
Alunite Gd 14	-16.8	17.45
Jarosite Gd 19	-22.1	12.45
Jarosite Gd 20	-33.3	5.4

Table 5.3.4. Stable isotopic composition of barite, alunite and jarosite associated with the ore deposits.

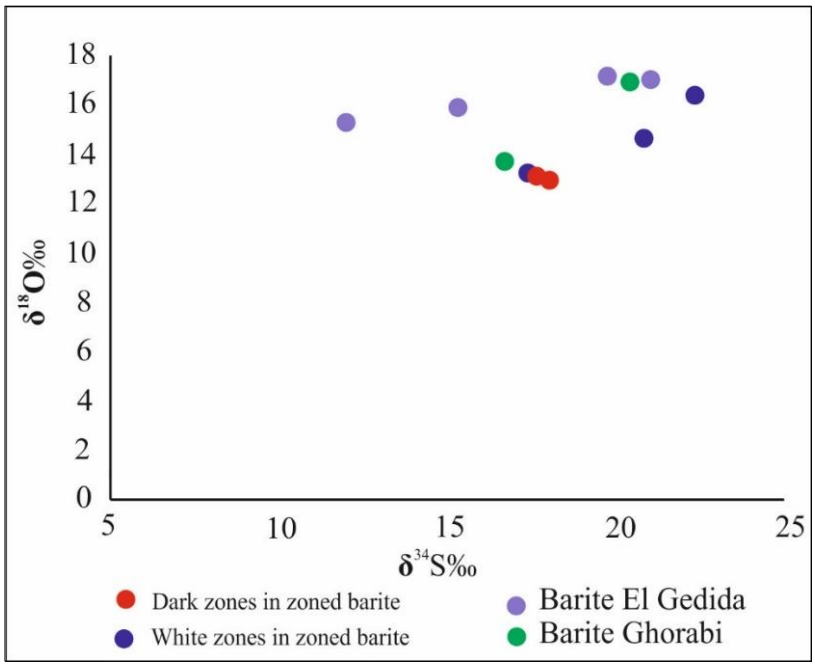

Figure 5.3.9. Sulfur and oxygen isotope compositions of barite crystals collected at the Ghorabi and El Gedida areas.

5.3.5. Fluid inclusions geochemistry

Fluid inclusions micro-thermometry was performed on barite and quartz crystals associated with the ironstones of the Ghorabi, El Harra and El Gedida areas. The fluid inclusion analyses were undertaken to trying to develop a model for the origin and evolution of fluids responsible for the

formation of the different ore-bearing minerals forming the Bahariya ore deposits.

Petrography of the barite reveals that it formed later than quartz and iron oxyhydroxides (Afify et al., 2015b). Most of the fluid inclusions in the barite crystals are primary (i.e. entrapped during the formation of the crystals) while a minor part is represented by pseudo-secondary and secondary inclusions (i.e. formed along micro-fractures during and after crystal growth). Primary fluid inclusions are commonly concentrated along growth zones and/or randomly distributed forming clouds within the barite crystals (Fig. 5.3.10A–D). The inclusions in barite consist of primary monophasic liquid fluids as well as minor two-phase aqueous inclusions, ranging in size from 4 to 32 µm and showing variable liquid/vapour ratios (Fig. 5.3.10A-D). The primary monophasic liquid fluid inclusions were affected by stretching. It resulted in formation of biphasic fluids with variable-sized bubbles that are composed of water vapour. The presence of CO_2 or other gases in the fluid inclusions was ruled out by using Raman spectroscopy. The salinity measurements suggest aqueous solution of low salinity (0.18-4.96 eq. wt.% (NaCl)) (Fig. 5.3.11).

The preliminary fluid inclusions studies on quartz crystals associated with the ironstone rocks, especially those of the Ghorabi and El Harra area, revealed few biphasic fluid inclusions with very small size not exceeding 8 µm and with 95:5, 90:10 and few 70:30 liquid/vapour ratios (Fig. 5.3.10E, F). The biphasic fluid inclusions homogenized to the liquid in a temperature range 90-283 °C. Due to their small sizes, it was difficult to determine neither their composition nor salinity of the fluids forming this mineral.

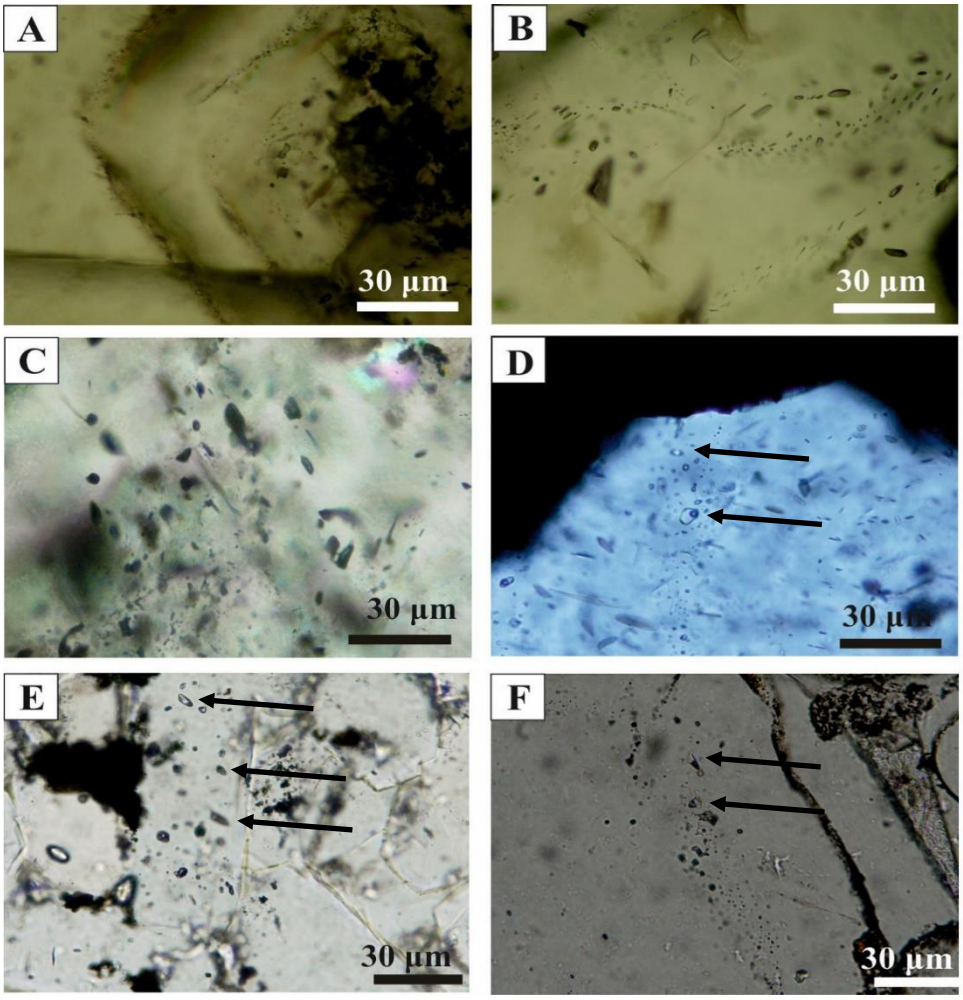

Figure 5.3.10. Petrography of fluid inclusions in barite (A–D) and quartz (E–F) crystals, A) Primary fluid inclusions along a zone of a barite crystal, B), C) Monophasic fluid inclusions with dark color, D) Monophasic liquid fluid inclusions with few biphasic (arrows) fluid inclusions. E), F) Biphasic fluid inclusions in quartz crystals (arrows).

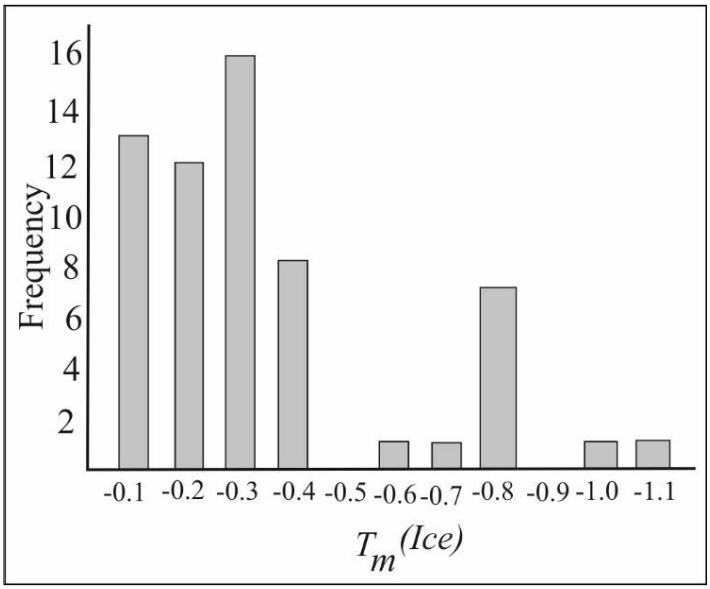

Figure 5.3.11. Histogram showing the temperature melting of ice (Tm (ice)) in the studied barite crystals.

5.4. Discussion and interpretation of the Eocene ore-bearing minerals

5.4.1. Ferromanganese minerals and quartz
5.4.2. Phosphates
5.4.3. Sulfate minerals
5.4.4. Clay minerals – clays as geothermal indicators

5.4. Discussion and interpretation of the Eocene ore-bearing minerals

The following discussion is an integration of those presented in previous articles dealing with the Eocene ironstones. The additional results and observations support the hydrothermal model of formation proposed by Afify et al. (2015b) and give new insight into the fluid types and their origin. Likewise, these new data contribute to refine the timing and mineral paragenesis of the mineralization proposed by Afify et al. (2015b; 2016).

5.4.1. Ferromanganese minerals and quartz

Tectonically driven fluid flow during faulting and thrusting plays a key role in controlling mineralization processes (Ceriani et al., 2011). Likewise, the types of hydrothermally precipitated minerals may be a function of the thermal regime of the system (Puteanus et al., 1991). From these points of view, the mineralogy, morphology and distribution of the ferromanganese minerals and their associated gangue minerals should reflect the thermal regime in the Bahariya area.

In this context, the presence of well-crystallized manganese oxides (e.g., pyrolusite and jacobsite) and iron oxyhydroxides, especially in the lower part of the ironstone succession reflects low temperature hydrothermal solutions (Cornell and Giovanoli, 1987). The occurrence of ferromanganese minerals in different fabrics subsequently reflects their formation after isomorphous substitution.

The formation of the studied ferromanganese minerals was probably favoured by microbial activity. However, the preservation of the

original biotic features and fabrics of the precursor carbonates (e.g., micritization, oolitic and stromatolite-like fabrics) may make some confusion between the biotic and abiotic origin of the minerals (Afify et al., 2015b, c, d). Mineral preservation in those structures is not clear evidence of bio-mediation. Actually, the filamentous and bacterial-like morphologies observed only as secondary pore-filling goethite could reflect a younger stage of bio-mediated iron oxyhydroxides (Afify et al., 2015b, c, d). The association of the secondary pore-filling bacterial-like goethite with the pyrite pseudomorphs could enhance the oxidation of pyrite to goethite and hematite by sulfur-oxidizing bacteria. Otherwise, local occurrence of the iron oxyhydroxides in bacterial-like morphologies associated with the hematite after pyrite pseudomorphs could reflect the spatial biotic mediation for some iron oxyhydroxides in the ironstone deposits.

In summary, the recorded ferromanganese minerals are mostly abiotic; however, some preserve the original biotic fabrics of the precursors. The biotic ferromanganese minerals occur only as localized secondary pore-fillings mostly replacing pyrite at El Gedida area.

As regards the REY geochemistry of the ironstones, it is typical of hydrothermal origin (Bau et al., 2014; Hein et al., 2016) as they are characterized by negative Ce anomalies, positive Y anomalies, and low Nd concentrations of mostly less 10 ppm. The positive Y anomalies suggest that ferromanganese precipitation occurred very rapidly and immediately after reducing, slightly acidic solution reached a more oxidizing and more alkaline shallow-water environment (Bau and Dulski, 1996). Our data oppose against the hydrogenetic origin proposed in previous literature (Salama et al., 2014; Baiuomy et al., 2014). The hydrogenetic ironstones are usually characterized by HREE enrichment, positive Ce anomaly and negative Y values at high REY concentrations and high Nd concentrations of >100 ppm (Bau and Dulski, 1996; Bau et al., 2014). Along the same terms, the small positive Eu anomaly could be a signature inherited from either low-temperature hydrothermal solutions or high-temperature hydrothermal solutions (Bau and Dulski, 1996) that lost their positive Eu anomaly, due to a

relatively high oxygen level. This is supported by the fact that in present oceans, high-temperature hydrothermal solutions lose their Eu anomaly within a few hundred meters away from vent sites due to the rapid oxidation of Eu derived from mixing with oxidized seawater (Klinkhammer et al., 1983).

The positive Ce anomalies indicate anoxic conditions in the water column, enhancing Ce^{3+} concentrations in the sediment whereas the negative Ce anomaly arises from oxidation of trivalent Ce to Ce^{4+} and subsequent decoupling of Ce from the other REEs (Sholkovitz et al., 1992; Kato et al., 2002). Thus, presence of a negative Ce anomaly in samples of the studied ironstones is attributed to oxidize surface.

The association of silica with the iron oxyhydroxides as well as the nearly absence of silica in the ironstone deposits in El Gedida area could relate these minerals to the vulcanicity of the area through the movement of the fluids along the main faults and discontinuities depending on the proximity from the hydrothermal sources (Afify et al., 2015b). More discussion about the ferromanganese minerals and quartz was reported in Afify et al. (2015b).

5.4.2. Phosphates

Association of microcrystalline apatite with the pore-filling microbe-like goethite crystals suggests late precipitation of microbially mediated minerals in pores. The iron-rich sediments are considered traps for phosphates (Mortimer, 1971) because of the strong affinity of iron oxides for them. Barale et al. (2013) described that decomposition of organic matter and release of P bound on Fe-oxides increase pore-water concentration of phosphate, which is precipitated as well-crystallized fluorapatite on hematite surfaces.

5.4.3. Sulfate minerals

The studied sulfate minerals, i.e. barite, alunite and jarosite, could reflect variable mechanisms of formation and several sources. Barite precipitation is driven usually by mixing of Ba-rich and sulfate-rich fluids due to its low solubility under hydrothermal conditions (Holland and Malinin, 1979). This reflects that appreciable amount of Ba^{2+} and SO_4^{2-} species cannot be transported together by the same fluid. The isotopic data of the studied barite crystals further confirm that

hydrothermal convection may have affected the mine areas along the major faults. The sulfur and oxygen isotopic data ($\delta^{34}S$ and $\delta^{18}O$ (SO_4)) are typical for barite that is formed from mixing of hydrothermal steam-heated fluids and meteoric water (Rye, 2005). The sulfur and oxygen isotope data show positive correlation indicating a mixing trend recognized at almost every magmatic hydrothermal acid sulfate system (Rye and Alpers, 1997; Rye, 2005). The temperature fluctuations were mostly from the flux of the magmatism and the magmatic activity south of the study area. Precipitation of barite, as the last phase of the studied ore deposits after silica and ferromanganese minerals, mostly represents a function of decreasing temperatures.

The maximum value of $\delta^{34}S$ (20.5-22.4‰) in some barite samples is similar to that of the SO_4^{-2} ions dissolved in seawater during the Eocene period. However, the fluid inclusion salinity reflects very low salinity and suggests that hydrothermal fluids rose until shallow level and mixed with meteoric water. The liquid monophasic inclusions of barite crystals reflect their formation in low temperature (<50 °C) phreatic environment.

Both jarosite ($KFe_3(SO_4)_2(OH)_6$) and alunite ($KAl_3(SO_4)_2(OH)_6$) can form after hydrous sulfate minerals under strongly acid and oxidizing conditions typical of epithermal environments and hot springs associated with volcanism as well as the oxidation of hydrogen sulfides from hydrothermal magmatic sources (Rye and Alpers, 1997). Jarosite specifically forms in highly acid and oxidizing environments (Stoffregen, 1993; Rye and Alpers, 1997). It is a relatively common mineral in the weathering zones of pyrite-bearing ore deposits (supergene jarosite) (Alpers et al., 1992). Precipitation of jarosite is favored where silicification and clay mineral formation neutralize the pH buffering capacity of limestone (Lueth et al., 2005).

In the study area, alunite and jarosite were interpreted as supergenetic minerals resulting from weathering of pyrite into goethite and hematite (Dabous, 2002). The occurrence of these two sulfate minerals as irregular thin bed and lenses at the top part of the ironstone succession mostly strongly acid and oxidizing conditions and K-rich environment after silicification of the Eocene carbonates. The presence of pyrite pseudomorphs totally replaced by

hematite at the El Gedida area, enhanced by the bacterial activity, where most of the associated iron oxyhydroxides were bio-mediated, could reflect the source of S from pyrite after replacement in oxidizing environment. The sulfur isotopic values for both minerals could indicate their formation from sulfate not depleted in $\delta^{32}S$, i.e. pore-water with open contact to overlying seawater after formation of barite, especially in the presence of the overlying K-rich glauconites.

5.4.4. Clay minerals – clays as geothermal indicators

Illite and smectite are often used as geothermometers (Weaver and Beck, 1971; Bethke et al., 1986; Glasmann et al., 1989) and geochemical indicators (Lahann, 1980; Freed and Peacor, 1989; Wintsch and Kvale, 1994). The reason is that the increase in the illite component of the I-S mixed layers is related to temperature (Hower et al., 1976), time (Pytte and Reynolds, 1989), K^+ concentration (Huang et al., 1993), and water/rock ratio (Whitney, 1990). Smectite illitization occurs at temperature ranges of ~80 to ~150 °C (Hower et al., 1976; Abid et al., 2004; Aróstegui et al., 2006), where smectite is transformed into randomly interstratified (R0) illite-smectite minerals (I-S) and to more illitic ordered (R1–R3) I-S (Hower et al., 1976; Velde and Vasseur, 1992).

The vertical evolution of the studied clay mineral assemblages in the Bahariya Formation described in chapter 4 (see Fig. 4.2.1) around the Ghorabi and El Harra mine areas as well as the slight illitization of smectite recorded within the ironstone hosted in the Eocene rock units could be interpreted as a result of increasing temperature at these areas. This interpretation is consistent with the migration of hydrothermal iron-rich fluids through faults in the Ghorabi and El Harra areas. By contrast, this trend is not seen in Gabal El-Dist where the capping Eocene beds are not replaced by iron and the area is not traversed by major faults.

VI

Diagenetic and hydrothermal models of ironstone formation: constraints and comparison

6.1. Constraints of host rock sedimentary features in occurrences of ore minerals
6.2. Geochemical constraints as genetic proxies for both ironstone types
6.3. Modelling and interpretation of the two ironstone types

6. Diagenetic and hydrothermal models of ironstone formation: constraints and comparison

This chapter deals with the comparison between the two previously described ironstone rock types (Upper Cretaceous and Eocene ironstones) occurring in the Upper Cretaceous – Lower Cenozoic sedimentary succession of the northern Bahariya Depression. The two iron-bearing rock occurrences in the same area provide an opportunity to update understanding ironstone genesis. The interpretation of the differentiated ironstones is closely related to the sedimentary features of the host rocks, which have deep implications on the ironstone distribution (section 6.1). Likewise, discrimination between ironstones is undertaken by determining the geochemistry of both rock types (section 6.2). A genetic model is proposed for the two differentiated ironstone types (section 6.3).

6.1. Constraints of host rock sedimentary features in occurrences of ore minerals

Differentiation between thin ironstone crusts and concretions from the Cenomanian Bahariya Formation and the big ore bodies replacing the Eocene Naqb, Qazzun and El Hamra formations was achieved on the basis of field, petrographic and mineralogical investigations (see chapters 4 and 5 for

details). Major similarities between the two ironstone types are that both were post-depositional and preserve many of the structures, fabrics and stratigraphic features, e.g., thickness, bedding, skeletal and non-skeletal fabrics, of their precursors. The two types show preferential replacement and/or cementation of carbonates by iron-rich minerals. However, they exhibit differences in morphology, textures and geometry that are coherent with different mechanisms of formation and timing.

The Cretaceous ironstones show concretionary, massive, colloidal, reiniform aggregates, leisegang rings and bands, and geode and brecciated fabrics. The crusts and concretions are widely distributed in the lower and upper units of the Bahariya Formation along the whole depression and can be traced laterally for hundreds of meters, thus reflecting formation from basinal iron-rich fluids. In contrast, the Eocene ironstones display oolitic, stromatolitic, pisolithic, coating boxwork, oncolitic-like, and brecciated fabrics, in addition to massive, colloidal and reiniform aggregates. The ironstones hosted in the Eocene carbonates are closely related to two major fault systems through the northern part of the depression so they do not have a basinal distribution.

The Cretaceous ironstones show selective replacement of the iron-rich carbonates (Fe-dolomite, ankerite) that in turn replaced and/or cemented the primary carbonate deposits, i.e. shell fragments, micrite, carbonate grains, calcrete fabrics. On the other hand, the large ironstone bodies hosted in the Eocene rocks show intensive and local replacement and cementation of the dolomites of the Naqb Formation as well as the calcite of the Qazzun and El Hamra limestones preserving the texture of precursors. By contrast, the interbedded thin clay facies are unaltered.

A summary of the main features, i.e. occurrences, grade, thickness, morphology and distribution, of both ironstone types is shown in Table 6.1.

6.2. Geochemical constraints as genetic proxies for both ironstone types

Variations in mineralogy and geochemistry (major and trace elements) can be used to ascertain the origin of ore fluids. On this basis, Bau et al. (2014) and Hein et al. (2016)

discriminated between hydrogenetic, hydrothermal and purely diagenetic Fe-Mn crusts and nodules by using rare earth elements and yttrium content. In this purpose, we studied the geochemistry of the two different ironstone rock types occurring in the Upper Cretaceous – Lower Cenozoic sedimentary succession of the Bahariya region.

The whole-rock composition of the Cretaceous ironstones (Table 4.2.2) shows lower Fe_2O_3 and MnO contents compared with the Eocene ironstones (Table 5.3.1). The Cretaceous ironstone samples show relative enrichment in detrital-derived elements, i.e. Al_2O_3, SiO_2 and Na_2O that are attributed to the presence of clay minerals compared with the Eocene ironstones. The Eocene ironstones show high content in Zn, Ni and Sr trace elements and lower content of detrital-derived elements, e.g., Zr and Nb, compared with the Cretaceous ironstones. The elemental analyses of iron-bearing minerals for both ironstone types reveal depletion in trace elements which support the exclusion of the marine (hydrogenetic) or terrigenous source for these minerals (Nicholson, 1992; Hein et al., 2008). The enrichment of manganese oxides and silica oxide in the Eocene ironstones along with the higher content of Ba, Cu, Zn, Ni and Sr trace elements enhance a hydrothermal input for these deposits (Hein et al., 2016).

The high contents of MgO and CaO in the iron-bearing minerals mainly reflects the replacement of carbonate minerals by iron-rich fluids and support the petrographic results by Afify et al. (2015a, b, c). The lower Ca and Mg concentrations in the Eocene ironstones indicates that the Eocene carbonates were highly replaced by Fe and Mn than that of the Cretaceous case study.

Total REE content in the Cretaceous ironstones shows a wide range from, 70 to 348 ppm (Table 4.2.2), whilst the Eocene ironstones show quite low content, mostly from 1.96 ppm to 31 ppm (Table 5.3.3). The silicified Eocene ironstones are depleted in REE, ranging from 1.96 to 6.85 ppm. These contents fall within the range of diagenetic (110–489 ppm) and hydrothermal (15–149 ppm) ferromanganese deposits reported by Bau et al. (2014) for the Cretaceous and Eocene ironstones, respectively. Our data are significantly lower than the range recorded by Bau et al. (2014) for

the hydrogenetic ironstones (1228–2282 ppm). REE concentration was higher in the Upper Cretaceous ironstones than in the Eocene ironstones, suggesting that there was some contribution from the associated clastic sediments.

Two discrimination diagrams reported by Bau et al. (2014), i.e. Ce/Ce* *vs*. Nd concentration and Ce/Ce* *vs*. Y_{SN}/Ho_{SN} values, were used to distinguish between different genetic ironstones. The two ironstone types studied in Bahariya show negative to no Ce anomaly (Fig. 6.1). The Upper Cretaceous ironstones show enrichment in Nd concentration and fall in the 10-100 ppm range with positive correlation between Nd concentration and Ce/Ce* ratio (Fig. 6.1. A). In contrast, the Eocene ironstones are characterized by low Nd concentration ranging from 0.39 to 8.2 (less than 10 ppm) (Fig. 6.1. A). In Ce anomaly *vs*. Y_{SN}/Ho_{SN} ratio diagram, the Cretaceous ironstones show negative Y_{SN} close to unity ($Y_{SN}/Ho_{SN} \leq 1$) whereas, the Eocene ironstones show positive Y_{SN} ($Y_{SN}/Ho_{SN} \geq 1$) (Fig. 6.1. B).

These discrimination diagrams also support diagenetic and hydrothermal origins for the Cretaceous and Eocene ironstones, respectively. The diagenetic ironstones display negative Y and Ce anomalies and intermediate Nd concentration, between 10 and 100 ppm (Bau et al., 2014; Hein et al., 2016). The Cretaceous ironstones do not show large positive Ce or any significant Y anomalies, which point to a diagenetic origin from anoxic pore water that passed to oxidized surface. On the other hand, the negative Ce anomaly, positive Y and Eu anomalies and the low Nd concentration in the Eocene ironstones suggest a hydrothermal origin for this rock type. Presence of positive Y anomalies in the Eocene ironstones suggests that the precipitation of Fe-Mn minerals occurred very rapidly and immediately after reducing, slightly acidic waters reached more oxidizing and more alkaline water (Bau and Dulski, 1996). Higher Eu anomaly in the Eocene ironstones than in the Cretaceous ironstones indicates considerably more important REY input from hydrothermal solutions for the Eocene ironstones.

Features	*Diagenetic*	*Hydrothermal*
	Upper Cretaceous ironstones	*Eocene ironstones*
Occurrence and extension	Occurrence in the lower and upper units of the Cenomanian Bahariya Formation along the whole depression. Ironstone is absent in the sandstones of the middle unit. They occur in permeable carbonate rocks and sedimentary discontinuities.	Local occurrence related to two major fault systems at three main areas in the carbonate plateau of the northern Bahariya region. They occur mainly replacing carbonate rocks (limestone and dolostone) of the Eocene formations.
Morphology	Thin crusts, irregular thin beds measuring up to 1 m thick; also as concretions up to 40 cm in diameter included in the clastic rocks.	Large bedded and stratiform ironstones reaching up to 13 m in thickness at the Ghorabi and El Harra areas, up to 30 m at the El Gedida mine.
Ore texture and structure	Massive, concretionary, brecciated, and leisegang-like rings and bands. Mainly replacive textures including fossiliferous carbonate beds, calcrete fabrics (rhizoliths, etc.).	Preserved textures of skeletal and non-skeletal grains as well as structures of the precursor carbonates, e.g., massive mud-supported, oolitic, stromatolitic and breccia fabrics. Pisolithic, box-work and concretionary fabrics are also common.
Iron-bearing minerals	Goethite, hematite, Fe-dolomite, ankerite and some siderite	Goethite, hematite, some jarosite and (pyrite?).
Associated non-iron	Pyrolusite, romanechite, todorokite, barite,	Quartz, pyrolusite, jacobsite, romanechite,

minerals	quartz and clay minerals (smectites, I/S mixed layer, kaolinite).	psilomelane, todorokite, barite, alunite, apatite, and clay minerals (smectites, I/S mixed layer, kaolinite, palygorskite).
Ore grade	Low-grade ironstone deposits in clastic sediments.	High-grade ironstone deposits, especially those of the El Gedida mine. The ore deposits of the Ghorabi and El Harra areas are of low to medium grade due to high silica content (quartz).
Mineral paragenesis	Subordinate iron oxyhydroxides formed during early diagenetic stages in paleosol horizons. Most iron oxyhydroxides precipitated in telogenetic stages after replacement of previously formed dolomite and ankerite phases.	Ferromanganese minerals formed after or coeval to silicification of the Eocene carbonates. Sulfate minerals like barite formed after silica and Fe, Mn minerals through fractures and other types of pores as a product of decreasing temperature.
Geochemical characteristics of ironstones	Low MnO and high CaO and MgO contents, high contents of detrital-derived major and trace elements. Wide range of REE (70-384 ppm), negative Y shale-normalized values, high Nd concentration (between 10 and 100 ppm).	High MnO and BaO contents, low CaO and MgO contents, and low contents of detrital-derived major and trace elements. Low REE content, positive Y shale-normalized values and low Nd concentration (less than 10 ppm).

Ore controls	Mainly facies control. Selective replacement of carbonates interbedded with the clastic rocks. Formations of the ironstones was favoured by the uplift of the Bahariya area responsible for folding and faulting during the Late Cretaceous.	Structurally- and facies- controlled. Ironstones formed along two major fault systems. This structure was related to the phase rifting and opening of the Gulf of Suez/Red Sea, which was accompanied by magmatic activity and generation of hydrothermal fluids.
Mechanisms of formation	Mixing of diagenetic iron-rich fluids with oxygenated meteoric water through permeable rocks and discontinuities.	Mixing of iron-rich hydrothermal fluids with meteoric water through faults. The fluids also supply Mn, Ba and silica in variable spatial proportions.
Fluid migration	Enhanced by hydrocarbon migration, organic matter decomposition and formation of bitumen (or oil migration) during diagenesis.	Enhanced by tectonic activity (faulting as structure conduits), high temperature, and magmatic activity.
Timing	. Turonian – Santonian uplift of the region.	Upper Eocene (mostly Priabonian).
Source of iron	Dissolution of pyrite, siderite, Fe- dolomite of the Jurassic rocks (hydrocarbon-source rock). Other possible sources, i.e. glauconite and iron-bearing minerals of the host Bahariya Formation.	Mainly from iron-rich hydrothermal fluids associated with magmatic activity in the northern part of the Bahariya Depression and south of the mine areas.

Table 6.1. Summary and comparison of the main characteristics (sedimentary features, mineralogy, constraints and origin) of the Upper Cretaceous and Eocene ironstones of the Bahariya region, Egypt.

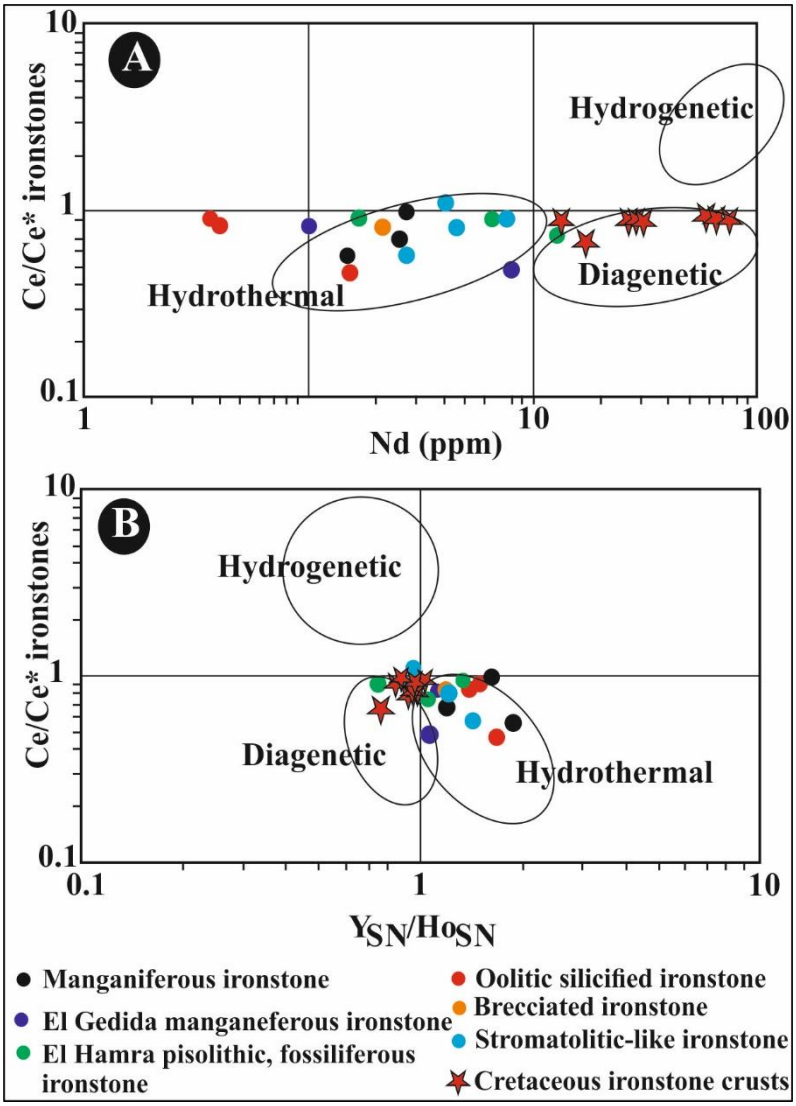

Figure 6.1. A. Graph of Ce/Ce* vs. Nd concentration for the different studied ironstones in the Bahariya area. B. Binary graph of Ce anomaly vs. Y_{SN}/Ho_{SN} values for the different studied ironstone types (SN: shale normalized). The encircled fields in the graphs are from Bau et al. (2014).

6.3. Modelling and interpretation of the two ironstone types

Two contrasted genetic models, i.e. diagenetically-formed Cretaceous ironstones versus hydrothermal Eocene ironstones, are proposed for the ironstones occurring in the Bahariya area (Fig. 6.2).

The ironstone crusts of the Cenomanian Bahariya Formation occurred replacing and/or cementing the dolomite and ankerite favoured by the migration of reducing iron-rich fluids mostly through discontinuities and permeable facies at a basinal scale (Fig. 6.2). Such conditions were enhanced

mostly by decomposition of organic matter and hydrocarbon migration. In contrast, the large ironstone bodies hosted in the Eocene rocks show intensive but local replacement and cementation of the dolostones and limestones.

The replacement of iron-rich carbonates by iron oxyhydroxides in the Cenomanian Bahariya Formation was related to tectonic activity during the Turonian-Santonian, which led to mixing of reducing and oxidizing fluids, whilst replacement of the Eocene carbonate rock units by iron minerals took place after Bartonian, most probably during the Priabonian. The Eocene ironstone deposits are mainly related to structural traps where hydrothermal reducing iron-rich fluids migrated through the major fault systems. In this setting, the reduced iron-rich fluids mixed with meteoric water in phreatic zones and a subsequent vadose phase.

Iron resulting in the formation of the Cretaceous ironstone was probably sourced by iron-bearing minerals of the underlying rock units that after dissolution were leached in a divalent stage iron and precipitated under oxidizing conditions and mixed with meteoric water in fractures, discontinuities and permeable rocks. The iron-sourcing minerals could belong to the iron-bearing minerals associated with the Cenomanian Bahariya Formation or most likely the siderite, Fe-dolomite, and pyrite of the Jurassic Khatatba Formation since they are the hydrocarbon-source rocks in the area (Rossi et al., 2001, 2002). In contrast, source of iron for the Eocene ironstones was related to deep-seated hydrothermal iron-rich solutions that moved through major faults. We postulate that these fluids are due to the magmatic activity occurred in the northern Bahariya Depression during the Oligo-Miocene.

In spite of coincident geographic location, the two ironstone-bearing rocks that form the northern scarp of the Bahariya Depression exemplify two models of iron accumulation in carbonatic rocks under different geotectonic conditions. The different mechanisms of formation are proved by a number of features (mineralogical, geochemical, distribution patterns, etc.) that provide proxies for interpreting more ancient rocks.

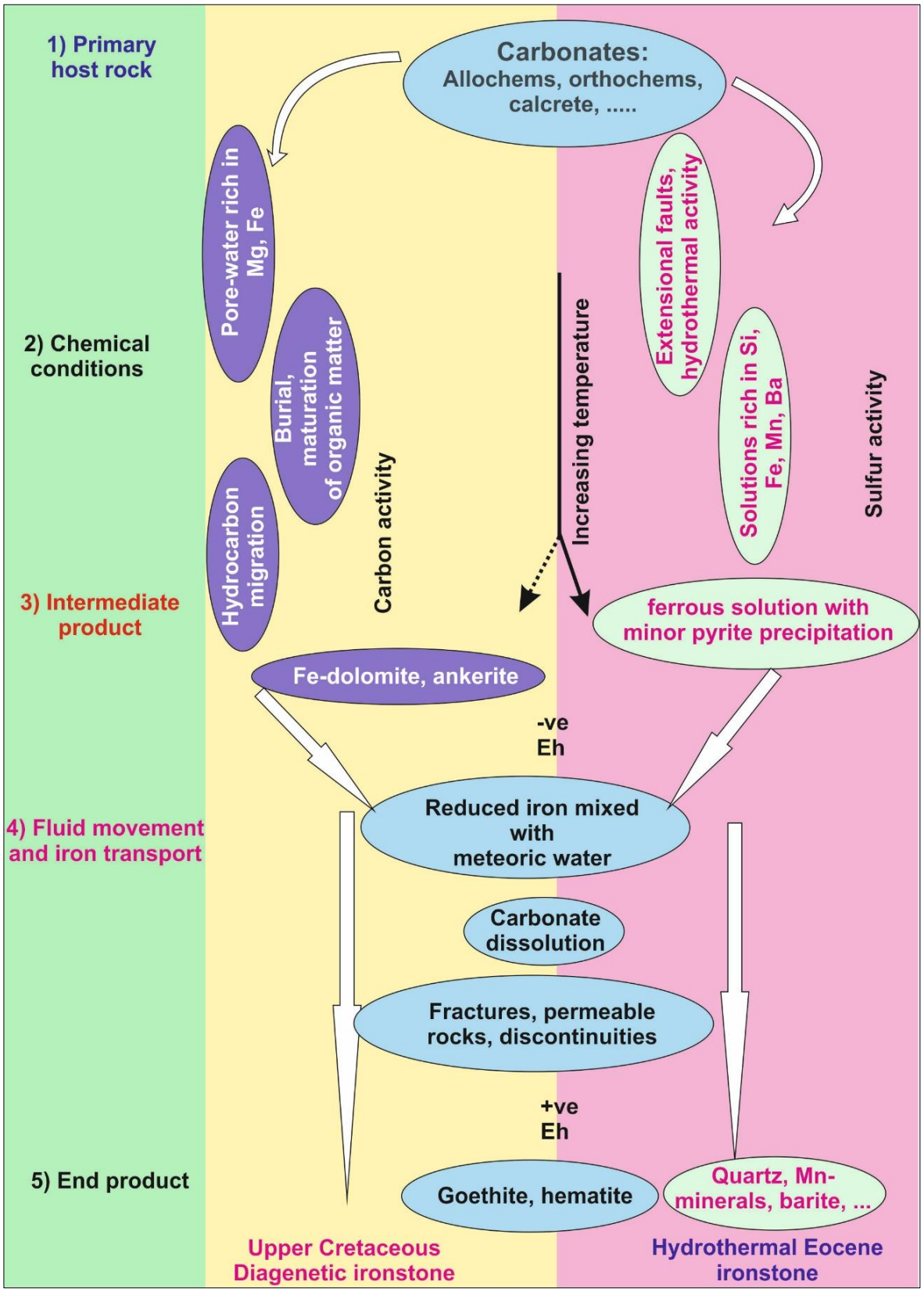

Fig. 6.2. Sketch showing comparison between two different models of ironstone formations: Upper Cretaceous diagenetic ironstones and Eocene hydrothermal ironstones, studied in the Bahariya Depression.

VII

Summary and conclusions

The study of the Upper Cretaceous and the Eocene ironstone deposits occurring in the Bahariya region, central Egypt, provided evidence that they formed according two different genetic models: the Upper Cretaceous ironstones are diagenetic in origin whilst the ironstones hosted in Eocene formations formed after Fe, Mn, Si, Ba- rich hydrothermal fluids. The two ironstone types show preferential replacement and cementation of carbonates by iron-rich minerals. In both cases, goethite and hematite are the main iron minerals, although subordinate ferroan-dolomite and ankerite were recorded in the Upper Cretaceous ironstones. There are similarities but also differences between the two ironstone types; thus, both are post-depositional, replace carbonates and preserve sedimentary structures, fabrics and thickness of their precursors. However, they are different in which relates to their origin, mechanism of formation and timing.

The ironstone present in Cenomanian clastic rocks of the Bahariya Formation occur mainly as crusts and concretions that spread out throughout all the depression. Detailed sedimentological, mineralogical and geochemical study of the ironstone and its hosting siliciclastic rocks indicates that the ironstone formed after selective replacement of the carbonate fraction, including fossil grains, depositional carbonates and calcareous paleosols. The carbonates were affected by dolomitization. Formation of iron-rich dolomite and ankerite was enhanced by decomposition of organic matter and presence of reduced Fe- and Mg- rich solutions. During hydrocarbon

migration, the solutions moved through fractures, permeable rocks, and inter- and intra-stratal discontinuities after dissolution of dolomite and ankerite minerals. The latter process was telodiagenetic, leading to partial or total dissolution of the carbonate, and concomitant with iron oxyhydroxide formation by mixing of the Fe-rich solutions with meteoric oxygenated water. This was favoured by tectonic movements in the region during the Turonian–Santonian. The iron-bearing minerals from the Bahariya Formation and the underlying Jurassic formations were the source of iron.

The ironstones associated with the Eocene carbonates in three mine areas to the north of the Bahariya Depression occur closely related to major faults. Its selective replacement of the carbonate host rocks nearby the faults reflects that they are structurally-controlled. The distribution of quartz, jacobsite, pyrolusite and barite in the ore deposits support their hydrothermal origin after Si, Fe, Mn, Ba- rich fluids. Sulfur and oxygen isotope analyses, fluid inclusions microthermometry and mineralogy of the ore deposits provide evidence for mixing of reduced iron-rich fluids with shallow oxygenated water. Goethite and hematite formed as a result of the process mostly related to the tectonic activity that affected the northern part of the Bahariya area during the Priabonian. Source of iron for the ironstones hosted in Eocene carbonate rocks was related to deep-seated hydrothermal iron-rich solutions that moved through major faults. We postulate that the fluids were due to the magmatic activity in the northern Bahariya Depression. The Eocene ironstone genetic type can be used as a recent analogue for better understanding of the genetic mechanisms of formation of banded iron formations (BIFs) that were abundant during the Precambrian.

In summary, the studied ironstone types show two different models of iron accumulation in carbonate rocks under contrasted geotectonic conditions. The different mechanisms of formation are supported by a number of features (mineralogical, geochemical, distribution patterns, etc.) that provide proxies for interpreting more ancient rocks.

VIII

References

Abd El-Aziz, M., Moustafa, A.R., Said, S.E., 1998. Impact of basin inversion on hydrocarbon habitat in the Qarun Concession, Western Desert, Egypt. Proceedings of the 14th Petroleum Exploration and Development Conference, Cairo. The Egyptian General Petroleum Corporation 1, 139–155.

Abid, I.A., Hesse, R., Harper, J.D., 2004. Variations in mixed-layer illite/smectite diagenesis in the rift and post-rift sediments of the Jeanne d'Arc Basin, Grand Banks offshore Newfoundland, Canada. Canadian Journal of Earth Sciences 41, 401–429.

Abouzeid, A.M., Khalid, A.M., 2011. Mineral Industry in Egypt-Part I: Metallic Mineral Commodities. Natural Resources 2, 35–53.

Afify, A.M., Sanz-Montero, M.E., Calvo, J.P., Wanas, H.A. 2015a. Diagenetic origin of ironstone crusts in the Lower Cenomanian Bahariya Formation, Bahariya Depression, Western Desert, Egypt. Journal of African Earth Sciences 101, 333–349.

Afify, A.M., Sanz-Montero, M.E., Calvo, J.P., 2015b. Ironstone deposits hosted in Eocene carbonates from Bahariya (Egypt) - New perspective on cherty ironstone occurrences. Sedimentary Geology 329, 81–97.

Afify, A.M., Sanz-Montero, M.E., Calvo, J.P., 2015c. Biotic versus abiotic iron: An example of the fault-related ironstone hosted in Eocene carbonates in the Bahariya area, Western Desert, Egypt. 31st IAS Meeting of Sedimentology, Kraków, Poland, Abstract, pp. 24.

Afify, A.M., Sanz-Montero, M.E., Calvo, J.P., 2015d. Cherty ironstone hosted in Eocene marine carbonates: Tectonic and sedimentological controls on iron and silica formation. 31st IAS Meeting of Sedimentology, Kraków, Poland, Abstract, pp. 25.

Afify, A.M., Serra-Kiel, J., Sanz-Montero, M.E., Calvo, J.P., Sallam, E.S., 2016. Nummulite biostratigraphy of the Eocene succession in the Bahariya Depression, Egypt: Implications for timing of iron mineralization. Journal of African Earth Sciences 120, 44–55.

Alpers, C.N., Rye, R.O., Nordstorm D.K., White, L.D., King, B.S., 1992. Chemical, crystallographic and stable isotopic properties of alunite and jarosite from acid—Hypersaline Australian lakes. Chemical Geology 96, 203–226.

Alt, J.C., 1988. Hydrothermal oxide and nontronite deposits on seamounts in the Eastern Pacific. Marine Geology 81, 227–239.

Aróstegui, J., Sangüesa, F.J., Nieto, F., Uriarte, J.A., 2006. Thermal models and clay diagenesis in the Tertiary-Cretaceous sediments of the Alava block (Basque-Cantabrian basin, Spain). Clay Minerals 41, 791–809.

Attia, M.I., 1955. Topography, Geology, and Iron Ore of the District East of Aswan. The Egyptian Geological Survey, 262 pp.

Bagge, M.A., Keeley, M.L., 1994. The oil potential of the Mid-Jurassic coals. In: Scott, A.C., Fleet, A.J., (Eds.), Northern Egypt, Coal and Coal-Bearing Strata as Oil-Prone Source Rocks?. Geological Society of London, Special Publication 77, pp. 183–200.

Baioumy, H.M., Ahmed H.H., Mohamed Z.K., 2014. A mixed hydrogeneous and hydrothermal origin of the Bahariya iron ores, Egypt: Evidences from the trace and rare earth elements geochemistry. Journal of Geochemical Exploration 146, 149–162.

Baioumy, H.M., Khedr, M.Z., Ahmed, A.H., 2013. Mineralogy, geochemistry and origin of Mn in the high-Mn iron ores, Bahariya Oasis, Egypt. Ore Geology Reviews 53, 63–76.

Barale, L., D'atri, A., Martire, L., 2013. The role of microbial activity in the generation of the lower Cretaceous mixed Fe-oxide-phosphate ooids from the Provencal Domain, French Maritime Alps. Journal of Sedimentary Research 83, 196–206.

Barnes, J.W., 1989. Ores and minerals: introducing economic geology. Open University Press, Milton Keynes—Philadelphia. 181 pp.

Basta, E.Z., Amer, H.I., 1969. El Gedida iron ores and their origin, Bahariya oasis, Western Desert, U.A.R. Economic Geology 64, 424–444.

Basta, F.F., Maurice, A.E., Fontboté, L., Favarger, P.Y., 2011. Petrology and geochemistry of the banded iron formation (BIF) of Wadi Karim and Um Anab, Eastern Desert, Egypt: Implications for the origin of Neoproterozoic BIF. Precambrian Research 187, 277–292.

Bau, M., 1996. Controls on the fractionation of isovalent trace elements in magmatic and aqueous systems: evidence from Y/Ho, Zr/Hf, and lanthanide tetrad effect. Contributions to Mineralogy and Petrology 123, 323–333.

Bau, M., Dulski, P., 1996. Distribution of yttrium and rare-earth elements in the Penge and Kuruman iron-formations, Transvaal Supergroup, South Africa. Precambrian Research 79, 37–55.

Bau, M., Koschinsky, A., Dulski, P., Hein, J.R., 1996. Comparison of the partitioning behaviours of yttrium, rare earth elements, and titanium between hydrogenetic marine ferromanganese crusts and seawater. Geochimica et Cosmochimica Acta 60, 1709–1725.

Bau, M., Schmidt, K., Koschinsky, A., Hein, J., Kuhn, T., Usui, A., 2014. Discriminating between different genetic types of marine ferro-manganese crusts and nodules based on rare earth elements and yttrium. Chemical Geology 381, 1–9.

Bekker, A., Planavsky, N.J., Krapež, B., Rasmussen, B., Hofmann, A., Slack, J.F., Rouxel, O.J., Konhauser, K.O., 2014. Iron Formations: Their Origins and Implications for Ancient Seawater Chemistry. In: Treatise on Geochemistry (Second Edition) 9, pp. 561–628.

Bekker A., Slack J.F., Planavsky N. et al., 2010. Iron formation: The sedimentary product of the complex interplay among mantle, tectonic, oceanic, and biospheric processes. Economic Geology 105, 467–508.

Bethke, C.M., Vergo, N., Altaner, S.P., 1986. Pathways of smectite illitization. Clays and clay minerals 34, 125–135.

Bhattacharyya, D.P., 1989. Concentrated and lean oolite: examples from the Nubia Formation at Aswan, Egypt, and significance of the oolite types in

ironstone genesis. In: Young, T.P., Taylor, W.G.E. (Eds.), Phanerozoic Ironstones. Geological Society of London Special Publication 46, pp. 93–103.

Bhattacharyya, D.P., Kakimoto, P., 1982. Origin of ferriferous ooids: An SEM study of ironstone ooids and bauxite pisoids. Journal of Sedimentary Petrology 52, 849–857.

Blatt, H., 1982. Sedimentary Petrology: W.H. Freeman, San Francisco, C.A.

Boggs, S.Jr., 2006. Principles of Sedimentology and Stratigraphy, 4th edition, Prentice Hall, 662 p.

Bolhar, R., Kamber, B.S, Moorbath S., Fedo C.M., Whitehouse M.J., 2004. Characterization of Early Archaean chemical sediments by trace element signatures. Earth and Planetary Science Letters 222, 43–60.

Brookins, D.G., 1987. Eh-pH Diagrams for Geochemistry. Springer Verlag, Berlin, Heidelberg, New York, pp. 76 and 96.

Borchert, H., 1965. Formation of marine sedimentary iron ores. In: Riley, J.P., Skirrow, G. (Eds), Chemical Oceanography. Academic Press, London. pp. 159–204,

Botros, N.Sh., 1991. Geological and Geochemical Studies on Some Gold Occurrences in the North Eastern Desert. Ph.D. Thesis, Zagazig University, Zagazig, Egypt. 146 pp.

Bottke, H., 1981. Lagersta¨ttenkunde des Eisens. Verlag Glu¨ckauf GmbH, Essen, 75–97.

Budd, D.A., 1997. Cenozoic dolomites of carbonate islands: their attributes and origin. Earth-Science Reviews 42, 1–47.

Burkhalter, R.M., 1995. Ooidal ironstones and ferruginous microbialites: origin and relation to sequence stratigraphy (Aalenian and Bajocian, Swiss Jura mountains). Sedimentology 42, 57–74.

Catuneanu, O., Khalifa, M.A., Wanas, H.A., 2006. Sequence stratigraphy of the Lower Cenomanian Bahariya Formation, Bahariya Oasis, Western Desert, Egypt. Sedimentary Geology 190, 121–137.

Ceriani, A., Calabró, R., Di Giulio, A., Buonaguro, R., 2011. Diagenetic and thermal history of the Jurassic-Tertiary succession of the Zagros Mountains in the Dezful Embayment (SW Iran): constraints from fluid inclusions. International Journal of Earth Sciences 100, 1265–1281.

Chao, T.T., Theobald, J.P.K., 1976. The significance of secondary iron and manganese oxides in geochemical exploration. Economic Geology 71, 1560–1569.

Chung, F.H., 1974. Quantitative interpretation of X-ray diffraction patterns. I. Matrix-flushing method for quantitative multicompetent analysis. Journal of Applied Crystallography 7, 519–931.

Cornell, R.M., Giovanoli, R., 1987. Effect of manganese on the transformation of ferrihydrite into goethite and jacobsite in alkaline media: Clays and Clay Minerals 35, 11–20.

Dabous, A.A., 2002. Uranium isotopic evidence for the origin of the Bahariya iron deposits, Egypt. Ore Geology Reviews 19, 165–186.

Dahanayake, K., Krumbein, W.E., 1986. Microbial structures in ooidal iron formations. Mineralium Deposita 21, 85–94.

Deer, W.A., Howie, R.A., Zussman, J., 1992. An Introduction to the Rock-forming Minerals (second edition.). Essex: Longman Scientific and Technical; New York: Wiley, 696 pp.

Dreesen, R., 1989. Oolitic ironstones as event-stratigraphical marker beds within the Upper Devonian of the Ardeno-Rhenish Massif. In: Young, T.P., Taylor, W.E.G. (Eds.), Phanerozoic Ironstones. Geological

Society Special Publications London 46, pp. 65–78.

El Akkad, S.E., Issawi, B., 1963. Geology and iron ore deposits of Bahariya Oasis. Geological Survey of Egypt 18, 300 pp.

El Aref, M.M., El Sharkawi, M.A., Khalil, M.A., 1999. Geology and genesis of the stratabound and Stratiform Cretaceous–Eocene iron ore deposits of the Bahariya region, Western Desert, Egypt. GAW 4th International Conference, Cairo University, Egypt, 450–475.

El Aref, M.M., Mesaed, A.A., Khalil, M.A., Salama, W.S., 2006a. Stratigraphic setting, facies analyses and depositional environments of the Eocene ironstones of Gabal Ghorabi mine area, El Bahariya Depression, Western Desert, Egypt. Egyptian Journal of Geology 50, 29–57.

El Aref, M.M., Mesaed, A.A., Khalil, M.A., Salama, W.S., 2006b. Microbialite morphostructures and biogenic accretion mechanism of the Eocene ironstones of Gabal Ghorabi mine area, El Bahariya Depression, Western Desert, Egypt. Egyptian Journal of Geology 50, 59–81.

El Sharkawi, M.A., Higazi, M.M., Khalil, N.A., 1984. Three genetic iron ore dikes of iron ores at El Gedida mine, Western Desert, Egypt Geological Society of Egypt. 21st Annual Meeting, Cairo, Egypt, pp. 68.

El Shazly, M.M., El Ramly, I.M., Guindy, Kh.A., Abdel Aati, A., 1991. Bahariya formation water quality characteristics and its relationship to the hydrothermal activity in Bahariya Oasis, Western Desert, Egypt. Geological Society of Egypt. 29th Annual Meeting, Cairo, Egypt (Abstract).

Evans, A.M., 1993. Ore Geology and Industrial Minerals (third Edition). Blackwell Science. 389 pp.

Fortin, D., Langley, S., 2005. Formation and occurrence of biogenic iron-rich minerals. Earth Science Review 72, 1–19.

Freed, R.L., Peacor, D.R., 1989. Variability in temperature of the smectite/illite reaction on Gulf Coast sediments: Clay Minerals 24, 171–180.

Garrels, R.M., Christ, C.L., 1965. Solutions, Minerals, and Equilibria: Harper and Row, New York, NY.

Glassman, J.R., Larter, S., Briedis, N.A., Lundegard, P.D., 1989. Shale diagenesis in the Bergen High area, North Sea. Clays and Clay Minerals 37, 97–112.

Guiraud, R., 1998. Mesozoic rifting and basin inversion along the northern African Tethyan margin: an overview. In: Macgregor D.S., Moody, R.T.J., Clark-Lowes, D.D. (Eds.), Petroleum Geology of North Africa. Geological Society of London, Special Publications 132, pp. 217–229.

Guiraud, R., Binks, R.M., Fairhead, J.D., Wilson, M., 1992. Chronology and geodynamic setting of Cretaceous-Cenozoic rifting in West and Central Africa. Tectonophysics 213, 227–234.

Harder, H., 1989. Mineral genesis in ironstones: a model based upon laboratory experiments and petrographic observations. In: Young, T.P., Taylor, W.E.G. (Eds.), Phanerozoic Ironstones. Geological Society of London, Special Publication 46, pp. 9–18.

Hein, J.R., Conrad, T., Mizell, K., Banakar, K.V., Frey, F.A., Sager, W.W., 2016. Controls on ferromanganese crust composition and reconnaissance resource potential, Ninetyeast Ridge, Indian Ocean. Deep-Sea Research I 110, 1–19.

Hein, J.R., Koschinsky, A., Halbach, P., Manheim, F.T., Bau, M., Kang, J.-K., Lubick, N., 1997. Iron and manganese oxide mineralization in the Pacific. In: Nicholson, K., et al., (Eds.), Manganese Mineralization: Geochemistry and Mineralogy of Terrestrial and Marine Deposits. Geological Society, Special Publication 119, pp. 123–138.

Hein, J.R., Mizell, K., Koschinsky, A., Conrad, T.A., 2013. Deep-ocean

mineral deposits as a source of critical metals for high- and green-technology applications: comparison with land-based deposits. Ore Geology Review 51, 1–14.

Hein, J.R., Schulz, M.S., Dunham, R.E., Stern, R.J., Bloomer, S.H., 2008. Diffuse flow hydrothermal manganese mineralization along the active Mariana and southern Izu-Bonin arc system, western Pacific, Journal of Geophysical Research 113, 1–29.

Helba, A.A., El Aref, M.M., Saad, F., 2001. Lutetian oncoidal and ooidal ironstone sequence; depositional setting and origin; northeast El Bahariya Depression, Western Desert, Egypt. Egyptian Journal of Geology 45, 325–351.

Hendry, J.P., Wilknson, M., Fallick, A.E., Haszeldine, R.S., 2000. Ankerite cementation in deeply buried Jurassic sandstone reservoirs of the central North Sea. Journal of Sedimentary Research 70, 227–239.

Heikoop, J.M., Tsujita, C.J., Risk, M.J., Tomascik, T., Mah, A.J., 1996. Modern iron ooids from a shallow-marine volcanic setting: Mahengetang, Indonesia. Geology 24, 759–762.

Holland, H.D., 1984. The Chemical Evolution of the Atmosphere and Oceans. Princeton, N.J.: Princeton University Press.

Holland, H.D., Malinin, S.D., 1979. The solubility and occurrence of non-ore minerals. In: Barnes, H.L. (Ed.), Geochemistry of hydrothermal solutions (second edition). John Wiley and Sons, pp. 461–508.

Hower, J., Eslinger, E.V., Hower, M., Perry, E.A., 1976. Mechanism of burial metamorphism of argillaceous sediments. I. Mineralogical and chemical evidence. Geological Society of American Bulletin 87, 725–737.

Huang, W.L., Longo, J.M., Pevear, D.R., 1993. An experimentally derived kinetic model for smectite-to- illite conversion and its use as a geothermometer. Clays and Clay Minerals 41, 162–177.

Irwin, H., Curtis, C., Coleman, M., 1977. Isotopic evidence for source of diagenetic carbonates formed during burial of organic-rich sediments. Nature 269, 209–213.

Issawi, B., Francis, M., Youssef, A., Osman, R., 2009. The Phanerozoic of Egypt: a Geodynamic Approach. Egyptian Geological Survey. Special publication 81, 589 pp.

James, H.L., 1966, Chemistry of Iron-Rich Sedimentary Rocks: Data of Geochemistry, 6th edition: US Geological Survey Professional Paper 440-W.

James H.L., 1983. Distribution of banded iron formation in space and time. In: Trendall A.F., Morris R.C. (Eds.), Iron-Formation: Facts and Problems. Amsterdam: Elsevier, pp. 471-490.

James, H.L., 1992. Precambrian iron-formations: Nature, origin, and mineralogic evolution from sedimentation to metamorphism. In: Wolf, K.H., Chilingarian, G.V. (Eds.), Diagenesis III: Developments in Sedimentology 47, pp. 543–589.

James, H.L., Trendall, A.F., 1982, Banded iron formation: Distribution in time and paleoenvironmental significance. In: Holland, H.D., Schidlowski, M. (Eds.), Mineral Deposits and the Evolution of the Biosphere: Springer-Verlag, Berlin, pp. 199–218.

Kakuwa, Y., Matsumoto, R., 2006. Cerium negative anomaly just before the Permian and Triassic boundary event–The upward expansion of anoxia in the water column. Palaeogeography, Palaeoclimatology Palaeoecology 229, 335–344.

Kappler, A., Pasquero, C., Konhauser, K.O., Newman, D.K., 2005. Deposition of banded iron formations by anoxygenic phototropic Fe(II)-oxidizing bacteria. Geology 33, 865–868.

Kato, Y., Nakao, K., Isozaki, Y., 2002. Geochemistry of Late Permian to Early Triassic pelagic cherts from

southwest Japan: implications for an oceanic redox change. Chemical Geology 182, 15–34.

Khalid A.M., Diaf, A.A., 1996. Geological and Geochemical Exploration for Gold and REE at Jabal Nazar and Jabal Arkenu, Egypt-Libya. Proceedings of Geological Survey, Egypt, 425-446.

Khattab, M., Greiling, O.R., Khalid, A.M., Said, M., Kontany, A., Abu Salem, A., 2002. Uwaynat Banded Iron Formation (SW Egypt) Distribution and Related Gold Mineralization. Annals of the Geological Survey of Egypt 25, 343–364.

Kimberley, M.M., 1979. Origin of oolitic iron formations: Journal of Sedimentary Petrology 49, 111–132.

Kimberley, M.M., 1989. Exhalative origins of iron formations. Ore Geology Review 5, 13–145.

Kimberley, M.M., 1994. Debate about ironstone: has solute supply been surficial weathering, hydrothermal convection, or exhalation of deep fluids?. Terra Nova 6, 116–132.

Kimberley, M.M., 2005. Dynamic Earth: Chemistry: New York, Wiley and Sons, 369 pp.

Klein, C., Beukes N.J., 1993. Sedimentology and geochemistry of the glaciogenic Late Proterozoic Rapitan iron-formation in Canada. Economic Geology 88, 542–565.

Klinkhammer, G., Elderfield, H., Hudson, A., 1983. Rare earth elements in seawater near hydrothermal vents. Nature 305, 185-188.

Klitzsch, E., 1986. Plate tectonics and cratonal geology in Northeast Africa (Egypt, Sudan). Geologische Rundschau 75, 755–768.

Korany, E.A., 1995. Hydrogeologic evaluation of the deeper aquifer in Bahariya mines area, Egypt. Symp. Nubian Sandstone rocks, Bengazy, Libya, Gume, 1–38.

Krauskopf, K.B., Bird, D.K., 1995. Introduction to Geochemistry. McGraw-Hill, 647 pp.

Lahann, R.W., 1980. Smectite diagenesis and sandstone cements: the effect of reaction temperature. Journal of Sedimentary Petrology 50, 755–760.

Land, L.S., 1980. The isotopic and trace element geochemistry of dolomite: the state of the art. In: Zenger, D.H., Dunhan, J.B., Ethington R.L. (Eds.), Concepts and Models of Dolomitization Geology. Society of Economic Palaeontologists and Mineralogists Special Publication 28, 87–110.

Land, L.S., 1983. The application of stable isotopes to studies of dolomite and to problems of diagenesis of clastic sediments. In: Stable Isotopes in Sedimentary Geology. Society of Economic Palaeontologists and Mineralogists (shortcourse) 10, 4.1–4.22.

Lindholm, R.C., Finkelman, R.B., 1972. Calcite staining: semiquantitative determination of ferrous iron: Journal of Sedimentary Petrology 42, 239–242.

Loope, D.B., Kettler, R.M., Webber, K.A., 2011. Morphologic clues to the origins of iron oxide–cemented spheroids, boxworks, and pipelike concretions, Navajo Sandstone of South-Central Utah, U.S.A. Journal of Geology 119, 505–520.

Lueth, V.W., Rye, R.O., Peters, L., 2005. "Sour gas" hydrothermal jarosite: ancient to modern acid-sulfate mineralization in the southern Rio Grande Rift. Chemical Geology 215, 339–360.

Mamet, B., Préat, A., 2006. Iron-bacterial mediation in Phanerozoic red limestones: State of the art. Sedimentary Geology 185, 147–157.

Mansburg, H., Morad, S., Salem A., Marfil R., El−Ghali. M.A.K., Nystuen, J.P., Caja, M.A., Amorsi, A., Garcia, D., La Iglesia, A., 2008. Diagenesis and reservoir quality evolution of Paleocene deep−water marine sandstones, the Shetland−Faroes

Basin, British continental shelf. Marine and Petroleum Geology 25, 514–543.

Maynard, J.B., 1983. Geochemistry of Sedimentary Ore Deposits. Springer-Verlag, New York, 305 pp.

Maynard, J.B., 1991. Iron: Syngenetic deposition controlled by the evolving ocean-atmosphere system. In: Force, E., Eidel, J.J., Maynard, J.B., (Eds.), Sedimentary and diagenetic mineral deposits: A basin analysis approach to exploration: El Paso, Texas, Society of Economic Geologists, Reviews in Economic Geology 5, pp. 141–145.

Mazzullo, S.J., 2000. Organogenic dolomitization in peritidal to deep-sea sediments. Journal of Sedimentary Research 70, 10–23.

McLennan, S.M., 1989. Rare earth elements in sedimentary rocks: Influence of provenance and sedimentary processes. In: Lipin, B.R., McKay, G.A. (Eds.), Geochemistry and Mineralogy of Rare Earth Elements. Reviews in Mineralogy and Geochemistry 21, Mineralogical Society of America, Washington, D.C., pp. 169–200.

Meneisy, M.Y., 1990. Vulcanicity. In: Said, R. (Ed.), The Geology of Egypt. A.A. Balkema, Rotterdam, pp. 57–172.

Meneisy, M.Y., El Kalioubi, B., 1975. Isotopic ages of the volcanic rocks of the Bahariya Oasis. Annal Geological Survey of Egypt 5, 119–122.

Mesaed, A.A., 2006. Mechanism of formation of the Cenomanian glauconitic ironstones of the Bahariya Formation, Gabal el Dist, Bahariya Oases, Western Desert, Egypt. Bulletin Tethys Geological Society, Cairo 1, 17–36.

Metwalli, F., Pigott, J., 2005. Analysis of petroleum system criticals of the Matruh-Shushan Basin, Western Desert, Egypt. Petroleum Geoscience 11, 157–178.

Moore, D.M., Reynolds, R.C.Jr., 1989. X-Ray Diffraction and the Identification and Analysis of Clay Minerals. Oxford University Press, 322 pp.

Moretti, I., Kerdraon, Y., Rodrigo, G., Huerta, F., Griso, J.J., Sami, M., Said, M., Ali, H., 2010. South Alamein petroleum system (Western Desert, Egypt). Petroleum Geoscience 116, 121–132.

Moustafa, A.R., Saoudi, A., Moubasher, A., Ibrahim, I.M., Molokhia, H., Schwartz, B., 2003. Structural setting and tectonic evolution of the Bahariya Depression, Western Desert, Egypt. GeoArabia, 8. Gulf Petrolink, Bahrain, 91–124.

Mücke, A., 2000. Environmental conditions in the late Cretaceous African Tethys: conclusions from a microscopic-michrochemical study of ooidal ironstones from Egypt, Sudan and Nigeria. Journal of African Earth Sciences 30, 25–46.

Mücke, A., Agthe, Ch., 1988. Mineralization, origin and age classification of ferruginized sandstone in the Bahariya Oasis, Western Desert, Egypt: A contribution to the origin of red beds. Lithos 22, 59–73.

Mücke, A., Farshad, F., 2005. Whole-rock and mineralogical composition of Phanerozoic ooidal ironstones: comparison and differentiation of types and subtypes. Ore Geology Reviews 26, 227–262.

Murray, J.W., 1979. Iron oxides. In: Burns, R.G. (Ed.), Marine Minerals. Mineralogical Society of America, Washington, pp. 47–98.

Needham, S.J., Worden, R.H., Mcilroy, D., 2004. Animal–sediment interactions: the effect of ingestion and excretion by worms on mineralogy: Biogeosciences, 1, 113–121.

Needham, S.J., Worden, R.H., Mcilroy, D., 2005. Experimental production of clay rims by macrobiotic sediment ingestion and excretion processes. Journal of Sedimentary Research 75, 1028–1037.

Nicholson, K., 1992. Contrasting mineralogical – geochemical signatures of manganese oxides: guides to

metallogenesis. Economic Geology 87, 1253–1264.

Petránek, J., Van Houten, F.B., 1997. Phanerozoic ooidal ironstones. Czech Geological Survey Special paper 7, 71 pp.

Pichler, T, Veizer, J., 1999. Precipitation of Fe (III) oxyhydroxide deposits from shallow-water hydrothermal fluids in Tutum Bay, Ambitle Island, Papua New Guinea. Chemical Geology 162, 15–31.

Pichler, T., Veizer, J., Hall, G.E.M., 1999. The chemical composition of shallow-water hydrothermal fluids in Tutum Bay, Ambitle Island, Papua New Guinea and their effect on ambient seawater. Marine Chemistry 64, 229–252.

Préat, A., Mamet, B., De Ridder, C., Boulvain, F., Gillan, D., 2000. Iron bacterial and fungal mats, Bajocian stratotype (Mid-Jurassic, northern Normandy, France). Sedimentary Geology 137, 107–126.

Puteanus, D., Glasby, G.P., Stoffers, P., Kunzendorf, H., 1991. Hydrothermal iron-rich deposits from the Teahitia-Mehitia and Macdonald hot spot areas, Southwest Pacific. Marine Geology 98, 389–409.

Pytte, A.M., Reynolds R.C., Jr., 1989. The thermal transformation of smectite to illite. In: Naeser, N.D., McColloh, T.H. (Eds.), Thermal History of Sedimentary Basins. Springer-Vedag, New York, pp. 133–140.

Rasmussen, B., Krapez, B., Meier, D.B., 2014. Replacement origin for hematite in 2.5 Ga banded iron formation: evidence for postdepositional oxidation of iron-bearing minerals. Geological Society of America Bulletin 126, 438–446.

Reynolds, R.C.Jr., 1980. Interstratified clay minerals: In: Brindley, G.W., Brown, G. (Eds.), Crystal Structures of Clay Minerals and Their X-Ray Diffraction: Monograph No. 5, Mineralogical Society, London, pp 249–303.

Rivas-Sánchez, M.L., Alva-Valdivia, L.M., J. Arenas-Alatorre, J., Urrutiafucugauchi, J., Ruiz-Sandoval, M., Ramos-Molina, M.A., 2006. Berthierine and chamosite hydrothermal: Genetic guides in the Peña Colorada magnetite-bearing ore deposit, Mexico: Earth, Planets and Space 58, 1389–1400.

Robb, L., 2004. Introduction to Ore-Forming Processes, Wiley, 384 pp.

Rossi, C., Goldstein, R.H., Ceriani, A., Marfil, R., 2002. Fluid inclusions record thermal and fluid evolution in reservoir sandstones, Khatatba Formation, Western Desert, Egypt: A case for fluid injection. American Association of Petroleum Geologists (AAPG) Bulletin 86, 1773–1799.

Rossi, C., Marfil, R., Ramseyer, K., Permanyer, A., 2001. Facies-related diagenesis and multiphase siderite cementation and dissolution in the reservoir sandstones of the Khatatba Formation, Egypt's Western Desert. Journal of Sedimentary Research 71, 459–472.

Rye, R.O., 2005. A review of the stable-isotope geochemistry of the sulfate minerals in selected igneous environments and related hydrothermal systems. Chemical Geology 215, 5–36.

Rye, R.O., Alpers, C.N. 1997. The stable isotope geochemistry of jarosite. U.S. Geological Survey Open-File Report, 88–97.

Said, R., 1962. The Geology of Egypt. Elsevier, Amsterdam, 377 pp.

Said, R., 1990. The Geology of Egypt. Elsevier, New York, 734 pp.

Said, R., Issawi, B., 1964. Geology of the northern plateau, Bahariya Oasis, Egypt. Geological Survey of Egypt 29, 41 pp.

Salama, W., El Aref, M.M., Gaupp, R., 2012. Mineralogical and geochemical investigations of the Middle Eocene ironstones, El Bahariya Depression,

Western Desert, Egypt. Gondwana Research 22, 717–736.

Salama, W., El Aref, M.M., Gaupp, R., 2013. Mineral evolution and processes of ferruginous microbialite accretion – an example from the Middle Eocene stromatolitic and ooidal ironstones of the Bahariya Depression, Western Desert, Egypt. Geobiology 11, 15–28.

Salama, W., El Aref, M.M., Gaupp, R., 2014. Facies analysis and palaeoclimatic significance of ironstones formed during the Eocene greenhouse. Sedimentology 61, 1594–1624.

Sanz-Montero, M.E., Wanas, H., Muñoz-García, M.B., Gonzalez-Acebron, L., Lopez, M.V., 2013. The uppermost deposits of the stratigraphic succession of the Farafra Depression (Western Desert, Egypt): evolution to a Post-Eocene continental event. Journal of African Earth Sciences 87, 33–43.

Schwertmann, U., Murad, E., 1983. Effect of pH on the formation of goethite and haematite from ferrihydrite. Clays, Clay Minerals 31, 277–284.

Sholkovitz, E.R., Shaw, T.J., Schneider, D.L., 1992. The geochemistry of rare earth elements in the seasonally anoxic water column and porewaters of Chesapeake Bay. Geochimica et Cosmochimica Acta 56, 3389–3402.

Siehl, A., Thein, J., 1989. Minette-type ironstones. In: Young, T.P., Taylor, W.E.G. (Eds.), Phanerozoic Ironstones. Geological Society of London, Special Publication 46, 175–193.

Soliman, H.E., Khalifa, M.A., 1993. Stratigraphy, facies and depositional environments of the Lower Cenomanian Bahariya Formation, Bahariya Oasis, Western Desert, Egypt. Egyptian Journal of Geology 37, 193–209.

Stanton, R.L., 1972. Ore Petrology. McGraw-Hill, 771 pp.

Stoffregen, R.E., 1993. Stability relations of jarosite and natroalunite at 100-250 °C. Geochimica et Cosmochimica Acta 58, 903–916.

Sturesson, U., 1992. Volcanic ash: the source material for Ordovician chamosite ooids in Sweden: Journal of Sedimentary Petrology 62, 1084–1094.

Sturesson, U., 2003. Lower Palaeozoic iron oolites and volcanism from a Baltoscandian perspective. Sedimentary Geology 159, 241–256.

Sturesson, U., Dronov, A., Saadre, T., 1999. Lower Ordovician iron ooids and associated oolitic clays in Russia and Estonia. Sedimentary Geology 123, 63–80.

Sturesson, U, Keikoop, J.M., Risk, M.J., 2000. Modern and Paleozoic iron ooids- a similar volcanic origin. Sedimentary Geology 136, 137–146.

Suchecki, R.K., Hubert, J.F., 1984. Stable and isotopic elemental relationship of ancient shallow-marine and slope carbonates, Cambro-Ordovician Cow Head Group, Newfoundland: implications for fluid flux. Journal of Sedimentary Petrology 54, 1062–1080.

Sultan, N., Halim, M.A., 1988. Tectonic framework of northern Western Desert, Egypt and its effect on hydrocarbon accumulations. Proceedings of the 9th Petroleum Exploration and Production Conference, Cairo 1988. The Egyptian General Petroleum Corporation 2, 1–22.

Sun, S., Konhauser, K.O., Kappler, A., Li, Y.L., 2015. Primary hematite in Neoarchean to Paleoproterozoic oceans. Geological Society of America Bulletin 127, 850–861.

Takeno N., 2005. Atlas of Eh-pH diagrams. Intercomparison of thermodynamic databases. Geological Survey of Japan 419, 285 pp.

Tanner, L.H., Khalifa, M.A., 2010. Origin of ferricretes in fluvial-marine deposits of the Lower Cenomanian Bahariya Formation, Bahariya Oasis, Western Desert, Egypt. Journal of African Earth Sciences 56, 179–189.

Trendall A., Blockley, J., 1970. The iron formations of the Precambrian Hamersley Group, Western Australia with special reference to the associated crocidolite. Geological Survey of Western Australia Bulletin 119. Perth: Geological Survey of Western Australia.

Tucker, M.E., 1981. Sedimentary petrology, an introduction, Blackwell Scientific Publications, Oxford, 252 pp.

Tucker, M.E., Wright, V.P., 1990. Carbonate Sedimentology. Blackwell, Oxford, 482 pp.

Van Houten, F.B., 1973. Origin of red beds. A review. Annual Review of Earth and Planetary Sciences 1, 39–61.

Van Houten, F.B., 1992. Review of Cenozoic ooidal ironstones. Sedimentary Geology 78, 101–110.

Van Houten, F.B., Arthur, M.A. 1989. Temporal patterns among Phanerozoic oolitic ironstones and oceanic anoxia. In: Young, T.P., Taylor, W.E.G. (Eds.) Phanerozoic Ironstones, Geological Society, London, Special Publication 46, pp. 33-50.

Van Houten, F.B., Purucker, M.E., 1984. Glauconitic peloids and chamositic ooids – favourable factors, constraints and problems. Earth Science Review 20, 211–243.

Veizer, J., 1983. Chemical diagenesis of carbonates: theory and application of trace element technique. In: Arthur, M.A., Anderson, T.F., Kaplan, I.R., Veizer, J., Land, I.S. (Eds.), Stable Isotopes in Sedimentary Geology, Society of Economic Palaeontologists and Mineralogists, Short Course 10, 3-1–3-100.

Velde, B., Vasseur, G., 1992. Estimation of the diagenetic smectite to illite transformation in time-temperature space. American Mineralogist 77, 967–976.

Von Stackelberg, U., 1997. Growth history of manganese nodules and crust of the Peru Basin. In: Nicholson, K., Hein, J.R., Buhn, B., Dasgupta, S. (Eds.), Manganese Mineralization: Geochemistry and Mineralogy of Terrestrial and Marine Deposits. Geological Society of London, Special Publication, pp. 153–176.

Weaver, C.E., Beck, K.C., 1971. Clay water diagenesis during burial: How mud becomes gneiss: Geological Society of America, Special Paper 134, 96 pp.

Whitney, G., 1990. Role of water in the smectite to illite reaction: Clays and Clay Minerals 38, 343–350.

Wintsch, R.P., Kvale, C.M., 1994. Differential mobility of elements in burial diagenesis of siliciclastic rocks. Journal of Sedimentary Research A64, 349–361.

Young, T.P., Taylor, W.G.E., 1989. Phanerozoic ironstones. Geological Society London Special Publication 46, 251 pp.

This PhD thesis explores the genesis, mechanisms of formation and modelling of ironstone mineralization, especially those occurring in Phanerozoic rocks. The present study deals with a variety of ironstone occurrences in the northern part of the Bahariya Depression, of the Western Desert of Egypt.

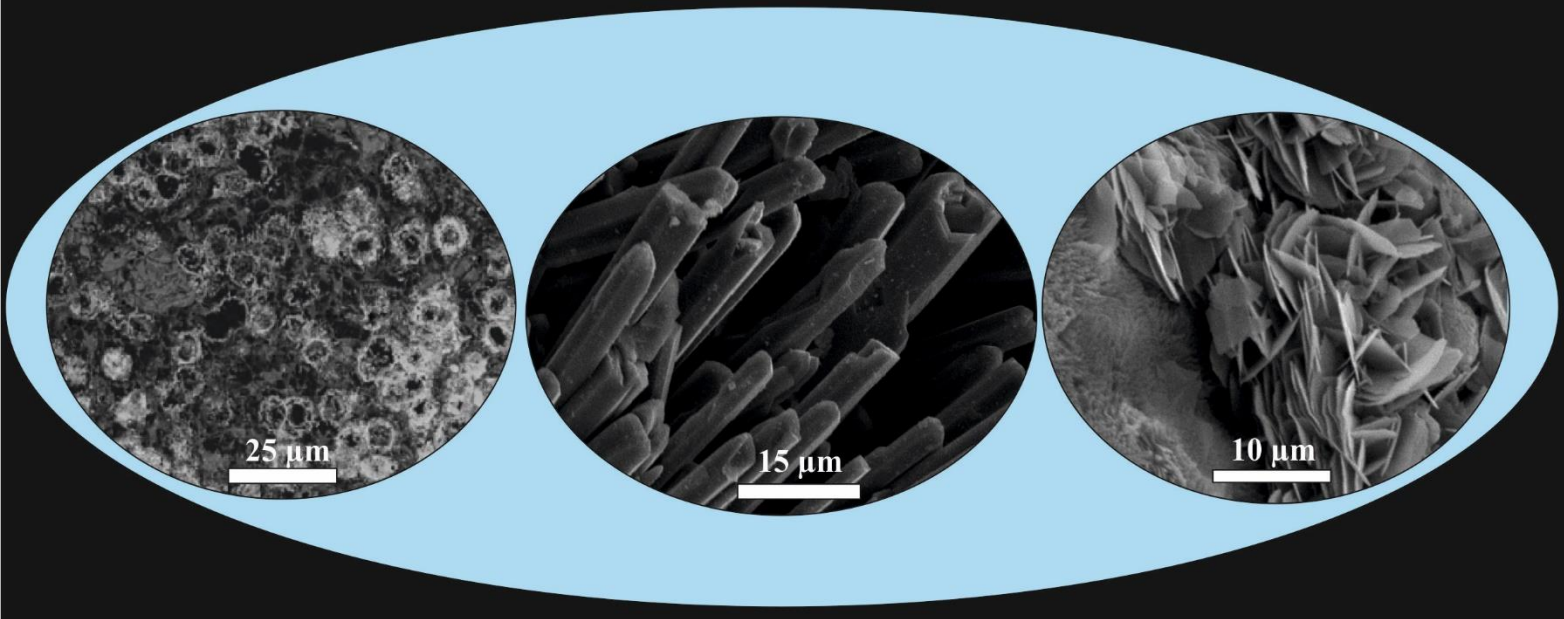

Front Cover - Upper image: Thin ironstone crusts within the Cenomanian clastic sediments, Lower left image : Prof. Dr. Jose Pedro Calvo with Dr. Mansour (Manager of the Bahariya ironstone mines) at the El Gedida mine, Lower right image: Prof. Dr. Esther Sanz showing the contact between the Eocene black ironstone and the underlying Cenomanian Bahariya Formation at the El Harra mine.

Back cover - Top image: Panoramic view of the Eocene ironstone of the Naqb Formation at the Ghorabi mine. Bottom images - SEM photos of: Iron oxyhydroxides replacing dolomite (left), Prismatic tubular-like goethite (middle) and platy rosette-like hematite (right).